TAILORING CROSSLINKED GELLED ELECTROLYTE AND PROBING ITS SYNERGISTIC PERFORMANCE WITH POLYMER-CERAMIC HYBRID SEPARATORS FOR HIGH ENERGY DENSITY LITHIUM-SULFUR BATTERY SYSTEMS

A Thesis

Presented to the Faculty of the Graduate School

of Cornell University

In Partial Fulfillment of the Requirements for the Degree of

Master of Science

by

Vaidik Shah

August 2021

ABSTRACT

The last two decades have seen an instrumental increase in the favor for renewable energy and the demand for electrical transport has significantly strengthened. With ever increasing demand for longer device duration especially for long-range electric transport, the existing Li-ion technology has eventually reached its limit. Meanwhile, Lithium Sulphur (Li-S) batteries, owing to their ultrahigh theoretical energy density of about 2600 $Whkg^{-1}$, low-cost, Earth abundant and environmentally friendly sulfur (S) cathode, are seen as promising replacements to realize energy densities beyond 500 $Whkg^{-1}$.

However, Li-S batteries still suffer from several challenges. (1) The loss of coulombic efficiency due to 'polysulfide shuttling' wherein lithium polysulfide intermediates formed during cell discharge, dissolve into the battery electrolyte and migrate and undergo side reactions at the Li anode. The instability caused due to (2) significant cathodic volume changes, (2) lithium dendritic formation and (3) the formation of an ionically insulating 'rough' passivation layer after repeated charge/discharge operations, limit the practical utility of Li-S batteries.

In this work, a novel solution in the form a facile, in-situ fabricated crosslinked Gel Electrolyte (GE) system has been proposed to tackle all the above issues. First, we present a comprehensive comparative analysis of the performance of GE cells with traditional liquid electrolyte (LE). The performance of GE cells was further enhanced using Polyethylene Glycol (PEG) as an additive. It was observed that the GE cells had

substantially lower capacity fade and performed better than LE cells at high-rate cycling.

Next, the GE system was paired with high-performance hybrid Polyimide (PI) / Organopolysilazane (OPSZ) separators. The synergistic performance of these two components in Li-S cell was probed and comparative analysis was conducted with conventional Celgard 2400 separator. The hybrid separator systems exhibit a ten-fold improvement in electrolyte uptake, a marked improvement in ionic conductivity and a high first cycle discharge capacity – close to that of LE cells.

Finally, to investigate the effectivity of the gelled separators at trapping the lithium polysulfide (LPS) intermediates, a diffusivity analysis was carried out using gel crosslinked and non-crosslinked Celgard 2400 and PI/OPSZ separators. Experimental analysis showed that the gelled separators were more effective at entrapping LPS migration. We have also built a numerical model solved using Finite Element Method on a mapped mesh grid using COMSOL Multiphysics 5.5 to supplement the experimental analysis.

BIOGRAPHICAL SKETCH

Vaidik Shah was born on October 19th, 1997, to Shital Shah and Rashesh Shah in Mumbai, India. In school, he naturally leaned towards Science and Mathematics and earned several accolades in national-level competitions. This interest led him to follow in the footsteps of his father and pursue Chemical Engineering at the Institute of Chemical Technology (ICT), Mumbai after graduating from Rustomjee Cambridge International School and Junior College. During his undergraduate studies, he was fortunate to obtain internships that helped him gain a well-rounded exposure to the vast field of Chemical Engineering. During his sophomore year, his internship at the Advanced Drying Laboratory, ICT Mumbai on simulation-based modeling of high-throughput, energy efficient drying systems developed his passion for research in the Energy domain. Having realized this passion, post his undergraduate studies in 2019, Vaidik chose to pursue the Master of Science program at Cornell University (CU). Since then, he has been working under the supervision of Prof. Yong L. Joo, on optimizing gel-electrolyte systems, and investigating their synergistic properties with polymer-ceramic hybrid separators in high-energy lithium sulfur (LiS) batteries. Vaidik has been accepted into the Ph.D. program at the Robert F. Smith School of Chemical and Biomolecular Engineering, Cornell University and will be continuing his graduate research on developing a deeper understanding of the chemistry and transport mechanisms of electrochemically active species in the electrolyte medium for LiS batteries.

Dedicated to my family, friends and all my loved ones.

ACKNOWLEDGMENTS

I would like to express my sincerest gratitude to my research advisor, Professor Yong Lak Joo for all his advice and guidance during the last two year and for accepting me into his group as a PhD student. I would like to acknowledge Prof. Jin Suntivich for being on my special committee and providing valuable feedback on my work. I would also like to extend my gratitude to Prof. Jefferson W. Tester and Prof. Nicholas L. Abbott for considering me worthy of their recommendation for my PhD applications. Without their help and guidance, I would not have been able to make my dream of pursuing a PhD a reality.

I acknowledge and appreciate all the support that I have received from my friends and colleagues especially in the trying pandemic time. In particular, I would like to thank Dr. Somayeh Zamani, Dr. Christopher Klaassen for all their guidance, patience and help throughout the 2 years. I have the deepest appreciation for Cecilia, Yash, Caspar, Jasper, Meichun, Ritika, Kyle, Sanjana, Naman and Dr. Min Nie for making the offices/labs enjoyable spaces to work in.

Finally, I would like to thank my family, without whom I wouldn't have been where I am today. It is your endless love and support that keeps me going.

TABLE OF CONTENTS

LIST OF FIGURES

LIST OF TABLES

CHAPTER 1

INTRODUCTION

1.1 The need for high-power, high-capacity energy storage

Why is there a need to store electrical energy? Electrical energy is the integral component of manufacturing industry, service industry, the ever-expanding renewable energy industry and of all the electronic peripherals that have become necessities of modern life!

The impact of climate change is more apparent today than ever before. The indiscriminate use of fossil fuels in the 19th and the 20th century has led to potentially catastrophic impacts to the environment (Höök & Tang, 2013). If the energy practices of the last two centuries are allowed to continue without check, the impacts will only worsen to the point of no return. The most promising, and, in fact the inevitable solution to this problem is shifting of the global energy portfolio to renewable sources of energy. The last decade has seen a significant increase in the awareness, interest, and investments in the renewable energy sector by major economies (Hasanuzzaman et al., 2017).

If renewable energy, or for the matter of fact even lower cost energy is to be made more ubiquitous in our energy landscape - high-capacity, high power output energy storage need be a critical component in assuaging issues like peak power demands and the inherent intermittent nature of conventional renewable energy technology like solar and wind (Whittingham, 2012).

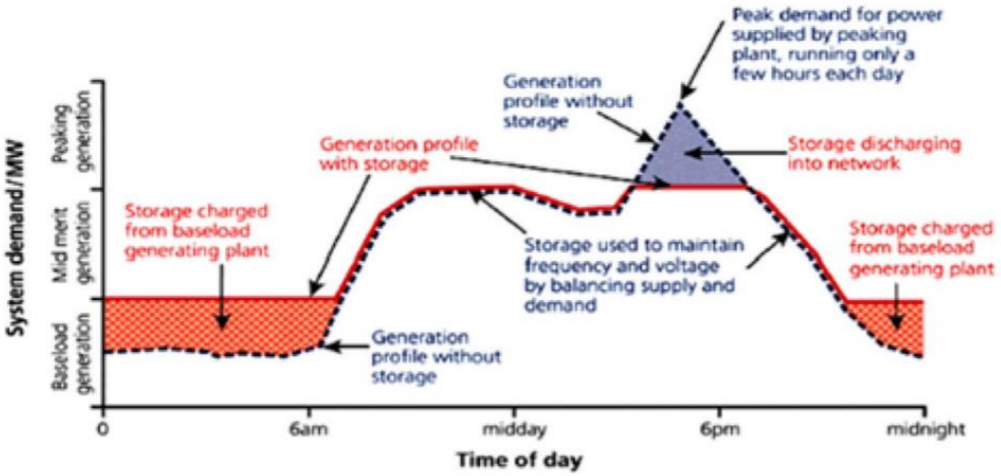

Figure 1.1: A typical renewable energy power profile augmented by energy storage(Whittingham, 2012).

Conventional renewable energy technologies, such as wind and solar, can only be the primary source of energy when supplemented with large-scale energy storage facility. Even if these sources are linked to the electric grid, an efficient high-capacity energy storage device is necessary to smoothen the electrical output as displayed in Fig. 1.1. Examples of this are the newly commissioned 310 MW solar power plant in Wisconsin which is paired with a 110 MW of battery storage and Japan's 'Tomatoh Abira Solar Park 2' with a capacity of 64.6 MW supplemented with 19MWh of onsite battery storage (Colthorpe, 2020)(Colthorpe, 2021). Today about 12% of the distributed solar generated energy in the United States is accounted by solar-plus-storage systems, and it is estimated that by 2023, about 27.4% of the total PV generation will be from solar-plus-storage sites accounting for about 21,000 MWp of electrical energy(Munsell, 2018).

Further, an electric economy would consequently necessitate the electrification of the transportation sector – it being, at present, the largest consumer of fossil fuel after grid-scale energy generation. The annual 'Long-Term Electric Vehicle Outlook' published on May 19, 2020, by BloombergNEF estimates electric vehicles (EVs) accounting for

58% of the new passenger car sales globally by 2040, and 31% of the whole car fleet. It also predicts EVs making up 67% of all municipal buses on the road by that year, with an additional 47% of two-wheelers and 24% of all light-commercial vehicles. With large EV players such as Tesla, Ford, and General Motors eyeing entry into untapped, high potential, developing economies like China and India, the demand and need for high-capacity battery systems is only expected to grow. For the EV technology to compete at such a scale with high range, long-lasting conventional internal combustion engine vehicles, there needs to be significant research into more robust, higher-capacity, lower cost battery systems. It is for these reasons, there is an inevitable and imperative need for research into high-power, high-capacity energy storage.

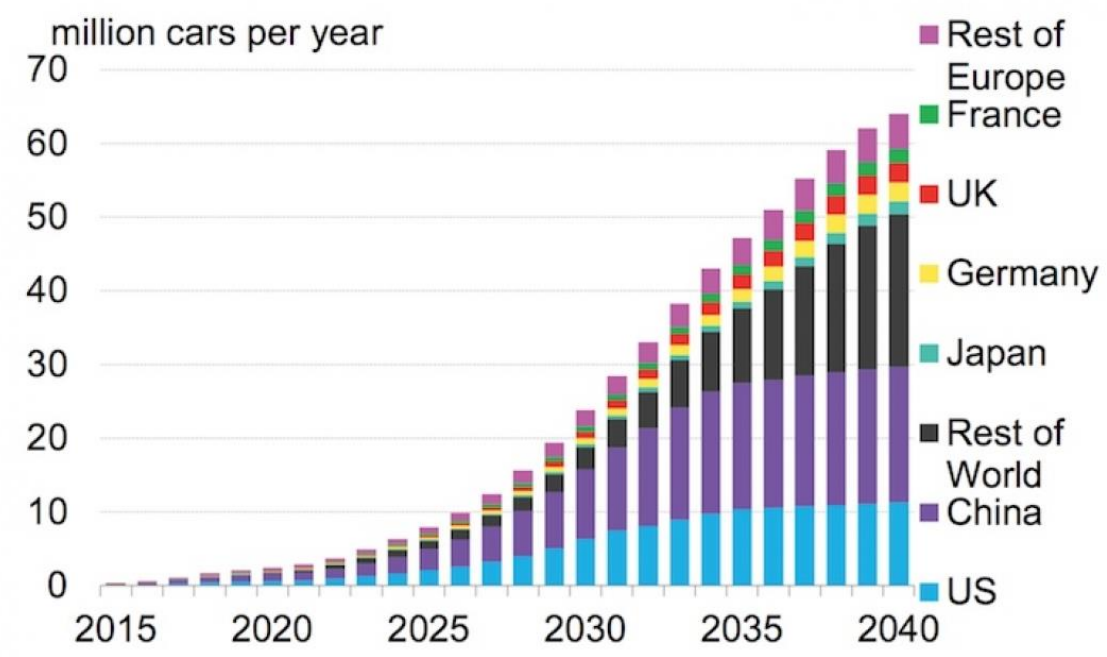

Figure 1.2: Electric Vehicle Market Projections till 2040

1.2 The Lithium-Sulphur Battery

1.2.1 Introduction

It has been well established via research trends that one of the primary motivators for research in secondary batteries is the pursuit for higher-and-higher specific capacity. From the previous generation of 40 $Whkg^{-1}$ lead-acid batteries to the high performance 260 $Whkg^{-1}$ Panasonic 6752.T 2170 lithium-ion batteries (LIBs), the specific gravimetric capacity of the secondary battery continues to rise (Rand, 2011)(Dunn et al., 2011) The most prominent secondary battery in use today is the lithium-ion battery (Li-ion). In this battery, external electric current is stored by electrochemically converting lithium ion (Li^+) stored in the nickel-manganese-cobalt (NMC) cathode into Li intercalated into the graphite anode. The reverse occurs upon discharge to produce electricity. The LIB technology, having matured over several decades, is capable of at least a couple of thousand cycles before battery failure (Cheng et al., 2018).

Today, LIBs have obtained widespread utilization in a vast range of applications ranging from personal electronics to electric vehicle applications and in some large applications like grid-scale energy storage applications. The need for higher capacity LIBs is only expanding. However, the issue with LIB technology is that the technology has almost reached the peak maturity, with several commercially available battery systems reaching close to their theoretical capacity performance and thus, there lies very little room for enhancing capacity to meet the ever-growing consumer demand.

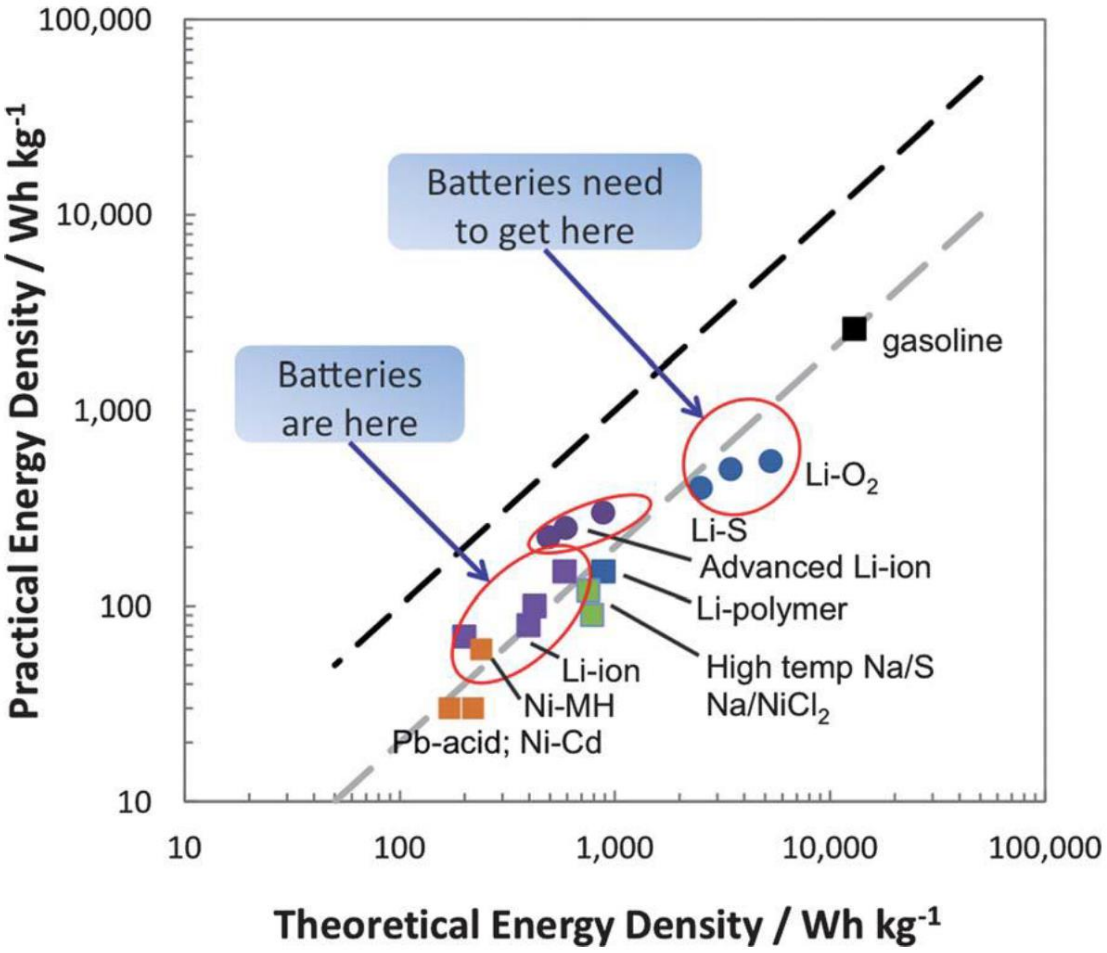

Figure 1.3: Energy densities of varying battery chemistries compared to gasoline (Thackeray et al., 2012).

The figure 1.3 shows an overview of the energy densities for different types of batteries. Lithium-oxygen/air (Li-O_2) and lithium-sulfur (Li-S) technologies have some of the highest theoretical energy densities for any secondary battery technology. With Li-O_2 comes the advantage of being able to use plentiful atmospheric oxygen as a reagent, however, in its current research stage, this technology suffers from severe challenges in terms of battery life and coulombic efficiency which require further research and development (Girishkumar et al., 2010). Li-S is closer to becoming a viable alternative to Li-ion, which has led government organizations like the Department of Energy, research universities, and private companies to devote substantial efforts towards Li-S research.

Throughout history, sulfur has been an essential commodity. In the medieval times, it was a crucial ingredient for black gunpowder which was a large leap in human innovation. Recently, it has been critical in developing state-of-the-art energy storage applications. Its small atomic number and its high multi-electron interaction with lithium metal, gives it a theoretical specific capacity of 1672 $mAhg^{-1}$ and specific energy of 2600 $Whkg^{-1}$, which are amongst the highest of any practical solid cathode materials (Ji & Nazar, 2010).

Furthermore, sulfur being a large volume waste product from petroleum refinement and its relative abundance in the Earth's crust make it a low environmental impact material and significantly more sustainable material than the heavy earth metals like Co, Mn and Ni required for LIB systems (Zhao et al., 2020).

The first development of the LiS battery technology dates back to 1962 which predates the first prototype LIB developed by Akira Yoshino in 1985 based on earlier research by John Goodenough, M. Stanley Whittingham, Rachid Yazami, and Koichi Mizushima during the 1970s and 1980s (Reddy et al., 2020). In 1962, Herbert and Ulam first introduced the concept of the S electrode (Herbert & Ulam, 1958). Building on that, in 1967, the Argonne National Laboratory developed a high-temperature Li-S system by using molten Li and S as the two electrodes (Birk & Steunenberg, 1974). This first showed the true potential of the technology, however, problems working around the low conductance of sulfur was still challenging. Later, E. Peled's research group analysed the electrochemical behavior of S cathodes in organic electrolytes at room temperature, which provided great insights into solvent-dependent redox cell mechanisms and paved the path for tailoring suitable electrolyte components in subsequent years (Yamin & Peled, 1983). Following that, another major leap in development of room temperature Li-S systems came with Nazar's

highly ordered mesoporous CMK-3 cathode design in 2009 which significantly improved the cycle life and capacity of the batteries (Ji et al., 2009). A year later, Sion Power's Zephyr, an unmanned aerial vehicle (UAV) powered by solar energy and the company's proprietary Li-S battery systems broke the then world record for longest unmanned flight by exceeding 336 hours of continuous flight – thus marking the first significant leap in commercial Li-S battery development.

Li-S batteries have grown even popular in the last 5 years which such great renewed interest in long-range electric vehicles and the strive towards long-lasting batteries for consumer electronics. Li-S batteries on the basis of their extremely high theoretical gravimetric capacity are the most well-suited to meet this demand. Li-S batteries are being studied quite extensively in both academia and industry across the world inorder to achieve capacities around 500 $Whkg^{-1}$. With such a high quantum of research on Li-S batteries, it can be assured that Li-S technology will achieve significant breakthroughs in the coming few years. This thesis outlines the work done on tailoring the electrolyte component and testing the synergy of the electrolyte component with high-performance polymer ceramic hybrid separators in order to maximize cell performance, life and safety standards for the Li-S battery technology.

1.2.2 Cell Chemistry

The Li-S battery is typically constructed using a lithium metal anode, a separator system – generally polyolefin but research by our group has showed that that polymer-ceramic hybrid separators exhibit better performance than traditional commercial Celgard 2400 separators, and a carbon/sulphide composite cathode. The battery electrolyte is generally organic glyme-based electrolyte with dissolved lithium salts, however, several broad types of electrolytes have been quoted in literature each having their merits and demerits (Angulakshmi & Stephan, 2015).

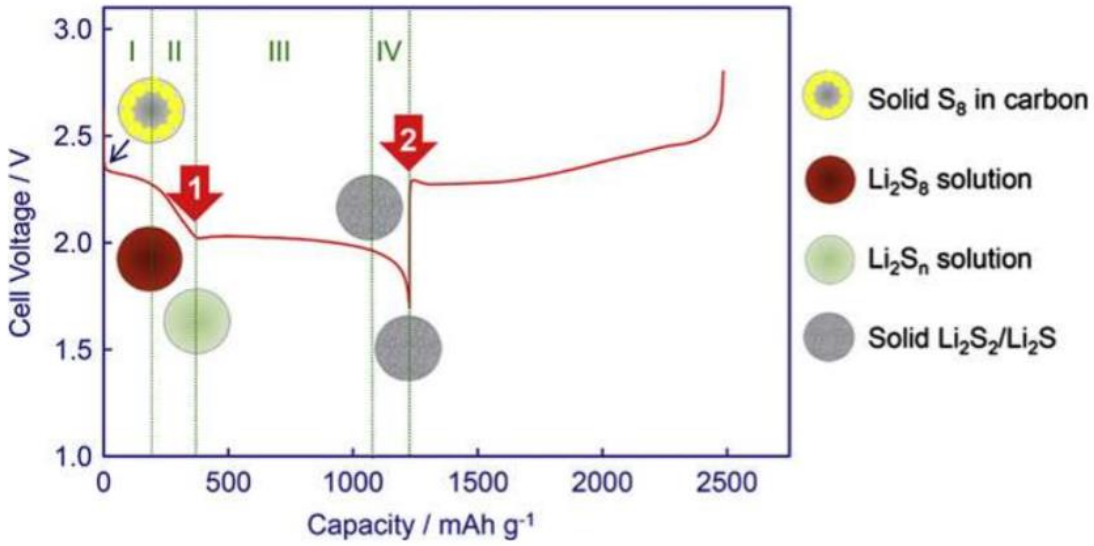

Figure 1.4: A typical charge-discharge profile of a traditional liquid electrolyte Li-S cell (Sheng S. Zhang, 2013).

During discharge, Li in the anode get converted to Li^+ ions and migrate towards the cathode in the electric field. Simultaneously, sulfur (S_8) gets reduced at the cathode and dissolves into the electrolyte where it reacts with the Li^+ to form lithium polysulfides (LPS) (Li_2S_x). These polysulfides are reactive intermediate species varying lengths of sulfur, with the longest being Li_2S_8. As the discharge cycle progresses, the longer chain

LPS are further reduced into shorter chain LPS such as Li_2S_6, Li_2S_4. These LPS are still soluble in the electrolyte and hence if they migrate towards the anode, may cause some unwanted side-reactions with the Li metal. The varying chemical reactivity and difference in kinetics and migration rates give Li-S batteries their characteristic discharge curve, shown in fig. 1.4.

1.2.3 Charge-Discharge profile characteristics of Li-S cell.

The fig 1.4 shows the typical charge-discharge profile for the first cycle of a traditional Li-S cell. As shown in the diagram, on the basis of the phase changes that Sulfur undergoes during a discharge cycle, the discharge process can be divided into 4 different reduction regions.

Region I: This region comprises of a solid-liquid two phase reduction reaction from elemental sulfur (S_8) to Li_2S_8 which is responsible for the first upper voltage plateau at 2.2-2.3 V. It is this region wherein the newly formed Li_2S_8 species dissolve into the liquid electrolyte to become a liquid cathode. This process leaves numerous voids in the cathode.

$$S_8 + 2Li \rightarrow Li_2S_8 \quad (1)$$

Region II: In this region, a liquid-liquid single phase reduction reaction from the dissolved Li_2S_8 to low-order LPS occurs. During this reaction, the cell voltage steeply declines and the electrolyte solution's viscosity is seen to increase gradually with a decrease in the S-S chain length and an increase in the concentration of LPS anions. The solution viscosity peaks at the end of this discharge region.

$$Li_2S_8 + 2Li \rightarrow Li_2S_{8-n} + Li_2S_n \quad (2)$$

Region III: In this region, a liquid-solid two-phase reduction reaction occurs converting the dissolved low-order LPS to insoluble Li_2S_2 or Li_2S. The following two reactions compete.

$$2Li_2S_n + (2n-4)Li \rightarrow nLi_2S_2 \quad (3)$$

$$Li_2S_n + (2n-2)Li \rightarrow nLi_2S \quad (4)$$

This region accounts for the second lower voltage plateau generally at 1.9 - 2.1 V at STP. It is this region that accounts for most of the cell's capacity.

Region IV: In this region, a solid-solid reduction reaction occurs that converts Li_2S_2 to Li_2S. This region is a kinetically slow step and suffers from high polarization due to the non-conductive and low diffusivity of the Li_2S_2 or Li_2S layer.

$$Li_2S_2 + 2Li \rightarrow 2Li_2S \quad (5)$$

Region I and II exhibit the greatest extent of redox shuttling, which causes the cell to suffer from high discharge rate and hence the cell's theoretical capacity is seldom achieved. Region II accounts for the major share of the battery capacity.

It is observed when eqn. 4 is dominant over eqn. 3, the cell exhibits an improved capacity performance, and the region IV is short-lived or in some cases absent. Aside from these electrochemical reduction reactions, complicated chemical reactions amongst the PS anions may also occur and the kinetics and thermodynamics of these

reactions are dependent on the type of solvents, concentration, and temperature etc. These double dissociation reactions may be written as:

$$Li_2S_n + Li_2S \rightarrow Li_2S_{n-m} + Li_2S_{1+m} \quad (6)$$

$$Li_2S_n \rightarrow Li_2S_{n-1} + \frac{1}{8}S_8 \quad (7)$$

Fig 1.4 shows 2 arrows that show a short peak in the discharge and charge voltage. Arrow 1 points towards the point where the viscosity of the solution is maximized due to the combined effect of S-S chain length and the concentration of PS anions. Arrow 2 indicates a reduction in polarization due to the phase transition from the solid, insoluble Li_2S_2 and Li_2S to the dissolved PS state. At the completely discharged state, the surface of the carbon at the cathode side is covered by a solid Li_2S_2/ Li_2S layer which causes the cell to suffer from high polarization. When charged, the solid layer oxidizes to form soluble PS which dissolves into the electrolyte and hence the cell's polarization is reduced. Based on this analysis it can be safely said that the Li-S cell is essentially a liquid electrochemical system (Sheng S. Zhang, 2013).

1.2.4 Polysulfide Redox Shuttling

Though the dissolved PS are critical for cell performance, they are also the most prominent reason for failure of cells. The dissolved PS cause severe and if unchecked, catastrophic redox shuttling between the S/C cathode and the Li metal anode. This results in reduced coulombic efficiency while charging and an enhanced self-discharging rate when stored. All in all, it severely affects the life of the cell (McBrayer et al., 2018).

At the anode, the PS dissolved in solution can be electrochemically and chemically reduced through these pathways:

Electrochemical Reduction

$$(n-1)\,Li_2S_n + 2Li^+ + 2e^- \rightarrow nLi_2S_{n-1}$$

Chemical Redox

$$(n-1)\,Li_2S_n + 2Li \rightarrow nLi_2S_{n-1}$$

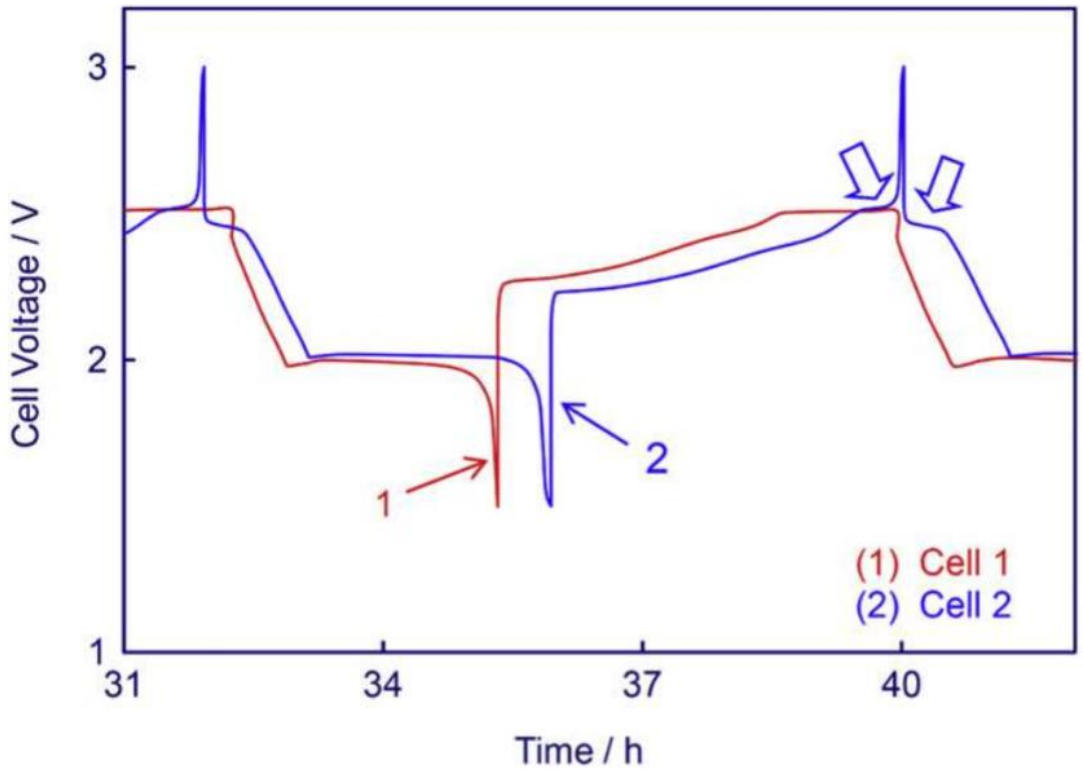

Figure 1.5: Charge and discharge voltage curves of Li-S cell. Cell 1 exhibits strong redox shuttling whereas Cell 2 has suppressed redox shuttling (Sheng S. Zhang & Read, 2012).

These parasitic reactions have severe impact on the cell performance. They consume active sulfur species, corrode Li anode, and polarize it once a solid Li_2S_2/ Li_2S layer form on the Li surface. The effect of LPS shuttling is evident in the charging and

discharging profiles seen in fig 1.5 (Sheng S. Zhang & Read, 2012)(Sheng S. Zhang, 2013). Cell 1 exhibits a strong redox shuttling effect and Cell 2 has suppressed redox shuttling because of $LiNO_3$ additive in the electrolyte (N. Ding et al., 2016a). It is observed that Cell 1 isn't able to be charge over 2.5V and the charging process must be stopped with a pre-set capacity cut-off (infinite charging). In this particular case, it is observed that the cell can be only charged to the end of Region I without the formation of sulfur. This is due to the high redox shuttle of dissolved Li_2S_8. Whereas Cell 2 can be charged to till the cut-off voltage with the formation of elemental sulfur and the next discharge cycle shows a plateau near 2.3 V and hence, shows a high cycling efficiency of over 99%.

1.3 Li-S: Challenges and Avenues for Research

Since the first initiation in 1960s, the Li-S battery technology has undergone several instrumental leaps in development. The cells today are much longer, can achieve significantly higher capacities, are much more practical in application. However, despite the great strides that Li-S technology has seen in the last few decades, true commercialization and complete replacement of the Li-ion technology is still a long curvy path ahead (T. Li et al., 2019).

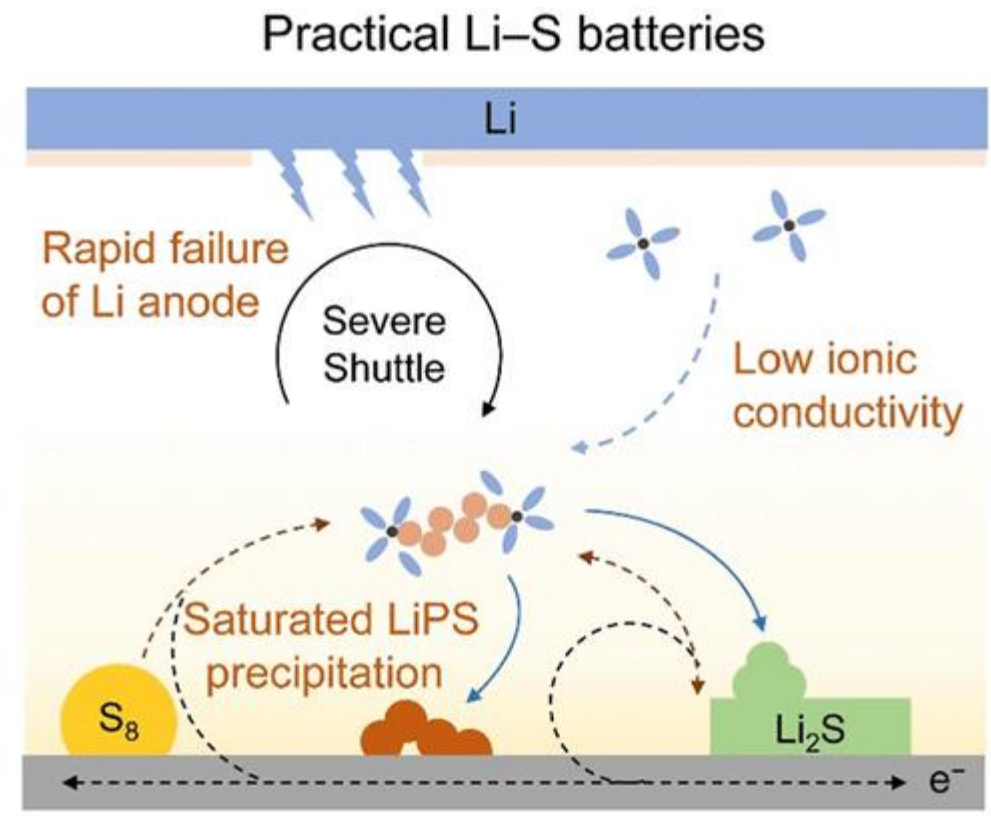

Figure 1.6: Problems associated with practical Li-S battery systems

For a Li-S battery be robust and commercially practical, it needs to overcome several issues. First, the end products of the discharging and charging are intrinsically ionic

insulating, and a thick, uneven coating renders a lot of kinetic difficulty in the battery system (Qie & Manthiram, 2016). To avoid this, the formation of the insoluble, non-conducting solid electrolyte interface (SEI) needs to be suppressed/regulated.

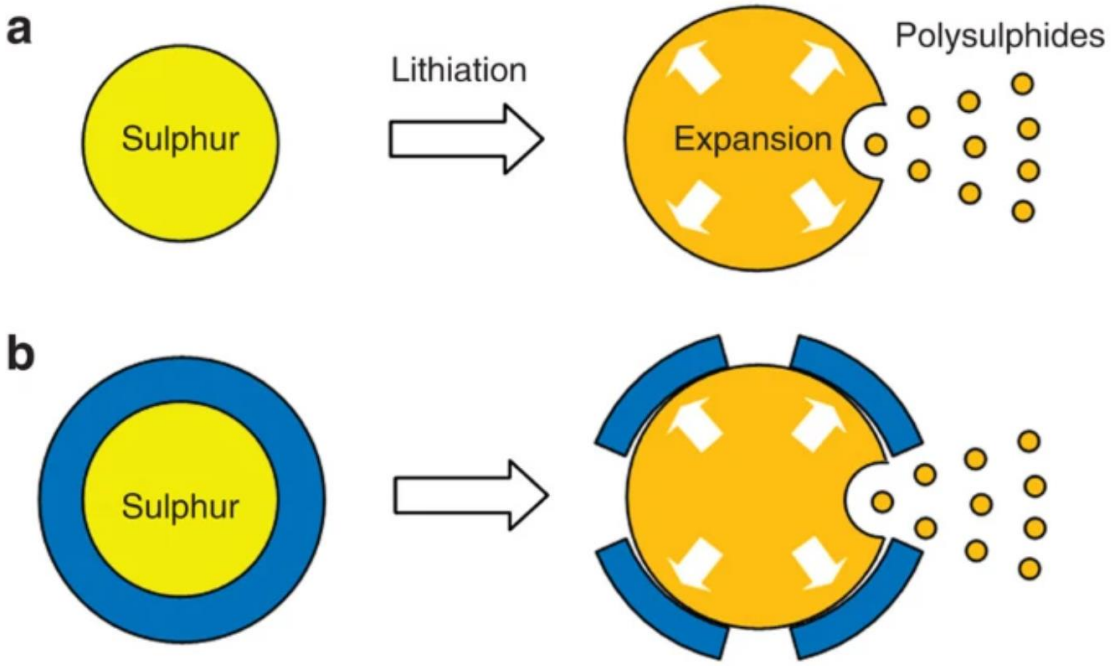

Figure 1.7: Schematic Diagram for cathodic expansion during charge-discharge cycle

Second, the cathode experiences significant volume changes during charging and discharging. The volume change is almost 80% and this leads to a lot of pressure on the system over multiple charge-discharge cycles. If the volume change is not properly mitigated, the cathode surface is seen to degrade over time which greatly minimizes the cell life and end-of-life capacity (Seh et al., 2013).

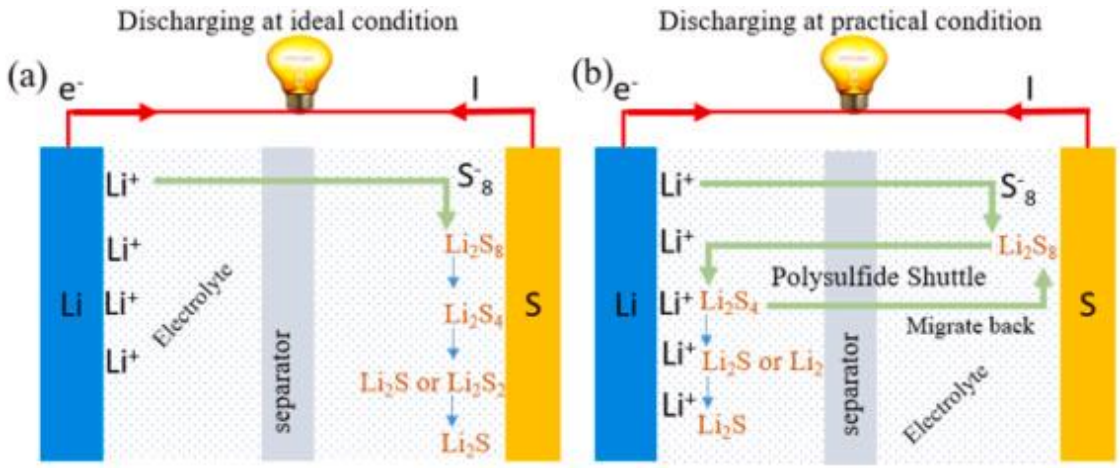

Figure 1.8: Schematic representation of a LSB condition in an (a) Ideal condition without shuttle effect and (b) Practical condition with shuttle effect caused by polysulfide migration (Rana et al., 2019).

Further, and probably the most important issue is that of the polysulfide shuttling. During discharge, The soluble LPS intermediates dissolve in the electrolyte and due to the electric field diffuse (or shuttle) from the cathodic half of the cell to the anodic half. Here, these LPS react with the lithium metal and form a passivation layer of Li_2S/Li_2S_2 on the lithium surface causing irreversible loss of the active material, reduction of coulombic efficiency and the eventual battery failure (Lei et al., 2018; Peled et al., 2018) (Rana et al., 2019).

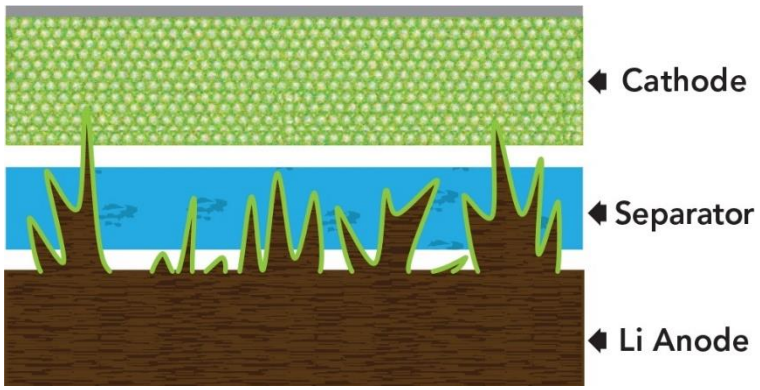

Figure 1.9: Schematic diagram for catastrophic dendritic growth

Lastly, one of the most common issues that plagues Li-based battery technology is the issue of Li dendritic growth. Lithium (Li) metal has the highest theoretical specific capacity (3,860 mA h g^{-1}) amongst all types of lithium battery anodes (Bruce et al., 2012). However, Li metal anode is plagued with the most severe safety risk, in the form of uncontrolled dendritic growth caused due to continuous lithiation and delithiation during repeated electrochemical charging/discharging. This dendritic growth if remained unchecked, lead to dendritic induced internal shorting.

These compounded issues are impeding the real commercialization of high-energy-density rechargeable lithium metal batteries (Zou et al., 2018). Several innovative efforts have been made towards addressing these issues in the form of employment of cathodic additives, modified cathodic surfaces(Ji et al., 2009; Qie & Manthiram, 2016; Seh et al., 2013), modified separator systems (K. Liu et al., 2017; Luo et al., 2015; Ryou et al., 2012), Li anode surface modifications (Park et al., 2016; Ryou et al., 2015), artificial anode surface coating (Kozen et al., 2015; Lee et al., 2016; N. W. Li et al., 2016; G. Zheng et al., 2014), enhanced current collector (Y. Liu et al., 2016; Yan et al., 2016; Yang et al., 2015; R. Zhang et al., 2016) and optimization of electrolyte (F. Ding et al., 2013; Y. Lu et al., 2012, 2014, 2015; Zhou et al., 2016) etc.

As seen above, there have been several solutions that aim towards mitigating one or a few of the issues but none tackle all the issues and so usually a combination of these systems are needed to be employed. This approach has its own flaws as battery systems are not modular in nature and the cell chemistry is dependent on all the components. Thus, there is always an issue with combinatory effects leading to the need for extensive synergistic studies.

In this thesis, a novel solution in the form a facile, in-situ fabricated Gel electrolyte system for the Li-S battery has been proposed. The Gel electrolyte tackles all the issues of suppressing passivation layer formation, dendritic growth, mitigating cathodic volume change pressures, and suppressing polysulfide shuttling.

1.4 Gel Electrolyte System

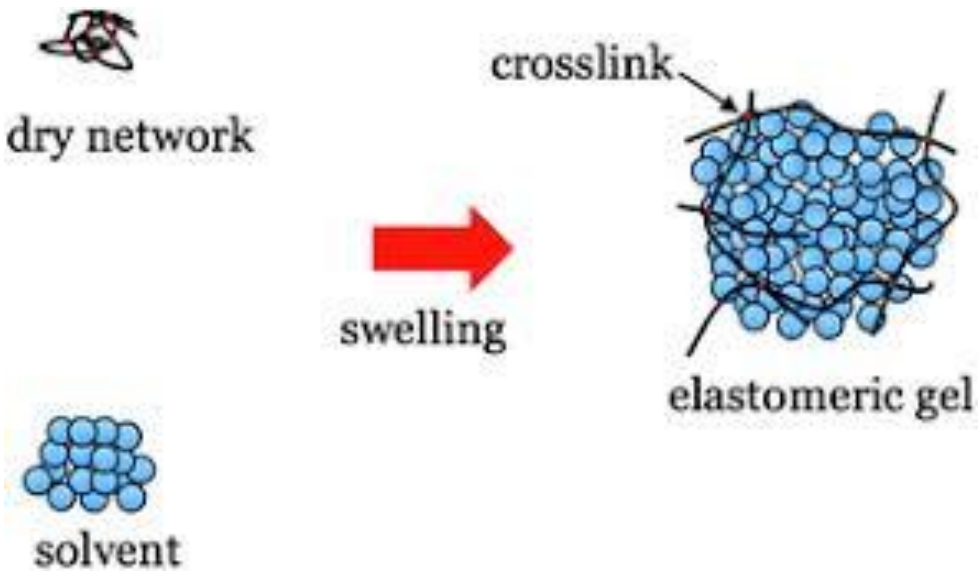

Figure 1.10: Schematic diagram to show the trapping of solvent molecules in a crosslinked 'Gel' network.

Although the performance of Li-S batteries have been well acknowledge, the safety hazards and electrochemical performance still remain as the biggest impeding factors towards real commercialization (Kamyshny Alexey et al., 2007)(Barchasz et al., 2012).

At present, most of the conventional Li-S batteries utilize liquid electrolyte with LiTFSI dissolved in ether solvents, such as 1, 3 dioxolane (DOL), dimethoxy ethane (DME), etc. Though these batteries have shown to have a high first cycle capacity however, the life of Li-S batteries is greatly limited due to the following reason: (a)During the charge/discharge cycling, long chain soluble lithium polysulfide intermediates are

formed at the cathode and these dissolve into the battery electrolyte. This continuous dissolution of LPS greatly increase the viscosity of the electrolyte, and in the meantime, also destroy the microporous structure of the sulfur impregnated cathode. Additionally, these LPS form a rough passive layer of Li_2S on the electrode surface and hence impede ionic conductivity. (b) The 'polyulfide shuttling'. (c) The electrolyte solvent becomes unstable and reacts with the fresh, porous Li anode after it has been corroded with polysulfides. The electrolyte continues to be consumed on the Li anode due to the reaction, and the reaction generates a gas which may cause the expansion of the the battery and may even lead to an explosion (Mikhaylik & Akridge, 2004)(Bruce et al., 2012). Given the electrolyte is pre-dominantly organic in nature, the risk of flammability at high temperature is also heightened. (d) The uncontrolled lithium growth in the liquid electrolyte causes the growth of dendrites, leading to the formation of 'dead lithium' with significant loss of coulombic efficiency, which may also cause internal short circuit and catastrophic failure(H. C. Wang et al., 2019) (Cao et al., 2015).

There have several potential solutions offered by researchers to these issues, including the optimizing the design of sulfur cathode, the protection of lithium anode and optimization of electrolytes. In terms of electrolyte optimization, recently, solid electrolytes have garnered a lot of research interest. They prevent dissolution of polysulfides into the electrolyte and their mechanical strength suppresses the formation of dendrites. However, solid electrolytes exhibit very little ionic conductivity at room temperature. Hence, the specific discharge capacity of solid electrolytes is well lower than needed for practical application. Additionally, the solid-solid interface between the electrodes and the electrolyte significantly reduces the kinetics of the cell chemistry.

Since, Li-S cell chemistry is extremely dependent on reactions of active materials in the liquid phase, the capacity is much lower than what conventional liquid electrolyte cells can achieve.

To solve the problems of low ionic conductivity at room temperature of the solid electrolyte, the Gel Electrolyte, which employs polymeric networks that immobilize the liquid electrolyte, was developed. Given the electrolyte is essentially, immobilized liquid electrolyte, the lithium-ion transport of the gel electrolyte is identical to that of the liquid electrolyte. Additionally, the gel electrolyte employed in the group have polar sites on the polymeric network and this helps trap the dissolved lithium polysulfide intermediates. These gel electrolytes have a significantly higher ionic conductivity of about 0.350 mS/cm. Moreover, gel electrolyte exhibits much lower interfacial impedance as before the gel is 'cured' at 70^{o}C, the electrolyte is liquid and so wets the cathode surface as a liquid. Additionally, the gel electrolyte system, owing to their relatively high mechanical strength, suppresses the formation of lithium dendrites and the inhibition of lithium polysulfide dissolution into the electrolyte means that the formation of passivation layer of Li_2S on the electrode surface is also curbed. The improved mechanical strength than liquid electrolyte also means that it is better able to withstand the pressures exerted by cathodic volumetric changes during charge/discharge process. These properties help improve both the electrochemical performance and the life of batteries.

Gel Electrolytes are defined widely as cross-linked polymeric networks that are swollen in the liquid electrolyte. This swelling of the polymeric networks immobilizes the liquid solvent molecules and produces a pseudo solid material with a gel-like consistency

shown in fig 1.10, and hence the name. In all chemical interaction, the crosslinked gel electrolyte still behaves as a liquid electrolyte, however, given the solvent molecules are immobilized, the physical properties of the gel systems are close to that of the solid-state electrolyte.

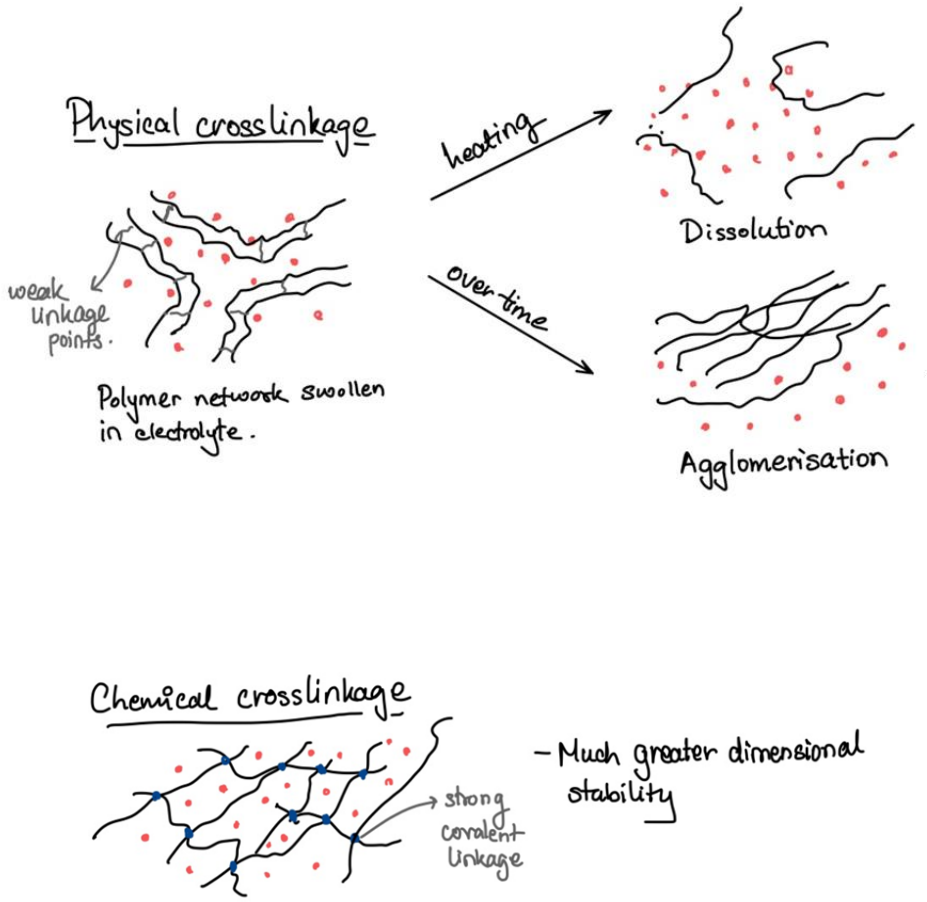

Figure 1.11: Schematic diagram for the two mechanisms of crosslinking - Physical and Chemical Crosslinkage

Crosslinking of polymeric strands can be achieved in two ways: physically and chemically. The bonds between the polymer strands in physical crosslinking is primarily

van der Waal's forces or hydrogen bonds and, in some cases, ionic interactions, whereas in chemical cross-linkage, the bonds are stable, strong covalent in nature. Given the weak van der Waal or hydrogen bonds in physically crosslinked systems, the polymer strands tend to agglomerate over time and under heat and at a temperature over the lower critical solution temperature (LCST), the polymer matrix may dissolve into the solution. Whereas gels made by chemical linkage show much greater dimensional stability and hence are ideal for usage in gel electrolytes.

There are several polymer matrices that have been researched each with their own merits, like polymethyl methacrylate (PMMA), polyethylene oxide (PEO), Poly(N-isopropylacrylamide) (PNIPAM) etc. (Sheng S. Zhang & Tran, 2013) (Jeddi et al., 2014).

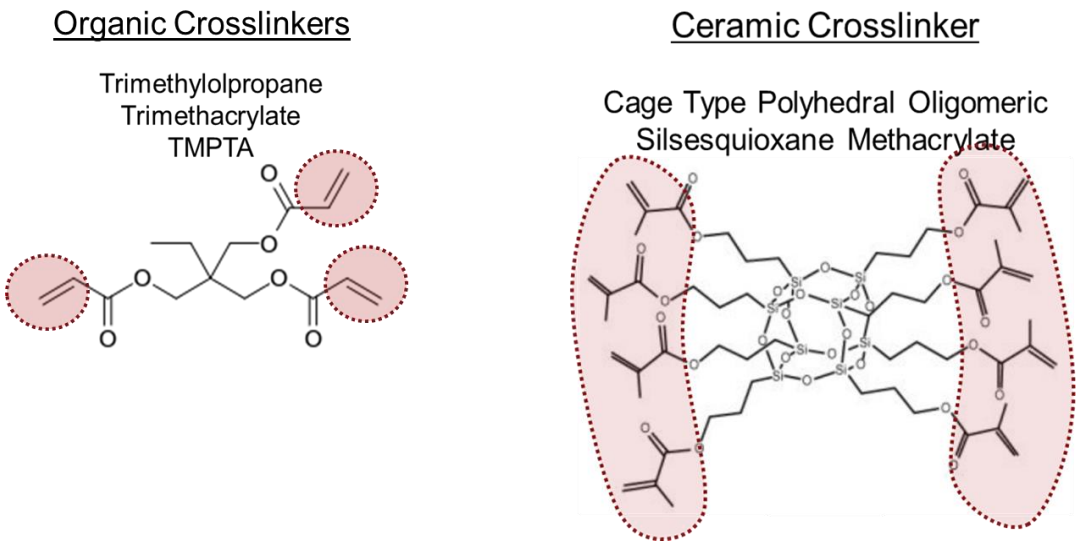

Figure 1.12: The organic and orano-ceramic crosslinkers used in this study.

The Joo Research Group primarily works on 2 crosslinkers. The organic Trimethylolpropane triacrylate (TMPTA or TPTA) crosslinker which is a trifunctional acrylate ester and the polymer-ceramic hybrid crosslinker – Cage Type Polyhedral

Oligomeric Silsesquioxane methacrylate (POSS-MA or POSS) as seen in fig. 1.12. The oxygen-rich functional group in TPTA and the charged silica cage in POSS-MA help in mitigating polysulfide shuttling and also help improve Li ion transport in the cell.

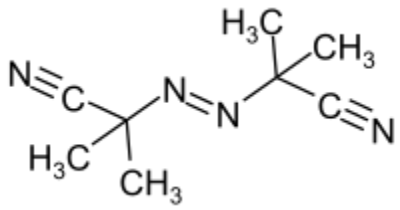

Figure 1.13: Azobisisobutyronitrile Initiator

To initiate the gelling process, an initiator is added to the solution of the liquid electrolyte and the polymeric monomers. The initiator used throughout this work is Azobisisobutyronitrile (AIBN) which is an organic compound that is commonly used as a radical initiator.

The next chapter includes a comprehensive analysis of the gel electrolyte with the traditional liquid electrolyte. Further, a novel improvement in the gel electrolyte is suggested and the resulting enhancement in performance has been reported.

1.5 References

Amine, K., Kanno, R., & Tzeng, Y. (2014). Rechargeable lithium batteries and beyond: Progress, challenges, and future directions. *MRS Bulletin*, *39*(5), 395–401. https://doi.org/10.1557/mrs.2014.62

Angulakshmi, N., & Stephan, A. M. (2015). Efficient electrolytes for lithium-sulfur batteries. In *Frontiers in Energy Research* (Vol. 3, Issue MAY, p. 17). Frontiers Media S.A. https://doi.org/10.3389/fenrg.2015.00017

Arora, P., & Zhang, Z. (2004). *Battery Separators*. https://doi.org/10.1021/cr020738u

Barchasz, C., Leprêtre, J. C., Alloin, F., & Patoux, S. (2012). New insights into the limiting parameters of the Li/S rechargeable cell. *Journal of Power Sources*, *199*, 322–330. https://doi.org/10.1016/j.jpowsour.2011.07.021

Birk, J. R., & Steunenberg, R. K. (1974). CHEMICAL INVESTIGATIONS OF LITHIUM-SULFUR CELLS. *Adv Chem Ser*, *140*, 186–202. https://doi.org/10.1021/ba-1975-0140.ch012

Bruce, P. G., Freunberger, S. A., Hardwick, L. J., & Tarascon, J. M. (2012). LigO2 and LigS batteries with high energy storage. In *Nature Materials* (Vol. 11, Issue 1, pp. 19–29). Nature Publishing Group. https://doi.org/10.1038/nmat3191

Cao, R., Xu, W., Lv, D., Xiao, J., & Zhang, J. G. (2015). Anodes for Rechargeable Lithium-Sulfur Batteries. In *Advanced Energy Materials* (Vol. 5, Issue 16, p. 1402273). Wiley-VCH Verlag. https://doi.org/10.1002/aenm.201402273

Carlin, J. M., Joo, Y. L., & Smith, S. (2018). *Hybrid separators and the manufacture thereof*.

Chen, R., Zhao, T., & Wu, F. (2015). From a historic review to horizons beyond: Lithium-sulphur batteries run on the wheels. In *Chemical Communications*

(Vol. 51, Issue 1, pp. 18–33). Royal Society of Chemistry. https://doi.org/10.1039/c4cc05109b

Cheng, X., Pan, J., Zhao, Y., Liao, M., & Peng, H. (2018). Gel Polymer Electrolytes for Electrochemical Energy Storage. In *Advanced Energy Materials* (Vol. 8, Issue 7). Wiley-VCH Verlag. https://doi.org/10.1002/aenm.201702184

Colthorpe, A. (2020, July 7). *Solar farm fitted with batteries to meet grid output control requirements goes online in Japan | Energy Storage News*. https://www.energy-storage.news/news/solar-farm-fitted-with-batteries-to-meet-grid-output-control-requirements-g

Colthorpe, A. (2021, March 23). *Wisconsin utilities plan 250MW solar project with 75MW of battery storage | Energy Storage News*. https://www.energy-storage.news/news/wisconsin-utilities-plan-250mw-solar-project-with-75mw-of-battery-storage

COMSOL AB. (n.d.). *COMSOL Multiphysics® v. 5.5*. Retrieved July 27, 2020, from www.comsol.com

Croce, F., Appetecchi, G. B., Persi, L., & Scrosati, B. (1998). Nanocomposite polymer electrolytes for lithium batteries. *Nature 1998 394:6692*, *394*(6692), 456–458. https://doi.org/10.1038/28818

Ding, F., Xu, W., Graff, G. L., Zhang, J., Sushko, M. L., Chen, X., Shao, Y., Engelhard, M. H., Nie, Z., Xiao, J., Liu, X., Sushko, P. v., Liu, J., & Zhang, J. G. (2013). Dendrite-free lithium deposition via self-healing electrostatic shield mechanism. *Journal of the American Chemical Society*, *135*(11), 4450–4456. https://doi.org/10.1021/ja312241y

Ding, L., Xu, G., Ge, Q., Wu, T., Yang, F., & Xiang, M. (2017). Effect of Fumed SiO 2 on Pore Formation Mechanism and Various Performances of β - i PP Microporous Membrane Used for Lithium-ion Battery Separator. *Chinese*

Journal of Polymer Science 2017 36:4, *36*(4), 536–545. https://doi.org/10.1007/S10118-018-2029-7

Ding, N., Zhou, L., Zhou, C., Geng, D., Yang, J., Chien, S. W., Liu, Z., Ng, M. F., Yu, A., Hor, T. S. A., Sullivan, M. B., & Zong, Y. (2016a). Building better lithium-sulfur batteries: From LiNO2 to solid oxide catalyst. *Scientific Reports*, *6*(1), 1–10. https://doi.org/10.1038/srep33154

Ding, N., Zhou, L., Zhou, C., Geng, D., Yang, J., Chien, S. W., Liu, Z., Ng, M.-F., Yu, A., Hor, T. S. A., Sullivan, M. B., & Zong, Y. (2016b). Building better lithium-sulfur batteries: from LiNO 3 to solid oxide catalyst. *Scientific Reports 2016 6:1*, *6*(1), 1–10. https://doi.org/10.1038/srep33154

Ding, Y., Hou, H., Zhao, Y., Zhu, Z., & Fong, H. (2016). Electrospun polyimide nanofibers and their applications. *Progress in Polymer Science*, *61*, 67–103. https://doi.org/10.1016/J.PROGPOLYMSCI.2016.06.006

Dunn, B., Kamath, H., & Tarascon, J. M. (2011). Electrical energy storage for the grid: A battery of choices. In *Science* (Vol. 334, Issue 6058, pp. 928–935). American Association for the Advancement of Science. https://doi.org/10.1126/science.1212741

Feng, X., Ouyang, M., Liu, X., Lu, L., Xia, Y., & He, X. (2018). Thermal runaway mechanism of lithium ion battery for electric vehicles: A review. *Energy Storage Materials*, *10*, 246–267. https://doi.org/10.1016/J.ENSM.2017.05.013

Girishkumar, G., McCloskey, B., Luntz, A. C., Swanson, S., & Wilcke, W. (2010). Lithium-air battery: Promise and challenges. *Journal of Physical Chemistry Letters*, *1*(14), 2193–2203. https://doi.org/10.1021/jz1005384

Halim, W., Lee, J. H., Park, S. M., Zhang, R., Sarkar, S., O'Neil, T., Chiang, Y. C., & Joo, Y. L. (2019). Directly deposited binder-free sulfur electrode enabled by air-controlled electrospray process. *ACS Applied Energy Materials*, *2*(1), 678–686. https://doi.org/10.1021/acsaem.8b01694

Hasanuzzaman, M., Zubir, U. S., Ilham, N. I., & Seng Che, H. (2017). Global electricity demand, generation, grid system, and renewable energy polices: a review. *WIREs Energy and Environment*, *6*(3), e222. https://doi.org/https://doi.org/10.1002/wene.222

Herbert, D., & Ulam, J. (1958). *United States Patent Office l 3,043,896 ELECTRIC DRY CELLS AND STORAGE BATTERES*.

Höök, M., & Tang, X. (2013). Depletion of fossil fuels and anthropogenic climate change-A review. *Energy Policy*, *52*, 797–809. https://doi.org/10.1016/j.enpol.2012.10.046

Javed, K., Krumme, A., Viirsalu, M., Krasnou, I., Plamus, T., Vassiljeva, V., Tarasova, E., Savest, N., Mere, A., Mikli, V., Danilson, M., Kaljuvee, T., Lange, S., Yuan, Q., Topham, P. D., & Chen, C. M. (2018). A method for producing conductive graphene biopolymer nanofibrous fabrics by exploitation of an ionic liquid dispersant in electrospinning. *Carbon*, *140*, 148–156. https://doi.org/10.1016/J.CARBON.2018.08.034

Jeddi, K., Sarikhani, K., Qazvini, N. T., & Chen, P. (2014). Stabilizing lithium/sulfur batteries by a composite polymer electrolyte containing mesoporous silica particles. *Journal of Power Sources*, *245*, 656–662. https://doi.org/10.1016/j.jpowsour.2013.06.147

Jeon, H., Yeon, D., Lee, T., Park, J., Ryou, M. H., & Lee, Y. M. (2016). A water-based Al2O3 ceramic coating for polyethylene-based microporous separators for lithium-ion batteries. *Journal of Power Sources*, *315*, 161–168. https://doi.org/10.1016/J.JPOWSOUR.2016.03.037

Ji, X., Lee, K. T., & Nazar, L. F. (2009). A highly ordered nanostructured carbon-sulphur cathode for lithium-sulphur batteries. *Nature Materials*, *8*(6), 500–506. https://doi.org/10.1038/nmat2460

Ji, X., & Nazar, L. F. (2010). Advances in Li-S batteries. *Journal of Materials Chemistry*, *20*(44), 9821–9826. https://doi.org/10.1039/b925751a

Kamyshny Alexey, Gun, J., Rizkov, D., Voitsekovski, T., & Lev, O. (2007). Equilibrium Distribution of Polysulfide Ions in Aqueous Solutions at Different Temperatures by Rapid Single Phase Derivatization. *Environmental Science & Technology*, *41*(7), 2395–2400. https://doi.org/10.1021/es062637+

Killis, A., le Nest, J. F., Gandini, A., Cheradame, H., & Cohen-Addad, J. P. (1984). Correlation among transport properties in ionically conducting cross-linked networks. *Solid State Ionics*, *14*(3), 231–237. https://doi.org/10.1016/0167-2738(84)90104-8

Kozen, A. C., Lin, C. F., Pearse, A. J., Schroeder, M. A., Han, X., Hu, L., Lee, S. B., Rubloff, G. W., & Noked, M. (2015). Next-Generation Lithium Metal Anode Engineering via Atomic Layer Deposition. *ACS Nano*, *9*(6), 5884–5892. https://doi.org/10.1021/acsnano.5b02166

Lee, D. J., Lee, H., Kim, Y. J., Park, J. K., & Kim, H. T. (2016). Sustainable Redox Mediation for Lithium-Oxygen Batteries by a Composite Protective Layer on the Lithium-Metal Anode. *Advanced Materials*, *28*(5), 857–863. https://doi.org/10.1002/adma.201503169

Lei, T., Chen, W., Lv, W., Huang, J., Zhu, J., Chu, J., Yan, C., Wu, C., Yan, Y., He, W., Xiong, J., Li, Y., Yan, C., Goodenough, J. B., & Duan, X. (2018). Inhibiting Polysulfide Shuttling with a Graphene Composite Separator for Highly Robust Lithium-Sulfur Batteries. *Joule*, *2*(10), 2091–2104. https://doi.org/10.1016/j.joule.2018.07.022

Li, N. W., Yin, Y. X., Yang, C. P., & Guo, Y. G. (2016). An Artificial Solid Electrolyte Interphase Layer for Stable Lithium Metal Anodes. *Advanced Materials*, *28*(9), 1853–1858. https://doi.org/10.1002/adma.201504526

Li, T., Bai, X., Gulzar, U., Bai, Y. J., Capiglia, C., Deng, W., Zhou, X., Liu, Z., Feng, Z., & Proietti Zaccaria, R. (2019). A Comprehensive Understanding of Lithium–Sulfur Battery Technology. In *Advanced Functional Materials* (Vol. 29, Issue 32). Wiley-VCH Verlag. https://doi.org/10.1002/adfm.201901730

Liu, K., Zhuo, D., Lee, H. W., Liu, W., Lin, D., Lu, Y., & Cui, Y. (2017). Extending the Life of Lithium-Based Rechargeable Batteries by Reaction of Lithium Dendrites with a Novel Silica Nanoparticle Sandwiched Separator. *Advanced Materials*, *29*(4). https://doi.org/10.1002/adma.201603987

Liu, Y., Lin, D., Liang, Z., Zhao, J., Yan, K., & Cui, Y. (2016). Lithium-coated polymeric matrix as a minimum volume-change and dendrite-free lithium metal anode. *Nature Communications*, *7*(1), 1–9. https://doi.org/10.1038/ncomms10992

Love, C. T. (2011). Thermomechanical analysis and durability of commercial micro-porous polymer Li-ion battery separators. *Journal of Power Sources*, *196*(5), 2905–2912. https://doi.org/10.1016/J.JPOWSOUR.2010.10.083

Lu, Y., Das, S. K., Moganty, S. S., & Archer, L. A. (2012). Ionic liquid-nanoparticle hybrid electrolytes and their application in secondary lithium-metal batteries. *Advanced Materials*, *24*(32), 4430–4435. https://doi.org/10.1002/adma.201201953

Lu, Y., Tikekar, M., Mohanty, R., Hendrickson, K., Ma, L., & Archer, L. A. (2015). Stable cycling of lithium metal batteries using high transference number electrolytes. *Advanced Energy Materials*, *5*(9). https://doi.org/10.1002/aenm.201402073

Lu, Y., Tu, Z., & Archer, L. A. (2014). Stable lithium electrodeposition in liquid and nanoporous solid electrolytes. *Nature Materials*, *13*(10), 961–969. https://doi.org/10.1038/nmat4041

Lu, Z., Sui, F., Miao, Y. E., Liu, G., Li, C., Dong, W., Cui, J., Liu, T., Wu, J., & Yang, C. (2021). Polyimide separators for rechargeable batteries. *Journal of Energy Chemistry*, *58*, 170–197. https://doi.org/10.1016/J.JECHEM.2020.09.043

Luo, W., Zhou, L., Fu, K., Yang, Z., Wan, J., Manno, M., Yao, Y., Zhu, H., Yang, B., & Hu, L. (2015). A Thermally Conductive Separator for Stable Li Metal

Anodes. *Nano Letters*, *15*(9), 6149–6154. https://doi.org/10.1021/acs.nanolett.5b02432

Marceaux, S., Bressy, C., Perrin, F. X., Martin, C., & Margaillan, A. (2014). Development of polyorganosilazane–silicone marine coatings. *Progress in Organic Coatings*, *77*(11), 1919–1928. https://doi.org/10.1016/J.PORGCOAT.2014.06.020

McBrayer, J. D., Beechem, T. E., Perdue, B. R., Apblett, C. A., & Garzon, F. H. (2018). Polysulfide Speciation in the Bulk Electrolyte of a Lithium Sulfur Battery. *Journal of The Electrochemical Society*, *165*(5), A876–A881. https://doi.org/10.1149/2.0441805jes

Mikhaylik, Y. v., & Akridge, J. R. (2004). Polysulfide Shuttle Study in the Li/S Battery System. *Journal of The Electrochemical Society*, *151*(11), A1969. https://doi.org/10.1149/1.1806394

Munsell, M. (2018, March 6). *US Energy Storage Market Tops the 1 GWh Milestone in 2017 | Greentech Media*. GTM Research Article: A Wood Mackenzie Business. https://www.greentechmedia.com/articles/read/us-energy-storage-market-tops-the-gwh-milestone-in-2017

Murata, K., Izuchi, S., & Yoshihisa, Y. (2000a). An overview of the research and development of solid polymer electrolyte batteries. *Electrochimica Acta*, *45*(8–9), 1501–1508. https://doi.org/10.1016/S0013-4686(99)00365-5

Murata, K., Izuchi, S., & Yoshihisa, Y. (2000b). Overview of the research and development of solid polymer electrolyte batteries. *Electrochimica Acta*, *45*(8), 1501–1508. https://doi.org/10.1016/S0013-4686(99)00365-5

Nunes-Pereira, J., Costa, C. M., & Lanceros-Méndez, S. (2015). Polymer composites and blends for battery separators: State of the art, challenges and future trends. *Journal of Power Sources*, *281*, 378–398. https://doi.org/10.1016/J.JPOWSOUR.2015.02.010

Park, J., Jeong, J., Lee, Y., Oh, M., Ryou, M. H., & Lee, Y. M. (2016). Micro-Patterned Lithium Metal Anodes with Suppressed Dendrite Formation for Post Lithium-Ion Batteries. *Advanced Materials Interfaces*, *3*(11). https://doi.org/10.1002/admi.201600140

Peled, E., Shekhtman, I., Mukra, T., Goor, M., Belenkaya, I., & Golodnitsky, D. (2018). Improving the Durability and Minimizing the Polysulfide Shuttle in the Li/S Battery. *Journal of The Electrochemical Society*, *165*(1), A6051–A6057. https://doi.org/10.1149/2.0101801jes

Pfleging, W. (2018). A review of laser electrode processing for development and manufacturing of lithium-ion batteries. *Nanophotonics*, *7*(3), 549–573. https://doi.org/10.1515/NANOPH-2017-0044

Qie, L., & Manthiram, A. (2016). High-Energy-Density Lithium-Sulfur Batteries Based on Blade-Cast Pure Sulfur Electrodes. *ACS Energy Letters*, *1*(1), 46–51. https://doi.org/10.1021/acsenergylett.6b00033

Rana, M., Ahad, S. A., Li, M., Luo, B., Wang, L., Gentle, I., & Knibbe, R. (2019). Review on areal capacities and long-term cycling performances of lithium sulfur battery at high sulfur loading. In *Energy Storage Materials* (Vol. 18, pp. 289–310). Elsevier B.V. https://doi.org/10.1016/j.ensm.2018.12.024

Rand, D. A. J. (2011). A journey on the electrochemical road to sustainability. *Journal of Solid State Electrochemistry*, *15*(7), 1579–1622. https://doi.org/10.1007/s10008-011-1410-z

Reddy, M. v., Mauger, A., Julien, C. M., Paolella, A., & Zaghib, K. (2020). Brief history of early lithium-battery development. *Materials*, *13*(8). https://doi.org/10.3390/MA13081884

Ryou, M. H., Lee, D. J., Lee, J. N., Lee, Y. M., Park, J. K., & Choi, J. W. (2012). Excellent cycle life of lithium-metal anodes in lithium-ion batteries with mussel-inspired polydopamine-coated separators. *Advanced Energy Materials*, *2*(6), 645–650. https://doi.org/10.1002/aenm.201100687

Ryou, M. H., Lee, Y. M., Lee, Y., Winter, M., & Bieker, P. (2015). Mechanical surface modification of lithium metal: Towards improved Li metal anode performance by directed Li plating. *Advanced Functional Materials*, *25*(6), 834–841. https://doi.org/10.1002/adfm.201402953

Salem, N., & Abu-Lebdeh, Y. (2012). *Effect of Nanoparticles on Electrolytes and Electrode/Electrolyte Interface*. 221–244. https://doi.org/10.1007/978-1-4614-4605-7_9

Seh, Z. W., Li, W., Cha, J. J., Zheng, G., Yang, Y., McDowell, M. T., Hsu, P. C., & Cui, Y. (2013). Sulphur-TiO 2 yolk-shell nanoarchitecture with internal void space for long-cycle lithium-sulphur batteries. *Nature Communications*, *4*. https://doi.org/10.1038/ncomms2327

Shebert, G. L., Zamani, S., Yi, C., & Joo, Y. L. (2020). Polysulfide entrapment and retardation in gel electrolyte Li–S batteries: experiments and modeling. *Journal of Materials Chemistry A*, *8*(8), 4341–4353. https://doi.org/10.1039/C9TA14234G

Thackeray, M. M., Wolverton, C., & Isaacs, E. D. (2012). Electrical energy storage for transportation - Approaching the limits of, and going beyond, lithium-ion batteries. In *Energy and Environmental Science* (Vol. 5, Issue 7, pp. 7854–7863). Royal Society of Chemistry. https://doi.org/10.1039/c2ee21892e

Vallée, A., Besner, S., & Prud'Homme, J. (1992). Comparative study of poly(ethylene oxide) electrolytes made with LiN(CF3SO2)2, LiCF3SO3 and LiClO4: Thermal properties and conductivity behaviour. *Electrochimica Acta*, *37*(9), 1579–1583. https://doi.org/10.1016/0013-4686(92)80115-3

Wang, D., Yu, J., Duan, G., Liu, K., & Hou, H. (2020). Electrospun polyimide nonwovens with enhanced mechanical and thermal properties by addition of trace plasticizer. *Journal of Materials Science 2020 55:13*, *55*(13), 5667–5679. https://doi.org/10.1007/S10853-020-04402-2

Wang, H. C., Cao, X., Liu, W., & Sun, X. (2019). Research Progress of the Solid State Lithium-Sulfur Batteries. In *Frontiers in Energy Research* (Vol. 7, p. 112). Frontiers Media S.A. https://doi.org/10.3389/fenrg.2019.00112

Wang, Q., Ping, P., Zhao, X., Chu, G., Sun, J., & Chen, C. (2012). Thermal runaway caused fire and explosion of lithium ion battery. *JPS*, *208*, 210–224. https://doi.org/10.1016/J.JPOWSOUR.2012.02.038

Wang, Q., Ping, P., Zhao, X., Chu, G., Sun, J., Chen, C., Wang, Q., Ping, P., Zhao, X., Chu, G., Sun, J., & Chen, C. (2012). Thermal runaway caused fire and explosion of lithium ion battery. *JPS*, *208*, 210–224. https://doi.org/10.1016/J.JPOWSOUR.2012.02.038

Whittingham, M. S. (2012). History, Evolution, and Future Status of Energy Storage. *Proceedings of the IEEE*, *100*(Special Centennial Issue), 1518–1534. https://doi.org/10.1109/JPROC.2012.2190170

Yamin, H., & Peled, E. (1983). Electrochemistry of a nonaqueous lithium/sulfur cell. *Journal of Power Sources*, *9*(3), 281–287. https://doi.org/10.1016/0378-7753(83)87029-3

Yan, K., Lu, Z., Lee, H. W., Xiong, F., Hsu, P. C., Li, Y., Zhao, J., Chu, S., & Cui, Y. (2016). Selective deposition and stable encapsulation of lithium through heterogeneous seeded growth. *Nature Energy*, *1*(3), 1–8. https://doi.org/10.1038/NENERGY.2016.10

Yang, C. P., Yin, Y. X., Zhang, S. F., Li, N. W., & Guo, Y. G. (2015). Accommodating lithium into 3D current collectors with a submicron skeleton towards long-life lithium metal anodes. *Nature Communications*, *6*(1), 1–9. https://doi.org/10.1038/ncomms9058

Yu, X., Wu, H., Koo, J. H., & Manthiram, A. (2020). Tailoring the Pore Size of a Polypropylene Separator with a Polymer Having Intrinsic Nanoporosity for Suppressing the Polysulfide Shuttle in Lithium–Sulfur Batteries. *Advanced*

Energy Materials, *10*(1), 1902872. https://doi.org/10.1002/AENM.201902872

Zhang, J., Yue, L., Kong, Q., Liu, Z., Zhou, X., Zhang, C., Xu, Q., Zhang, B., Ding, G., Qin, B., Duan, Y., Wang, Q., Yao, J., Cui, G., & Chen, L. (2014). Sustainable, heat-resistant and flame-retardant cellulose-based composite separator for high-performance lithium ion battery. *Scientific Reports 2014 4:1*, *4*(1), 1–8. https://doi.org/10.1038/srep03935

Zhang, R., Cheng, X. B., Zhao, C. Z., Peng, H. J., Shi, J. le, Huang, J. Q., Wang, J., Wei, F., & Zhang, Q. (2016). Conductive Nanostructured Scaffolds Render Low Local Current Density to Inhibit Lithium Dendrite Growth. *Advanced Materials*, *28*(11), 2155–2162. https://doi.org/10.1002/adma.201504117

Zhang, Sheng S. (2013). Liquid electrolyte lithium/sulfur battery: Fundamental chemistry, problems, and solutions. In *Journal of Power Sources* (Vol. 231, pp. 153–162). Elsevier. https://doi.org/10.1016/j.jpowsour.2012.12.102

Zhang, Sheng S., & Read, J. A. (2012). A new direction for the performance improvement of rechargeable lithium/sulfur batteries. *Journal of Power Sources*, *200*, 77–82. https://doi.org/10.1016/j.jpowsour.2011.10.076

Zhang, Sheng S., & Tran, D. T. (2013). How a gel polymer electrolyte affects performance of lithium/sulfur batteries. *Electrochimica Acta*, *114*, 296–302. https://doi.org/10.1016/j.electacta.2013.10.069

Zhang, Sheng Shui. (2007). A review on the separators of liquid electrolyte Li-ion batteries. *Journal of Power Sources*, *164*(1), 351–364. https://doi.org/10.1016/J.JPOWSOUR.2006.10.065

Zhao, M., Li, B.-Q., Zhang, X.-Q., Huang, J.-Q., & Zhang, Q. (2020). A Perspective toward Practical Lithium−Sulfur Batteries. *Cite This: ACS Cent. Sci*, *2020*, 1095–1104. https://doi.org/10.1021/acscentsci.0c00449

Zheng, C., Wang, K., Li, L., Huang, H., Liang, C., Gan, Y., He, X., Zhang, W., & Zhang, J. (2021). High-Performance All-Solid-State Lithium–Sulfur Batteries

Enabled by Slurry-Coated Li6PS5Cl/S/C Composite Electrodes. *Frontiers in Energy Research*, *8*, 416. https://doi.org/10.3389/FENRG.2020.606494

Zheng, G., Lee, S. W., Liang, Z., Lee, H. W., Yan, K., Yao, H., Wang, H., Li, W., Chu, S., & Cui, Y. (2014). Interconnected hollow carbon nanospheres for stable lithium metal anodes. *Nature Nanotechnology*, *9*(8), 618–623. https://doi.org/10.1038/nnano.2014.152

Zhong, W. (2016). Nanofibres for medical textiles. *Advances in Smart Medical Textiles: Treatments and Health Monitoring*, 57–70. https://doi.org/10.1016/B978-1-78242-379-9.00003-7

Zhou, D., Liu, R., He, Y. B., Li, F., Liu, M., Li, B., Yang, Q. H., Cai, Q., & Kang, F. (2016). SiO2 Hollow Nanosphere-Based Composite Solid Electrolyte for Lithium Metal Batteries to Suppress Lithium Dendrite Growth and Enhance Cycle Life. *Advanced Energy Materials*, *6*(7). https://doi.org/10.1002/aenm.201502214

Zou, P., Wang, Y., Chiang, S. W., Wang, X., Kang, F., & Yang, C. (2018). Directing lateral growth of lithium dendrites in micro-compartmented anode arrays for safe lithium metal batteries. *Nature Communications*, *9*(1), 1–9. https://doi.org/10.1038/s41467-018-02888-8

CHAPTER 2

OPTIMIZING GEL ELECTROLYTE SYSTEMS FOR ENHANCED CELL PERFORMANCE

2.1 Abstract

Though Li-S batteries have shown great potential in achieving the goal of secondary battery capacities of over 500 $Whkg^{-1}$(Barchasz et al., 2012; Bruce et al., 2012; K. Liu et al., 2017), issues such as polysulfide shuttling; formation of a nonconducting passive layer on the electrodes, lithium dendritic formation, and large cathodic volume changes impede the practical utility of this technology in commercial application(Amine et al., 2014; Chen et al., 2015; H. C. Wang et al., 2019). Several attempts have been made by researchers to tackle these issues in the form of cathodic, anodic surface design optimization, improved separator material, using additives in electrolyte etc.

In this chapter, a novel solution in the form a facile, in-situ fabricated crosslinked Gel Electrolyte (GE) system has been proposed to tackle all the above issues. First, we present a comprehensive comparative analysis of the performance of GE cells with traditional liquid electrolyte (LE). The performance of GE cells was further enhanced using Polyethylene Glycol (PEG) as an additive. It was observed that the GE cells had substantially lower capacity fade and performed better than LE cells at high-rate cycling.

Graphical Abstract

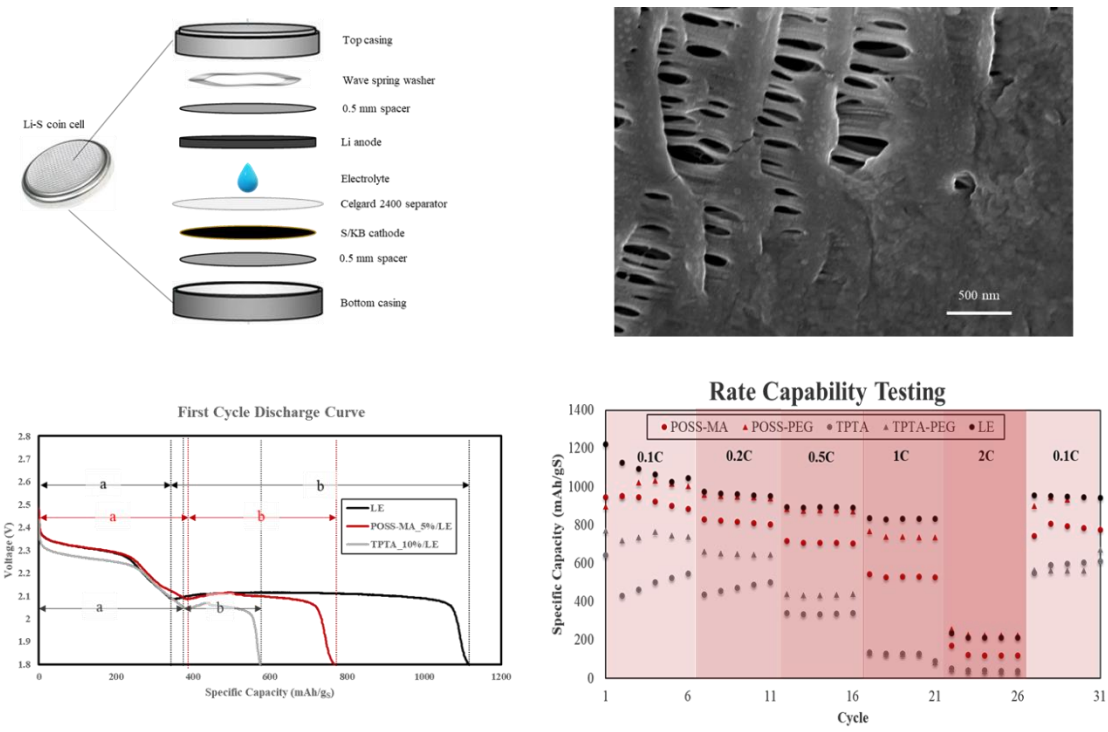

Figure 2.1: Graphical Abstract: Chapter 2

2.2 Experimental Methods

2.2.1 Synthesis of Sulfur-Ketjen Black Cathode Systems

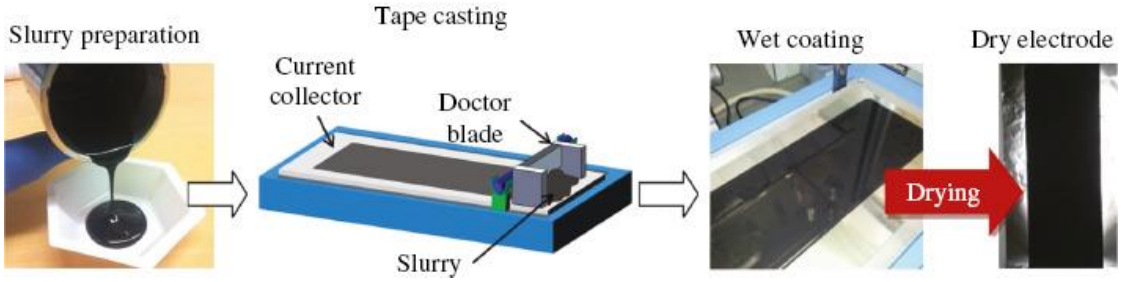

Figure 2.2: Process for tape casting (or slurry casting) S/KB electrodes using doctor-blade technique (Pfleging, 2018).

Sulfur powder (S, 1.5 g) was ground with Ketjen Black EC600JD (KB, 0.5 g, AkzoNobel) to obtain a 75:25 S:KB mixture. Then, the mixture was heat treated at 155 ^{0}C for at least 12 hours to ensure sulfur impregnation into the porous KB particles (Halim et al., 2019). The active material S/KB was then thoroughly mixed for 3 hours with Super C65 (MTI Corp.) and the binder polyvinylidene fluoride (PVDF, Aldrich) in N-methyl-2-pyrrolidone (NMP, BDH), in a weight ratio of 70 : 20 : 10 in a ball mill till honey-like consistency is achieved.

Figure 2.3: (a) Wet S/KB electrode slurry casted on Al foil. (b) Punched S/KB cathode disc for cell assembly

It was ensured that each milling session does not last over 10 mins for vibrations of over 20Hz to prevent overheating of the slurry. The slurry was then cast onto aluminum foil

using a doctor blade and the sheets were dried in a fume hood at room temperature overnight followed by heat treatment in a 55^0C oven as seen in figure 2.2. The total thickness of aluminum + cathode was 54 microns, and sulfur areal loading was around 1 mg/cm^2 for all cells.

2.2.2 Electrolyte Fabrication

For the liquid electrolyte cells prepared, the electrolyte used was 1 M LiTFSI (99.95% trace metal basis, Sigma-Aldrich) and 0.1 M $LiNO_3$ (99.99% trace metals basis, Sigma – Aldrich) in a 1:1 volumetric ratio of 1,3 dioxolane (DOL) (≥ 99.5% purity, MilliporeSigma) and 1,2 dimethoxyethane (DME) (anhydrous, 99.5%, inhibitor-free, Sigma-Aldrich).

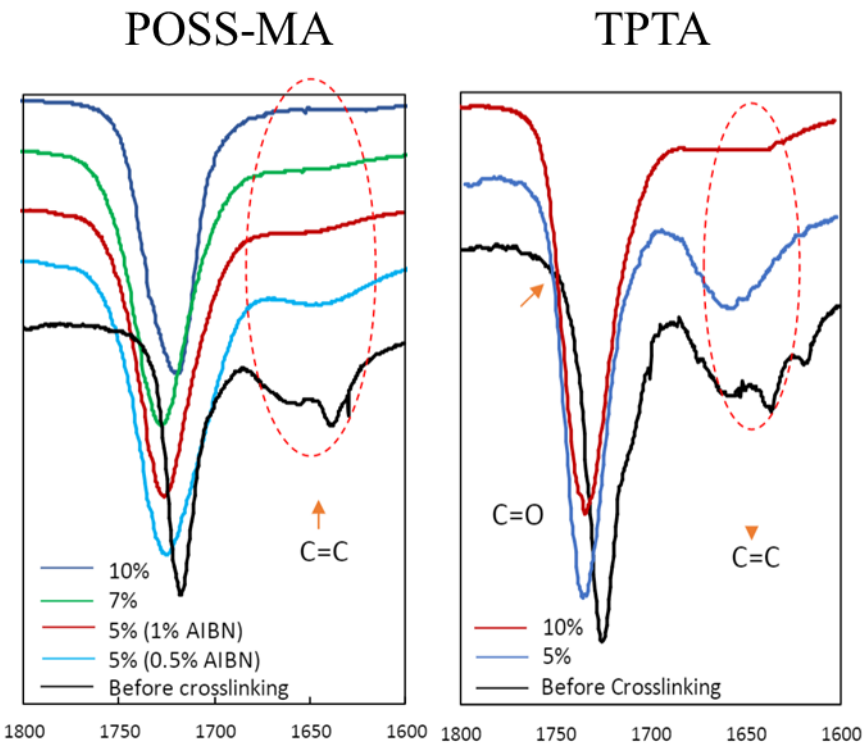

Figure 2.4: FTIR analysis of crosslinked gels at various crosslinker composition to achieve optimum crosslinking density.

For the gelled electrolyte cells prepared, the base liquid electrolyte solvent used was 1 M LiTFSI (99.95% trace metal basis, Sigma-Aldrich) and 0.1 M $LiNO_3$ (99.99% trace metals basis, Sigma – Aldrich) in a 1:1 volumetric ratio of 1,3 dioxolane (DOL) (≥ 99.5% purity, MilliporeSigma) and 1,2 dimethoxyethane (DME) (anhydrous, 99.5%, inhibitor-free, Sigma-Aldrich). To this solution, 10 wt% trimethylolpropane trimethacrylate (TPTA) (Technical grade, Sigma-Aldrich) was added as a crosslinker along with 1wt% azobisisobutyronitrile (AIBN) (98%, Sigma-Aldrich) as a free radical initiator to initiate the crosslinking process, to prepare TPTA gelled electrolyte cells. To make POSS gelled electrolyte cells, the base solution was mixed with 5 wt% polyhedral oligomeric silsesquioxane methacrylate (POSS-MA, ceramic-based) (99.99% pure, Sigma-Aldrich), a cage-like crosslinker, and 0.5 wt% AIBN were used instead. FTIR analysis was done to optimize the crosslinking density and it is observed that at 10% and 5% concentration of TPTA and POSS-MA respectively, the peak due to the C=C bond vanishes suggesting complete crosslinking. For those POSS-MA/PEG/LE and TPTA/PEG/LE electrolyte an additional 1% wt of Poly(ethylene glycol) (PEG, avg. M_n:1,500, High-purity, Sigma-Aldrich) is added to the electrolyte solution.

The electrolyte added to the cells was weighted on sulfur basis, and the general electrolyte-to-sulfur ratio was maintained at 30 μL per mg of sulfur (unless mentioned otherwise). The fabrication process for all the electrolyte was essentially the same, however, for the gel electrolyte cells, a 30 min heat treatment at 70^{o}C to the prepared cells was carried out after resting the cells for 3 hours to gel the electrolyte *in situ.* The entire electrolyte preparation process was conducted in an Argon environment glovebox with oxygen levels of lower than 0.1 ppm.

2.2.3 Coin Cell Assembly

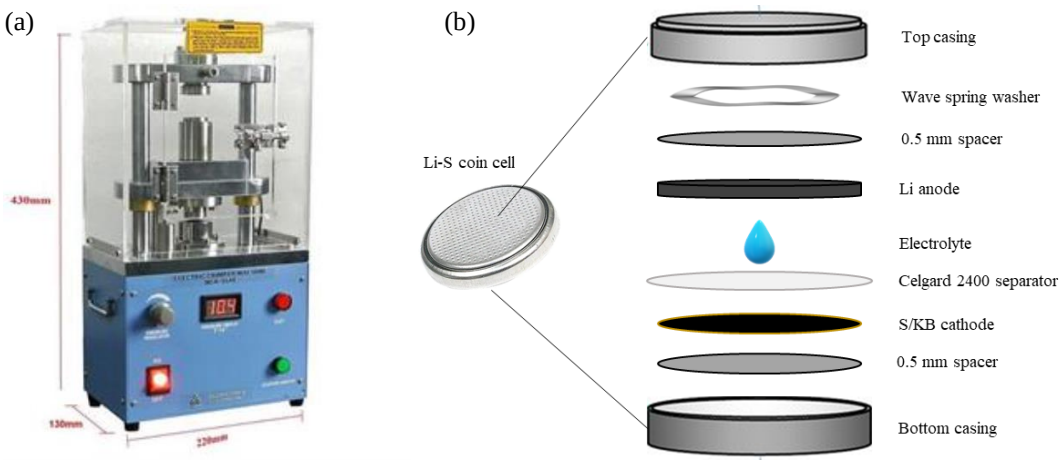

Figure 2.5: (a) MTI Automatic Digital Crimper. (b) Coin cell assembly components.

The 2032 CR coin cells were constructed in an oxygen-free, argon environment glovebox. The construction for these cells was done using the following components in order: (1) 2032 CR coin cell bottom; (2) 0.5 mm thick stainless steel spacer (16 mm diameter); (3) Punched S/KB Cathode discs with Al current collector (16 mm); (4) Celgard 2400 separator (19 mm diameter); (5) Electrolyte added at ratio of 30 μL per mg of sulfur (unless mentioned otherwise); (6) Punched Li anode discs (0.75 mm thick, 16 mm diameter); (7) 0.5 mm thick stainless steel spacer (16 mm diameter); (8) Wave spring washer. Once the assembly was finished, the coin cells were, first, hand crimped using a manual hand crimper in the Ar environment glovebox. Then, later, the cells were re-crimped using MTI digital pressure controlled electric crimper at 0.8 T pressure which seals the coin cell.

2.2.4 Electrochemical Measurements

The galvanostatic charge-discharge measurements were performed using MTI Corporation Battery Analyzer at room temperature using BTSDA (Battery Testing System Data Analyzer) software for cycling and rate capability tests. Each test began with resting the cells for 6 hours and cycling for first 5 cycles at a formation rate of 0.1 C (1C = 1675 mAh/g_S) in the range of 1.8-2.8 V versus Li^+/Li.

For cycling tests, the cells were run for 5 cycles at 0.1 C rate and then the next 200 cycles at 0.2 C rate (or till end of cell life). Each charge and discharge step had an intermediate 5-minute resting step.

For rate capability tests, the cells were run for 5 cycles at 0.1 C rate (formation step) and then followed by 5 charge/discharge cycles at 0.2C, 0.5C, 1C, 2C and finally back to 0.1C. All discharge capacities and current densities were standardized based on active sulfur mass in the cathode. Current densities were set according to a sulfur theoretical specific capacity of 1675 mAh/g.

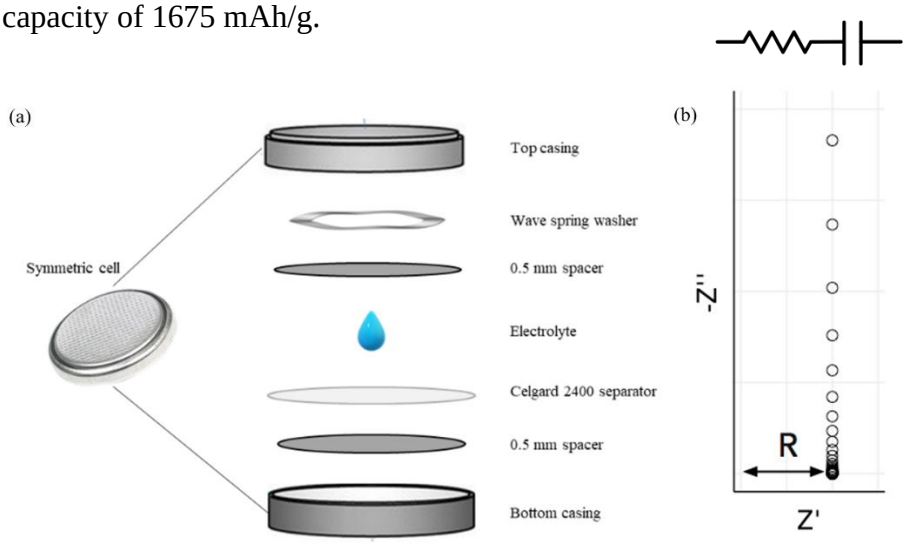

Figure 2.6: (a) Symmetric cell for EIS analysis. (b) Typical Nyquist plot for a R-C circuit. R: The ionic resistance of the electrolyte; C: The capacitance of double layer at the spacer/electrolyte interface

Ionic conductivity was measured using electrochemical impedance spectroscopy (EIS, Parstat 4000, Princeton Applied Materials).

For these tests, Celgard 2400 separators were soaked with 40 μL of electrolyte to mimic battery cell conditions and sandwiched between two stainless steel discs in a CR2032 coin cell. A frequency range from 100 kHz to 0.1 Hz was applied with an AC amplitude of 10 mV. Ionic conductivity was calculated according to the equation (C. Zheng et al., 2021):

$$\sigma = \frac{d}{R_b \times A}$$

Where d is the thickness of the separator, R_b is the bulk resistance, and A is the surface area of the stainless-steel electrode (1.96 cm^2). R_b is defined as the high frequency intercept of the real axis.

2.2.5 Other characterization techniques

Dimensional thermal stability of the gelled separator system was determined with a shrinkage test by placing them in a 150 °C oven for two hours under air with a 5 °C/min ramp rate. Flammability of the separator materials was tested by soaking each membrane in electrolyte and lighting the excess electrolyte with a butane torch.

Scanning Electron Microscopy (Zeiss Gemini 500) was carried at an accelerating voltage of 3keV.

2.3 Results and Discussion

2.3.1 Gel Electrolyte Performance with Conventional Celgard 2400 Separators.

Flammability Tests

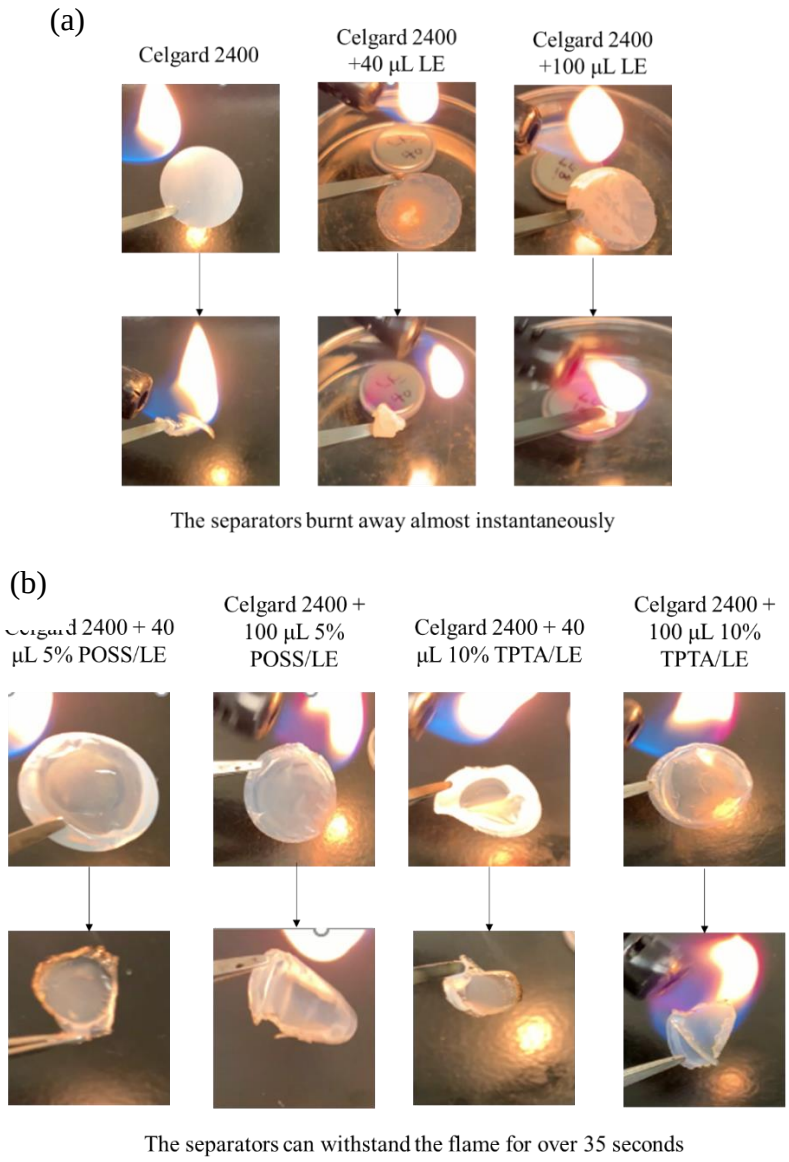

Figure 2.7: Results for flammability test for: (a) Celgard 2400 + liquid electrolyte; (b) Celgard 2400 + Gelled Liquid electrolyte

The flammability test results clearly show that the gelled electrolyte separators are much more flame resistant and can withstand direct contact with a naked flame for over 35

seconds. Even on long exposure to the flame, the gelled surface remains relatively unaffected with minimal charring at the edges.

This proves that the gel electrolyte significantly reduces flammability hazards in the Li-S battery, which is extremely important given, the battery electrolyte is predominantly a glyme-based organic solvent.

Ionic Conductivity

Table 2.1: Ionic Conductivity for symmetric cells with three sets of electrolytes

Electrolyte	**Conductivity (σ) mS/cm**
Liquid Electrolyte	0.709
POSS-MA 5%/LE	0.364
TPTA 10%/LE	0.138

*Values averaged for 3 sets of each cell type

The ionic conductivity was done by conducting an EIS analysis on symmetric cells with separators soaked the 3 types of electrolytes mentioned in Table 1. It was observed that ionic conductivity for the gelled liquid electrolyte was much lower than the liquid electrolyte system. This was expected as crosslinking immobilizes the electrolyte solvent molecules which in turn hinders lithium-ion migration. A similar observation is seen in solid electrolyte systems, however with solid electrolyte systems the ionic conductivity is usually in the range of 10^{-5} to 10^{-6} mS/cm (Murata et al., 2000b; H. C. Wang et al., 2019; C. Zheng et al., 2021). The gel electrolyte, meanwhile, showed an ionic conductivity of several orders greater.

The ionic conductivity of POSS-gelled LE is almost twice as much as TPTA-gelled LE, despite having significantly higher crosslinking density because of the silicon oxide (silica) cage-like structure in the molecule. It has been long established in Li-ion batteries and recently with Li-S batteries too, that ceramic additives help improve ionic conductivity by enhancing Li-ion transport pathways (N. Ding et al., 2016b).

With lower ionic conductivity than LE, it was expected that the discharge capacities for the gelled electrolytes would be lower than that of the cells containing only liquid electrolyte. This hypothesis was verified by data from the cyclability test in the next section (see fig 2.8).

Cyclability Test

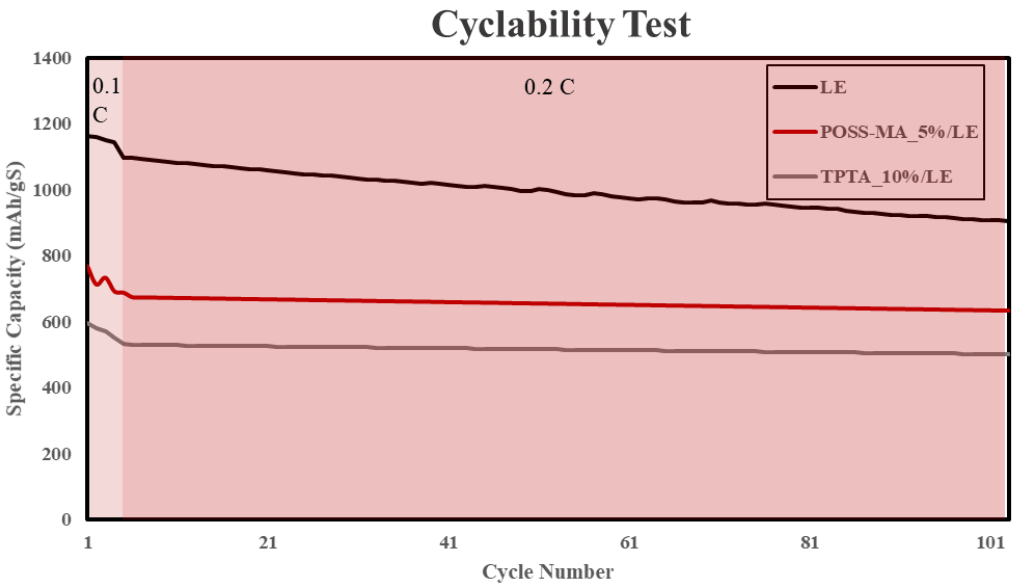

Figure 2.8: Cyclability Testing of 1mg/cm^2 loaded cells with various electrolytes

The cyclability test was carried out for the 3 electrolytes: (1) Liquid electrolyte, (2) Liquid electrolyte gelled by 5% wt POSS-MA, (3) Liquid electrolyte gelled by 10% wt

TPTA. In order to compare the cyclability performance, the S areal loading for each of the cells was maintained at ~1 mg/cm^2.

Fig 2.8 displays the cycling test results for the first 100 cycles run at 0.2 C charging/discharging rate (initial 5 formation cycles were run at 0.1 C rate). It was observed that the LE cells had the highest discharge capacity, followed by POSS-MA and then TPTA cells owing to the reduction in ionic conductivity as hypothesized in the previous section.

However, it was observed that the capacity retention of gelled electrolyte cells is better than liquid electrolyte cells. For POSS-MA cells, the capacity retention after 100 cycles was 82.3%; the capacity retention for TPTA cells was 84.1%; and the capacity retention for liquid electrolyte cells was 77.6%. This could be caused because the polysulfide diffusion rate through the gelled electrolyte separator is lower than when compared with just liquid electrolyte. This means that the polysulfide shuttling effect is less pronounced in the gelled electrolyte cells and hence the loss of active material is reduced leading to better retention of capacity over 100 cycles.

Cyclability tests help probe the overall performance and robustness of the cell. It gives an idea of how a cell is performing over continuous charge/discharge cycle. However, it gives very little additional information on characteristics of the cell performance. To do so, one must study the discharge curves, which has been done in the next section.

First Cycle Discharge Curve

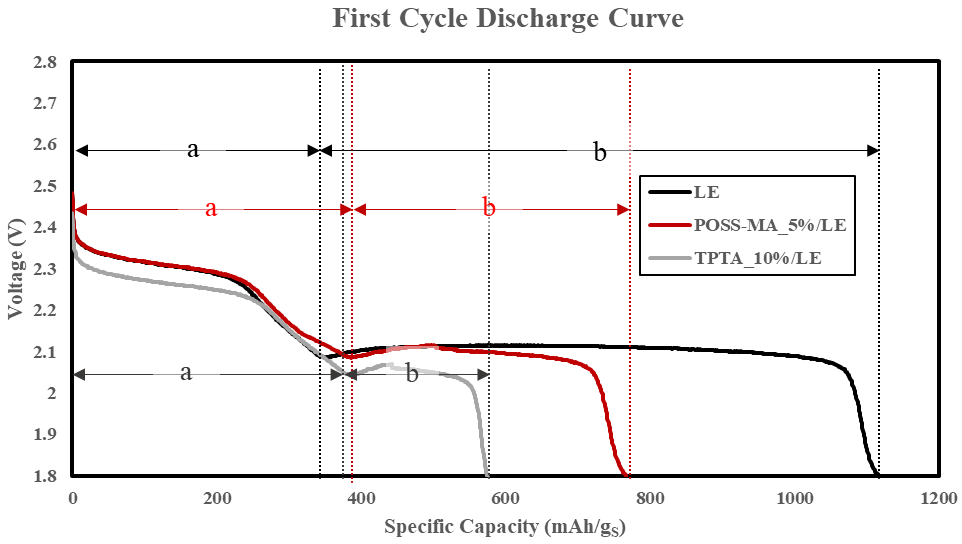

Figure 2.9: First Cycle Discharge Curve for LE, POSS/LE and TPTA/LE cells with voltage plateau comparison.

As explained in the Cell Chemistry section (see fig. 1.4), the first, shorter plateau region in the discharge curve for Li-S is associated with the formation of soluble long chain lithium polysulfides and the second, longer plateau is associated with the insoluble Li_2S layer formation on the electrode which is known to have slow kinetics. Figure 2.9 displays the first cycle discharge profiles of the 3 cells containing the 3 different electrolyte systems.

In congruence with the capacity observations in fig 2.8, here too liquid electrolyte cells showed a much higher capacity than both POSS/LE cells and the least capacity was displayed by the TPTA/LE cells. However, if one were to study the first plateau profile in detail, they would observe that the first plateau capacity for liquid electrolyte cells was the least, followed by gelled TPTA/LE cells and gelled POSS/LE cells had the highest capacity. This further points toward the conclusion that gel electrolytes are better able to trap the lithium polysulfide intermediates and hence are better able to

suppress the polysulfide shuttling effect in the cell leading to maximum utilization of the active material.

The theoretical maximum first plateau capacity is quoted to be about 25% of the maximum theoretical gravimetric capacity of the battery i.e., 418 mAh/g_S (McBrayer et al., 2018; Sheng S. Zhang, 2013). The gelled electrolyte cells with an excellent first plateau capacity of 372 mAh/g_S and 386 mAh/g_S for TPTA/LE and POSS/LE electrolytes respectively come very close to the theoretical maximum. Hence, it can be concluded that the gelled electrolyte is successful in trapping the soluble polysulfide intermediates.

For the second plateau, however, the capacity is maximum for the liquid electrolyte cells, lower for POSS/LE cells and the lowest for TPTA/LE cells. This trend fits well with ionic conductivity of these cells and understandably so because the second plateau is associated with the kinetically rate limiting Li_2S formation step and low ionic conductivity means that the Li_2S formation rate is reduced, hence lower capacity is extracted from this stage.

It was evident that though the gel electrolyte had an excellent first plateau capacity, the overall capacity of the cell was greatly reduced because of significantly lower ionic conductivity. To improve the total gravimetric capacity of these cells, it was imperative to try to improve the ionic conductance of these electrolyte systems.

The solution to this problem came in the form of poly(ethylene glycol) (PEG) additive to the electrolyte. The next section reports the results obtained on using PEG as an additive in the gelled electrolyte mixture.

2.3.2 Performance Improvement Via Addition of PEG Plasticizer to Gel Precursors

There are two means to increase the ionic conductivity of the crosslinked gel: (I) suppression of crystallization of polymer chains (or reducing the extent of crosslinking) to improve polymer chain mobility; (II) increase in the carrier concentration.

The suppression of crystallization (cross-linking) of polymer chains to improve polymer chain mobility can be realized by (i) co-polymerization; (ii) comb formation (side chains and dendritic polymers); (iii) polymer alloy (including IPN: Inter Penetrating Network), and (iv) inorganic filler blend. Among these, combinations of (i) co-polymerization, and (ii) comb formation and (iii) polymer alloying are useful for obtaining a high ionic conductivity (Murata et al., 2000a) (C. Zheng et al., 2021) (Killis et al., 1984; Vallée et al., 1992).

Adding PEG into the POSS or TPTA precured mixture and then letting the solution cure forms an intricate interpenetrating polymer network that significantly enhances the ionic conductivity. Additionally, the electron-rich oxygen groups on the PEG chain increases the carrier concentration leading to a higher Li^+ transference

In the next section, the ionic conductivity change due to PEG addition into the precured gel electrolyte mixture has been reported.

Ionic Conductivity

Table 2.2: Ionic conductivity data for gelled electrolytes with PEG additive.

Electrolyte	**Conductivity (σ) mS/cm**
Liquid Electrolyte	0.709
POSS-MA 5%/LE	0.364
POSS-MA 5%/PEG/LE	0.425
TPTA 10%/LE	0.138
TPTA 10%/PEG/LE	0.075

*Values averaged for 5 sets of each cell type

From the ionic conductivity data in Table 2, it is evident that the PEG additive enhances the ionic conductivity of POSS/LE gelled electrolyte system. There was a 18% increase in conductivity seen for POSS/LE system. However, for the TPTA/LE system, the PEG addition led to a further decrease in the ionic conductivity to almost half the original value. This observation is rather interesting and indicates the inherent differences in hybrid polymer-ceramic in POSS-MA and simple organo-polymeric linkages in TPTA. This observation could also be because the PEG polymer molecule used has a relatively similar molecular mass and chain length (1,500 Da) as compared to the large, caged structure of the POSS-MA molecule and so it is easier to form interpenetrating networks and comb formations with it. However, the PEG molecule being much larger than the TPTA monomeric unit disrupts the cross-linkages and hence, is relatively less compatible with the TPTA system. This reasoning is merely a hypothesis and may require additional testing and research to confirm. Additional testing is expected to be

done in the future to confirm this hypothesis. The following section reports the results of the rate capability test done on the cells with different combinations of the electrolyte. The results further are fit soundly with the results of the ionic conductivity testing.

Rate Capability Testing

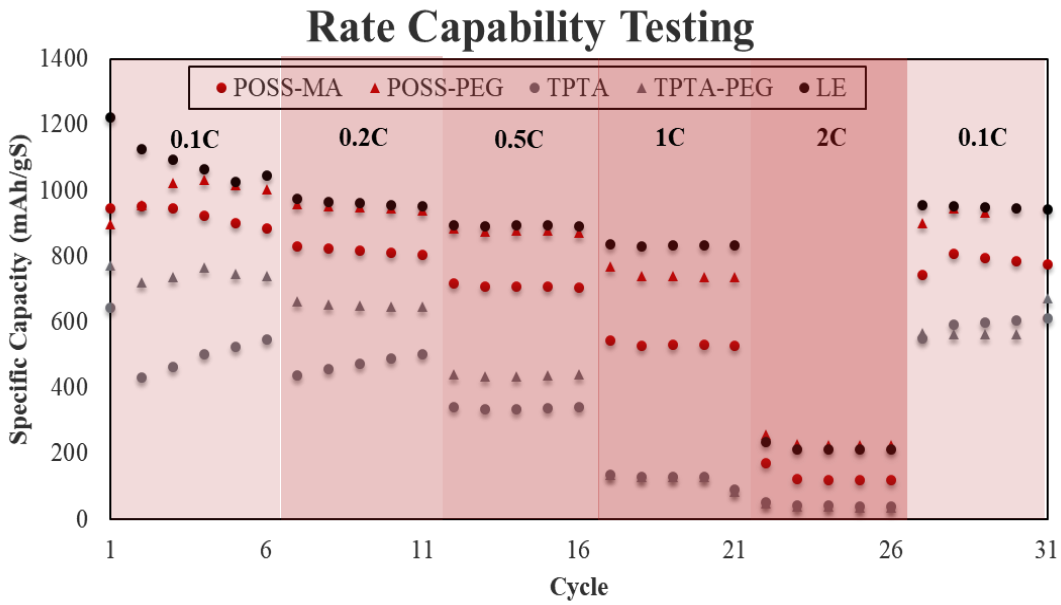

Figure 2.10: Rate Capability Testing for gelled and liquid electrolytes at 0.1 C, 0.2C, 0.5C, 1C, and 2C

Figure 2.10 shows the specific discharge capacities of cells with gelled and liquid electrolytes for 5 cycles at different charging/discharging rates. It was observed that POSS-PEG gelled cells had a higher capacity than all the other gelled electrolyte systems and the specific capacity was comparable to liquid electrolyte systems. This increase in capacity could be explained by the increase in the ionic conductivity on addition of PEG.

At high C rate charging/discharging, the polysulfide shuttling rate increases and that added on to the fact that due to the rate-limited electrochemical reaction there is

incomplete utilization of the active material, the discharge capacities for all the cells fades significantly at charge/discharges over 1C. The fade in capacity may be partially mitigated by improving the ionic conductivity as with better ionic conductivity, the strain on the kinetically rate controlled Li_2S step is reduced and so more capacity can be extracted from the cell.

This hypothesis was confirmed by the fact that the TPTA-PEG cells with lower ionic conductivity had significantly lower capacity (~50 mAh/g_S) than TPTA cells (~75 mAh/g_S) (not distinctly visible in the graph due to scaling) at 1C and 2 C cycling rates. POSS-PEG/LE cells having higher ionic conductivity (than POSS/LE) performed better than POSS/LE at high C cycling rates.

Another interesting observation seen in the rate capability testing is the fact that unlike liquid electrolyte cells, wherein the capacity fades over consecutive formation cycles, for the gelled electrolyte cells it was observed that the capacity slowly improves over the formation cycle. This may be hinting towards limited mass transport rate (or diffusion rate) in the gel matrix. Extensive pause recovery testing was done by (Shebert et al., 2020) to validate the hypothesis of polysulfide retardation in the gel matrix. The results of the diffusion experiment in Chapter 3 also confirmed this hypothesis.

2.3.3 Rest Time Analysis to Study the Wetting Characteristics of Gelled Electrolyte on the Slurry Casted S/KB Cathodes

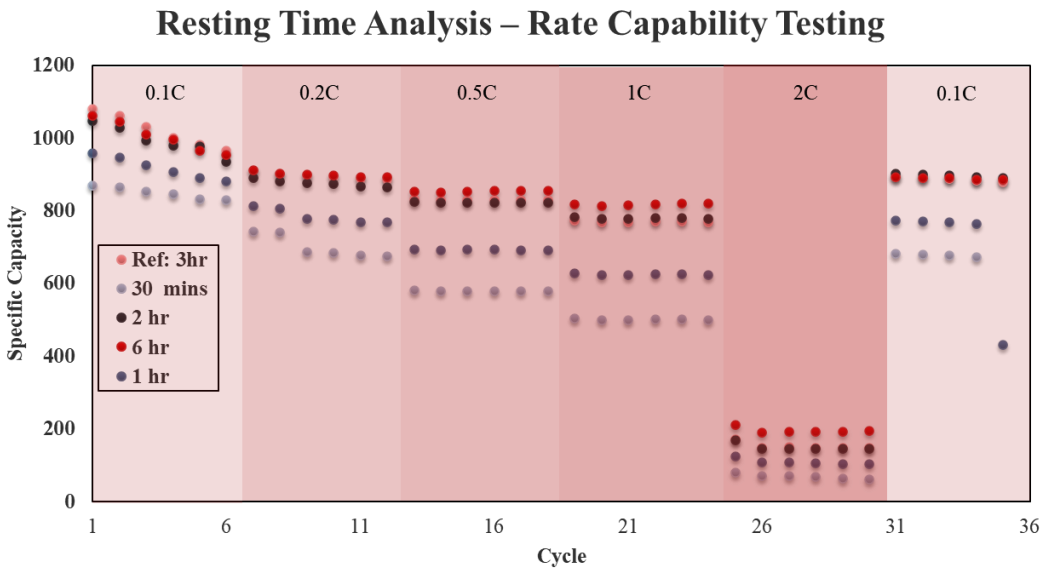

Figure 2.11: Resting Time Analysis for POSS/PEG/LE cells

An important characteristic that significantly influences the performance of any 'liquid' electrolyte cell system is the extent of cathode wetting. In Li-S cells especially this is of real importance, because the very first electrochemical reaction is the two-phase solid-liquid reduction of sulfur into lithium polysulfide intermediates that dissolve into the electrolyte solution. Any inadequate quenching/wetting of the cathode surface would lead to underutilization of the active material in the cathode and hence, affect the overall capacity and performance of the cell. It is for this reason, resting the cells after fabrication is essential to allow adequate time for the electrolyte to wet the entire surface of the cathode.

It is even more imperative that there is adequate wetting of the precured (pre-gelled) electrolyte onto the cathode surface because if the wetting is not adequate, (1) the

separators are not gelled properly and the gel coating is only partial; (2) the gelled matrix forms a resistive interface at the cathode and because of this high interfacial resistance, the resistivity of the entire cell increases by many folds.

Thus, the wetting time study was done for POSS/PEG/LE cells before they were cured at 70^{o}C for 30 mins, keeping 3 hours as reference time (3hr was a standard followed in the lab, though not much resting time analysis had been done before).

Figure 2.10 shows the results for the resting time analysis for the POSS 5%/PEG 1%/LE cells. The reference resting time was kept at 3hours and other sets of cells were rested for 30 mins, 1hr, 2hrs and 6hrs. It was observed that the performance for 2, 3 and 6 h was similar and that the capacity for 30 mins and 1 h was significantly lower than the reference 3 h which suggests that 1hr are inadequate for complete wetting of the S/KB electrode.

Though the test suggests that 2 h of resting time was enough for the gelled electrolyte cells, all the gelled electrolyte cells that have been tested have been rested for 3 h to ensure complete wetting.

2.4 Conclusion

The results reported in the previous section make a strong case for gelled electrolyte system to be used for the Li-S battery technology. Gelled electrolytes are effective at (1) reducing fire safety risks in the battery; (2) prevent leakage of electrolyte from the battery; (3) suppress potentially catastrophic polysulfide shuttling in the cell; (4) improve cell capacity retention over long cycling; and (5) help suppress dendritic formation (reduced percentage of cells shorting even after 200 cycles).

POSS/LE cells perform better at polysulfide retardation because of their high extent of cross linkage (8 sites per molecule) and also due to presence of the charged ceramic cage.

Addition of PEG improves the ionic conductivity of POSS/LE systems, and the discharge capacity of the cells is enhanced as well. The higher conductivity translates to better performance at high C cycling rate.

In a nutshell, the gelled electrolyte system forms a great intermediate between liquid electrolyte and solid-state electrolyte technology. It is not limited by the low ionic conductivity and high interfacial resistance of the solid electrolyte, but at the same time, they are safer and show performance comparable to liquid electrolyte. Further improvements in the gelled electrolyte technology will only cement its position as an effective solution to the problems posed by the Li-S technology.

2.6 Future Work

Building on to the experimental and cell performance characterization knowledge, we plan to work on these following research paths to further broaden our understanding of the gel electrolyte system in the lithium sulfur battery.

Several studies have shown a significant improvement on addition of ceramics in electrolytes in Li-based cell technology. Given the reduction in ionic conductivity in the gel electrolyte system, to further improve the conductivity of the gelled electrolyte, we plan to test out performance of ceramic and other high-conductance additives (Al_2O_3, SiO_2, TiO_2, rGO, graphene nanoribbons etc.) in the electrolyte.

Also, we aim to test out performance of pre-addition of Li_2S_x in electrolyte to minimize PS dissolution in the electrolyte. A higher initial polysulfide concentration in the electrolyte would reduce the solubility of the active material from the cathode and hence, may aid in reducing the losses due to polysulfide shuttling.

Next, we also plan to test different crosslinkers and other possible combination of polymer alloys and compare their performance. Additionally, we plan to test the performance of various ionic salt additives to improve Li^+ transference.

To better understand the chemistry of the gelled LiS system, we plan to perform extensive in-situ cell analysis while cycling and build a computational tool of the Li-S system to test the various failure modes of the cell.

2.5 References

Amine, K., Kanno, R., & Tzeng, Y. (2014). Rechargeable lithium batteries and beyond: Progress, challenges, and future directions. *MRS Bulletin*, *39*(5), 395–401. https://doi.org/10.1557/mrs.2014.62

Angulakshmi, N., & Stephan, A. M. (2015). Efficient electrolytes for lithium-sulfur batteries. In *Frontiers in Energy Research* (Vol. 3, Issue MAY, p. 17). Frontiers Media S.A. https://doi.org/10.3389/fenrg.2015.00017

Arora, P., & Zhang, Z. (2004). *Battery Separators*. https://doi.org/10.1021/cr020738u

Barchasz, C., Leprêtre, J. C., Alloin, F., & Patoux, S. (2012). New insights into the limiting parameters of the Li/S rechargeable cell. *Journal of Power Sources*, *199*, 322–330. https://doi.org/10.1016/j.jpowsour.2011.07.021

Birk, J. R., & Steunenberg, R. K. (1974). CHEMICAL INVESTIGATIONS OF LITHIUM-SULFUR CELLS. *Adv Chem Ser*, *140*, 186–202. https://doi.org/10.1021/ba-1975-0140.ch012

Bruce, P. G., Freunberger, S. A., Hardwick, L. J., & Tarascon, J. M. (2012). LigO2 and LigS batteries with high energy storage. In *Nature Materials* (Vol. 11, Issue 1, pp. 19–29). Nature Publishing Group. https://doi.org/10.1038/nmat3191

Cao, R., Xu, W., Lv, D., Xiao, J., & Zhang, J. G. (2015). Anodes for Rechargeable Lithium-Sulfur Batteries. In *Advanced Energy Materials* (Vol. 5, Issue 16, p. 1402273). Wiley-VCH Verlag. https://doi.org/10.1002/aenm.201402273

Carlin, J. M., Joo, Y. L., & Smith, S. (2018). *Hybrid separators and the manufacture thereof*.

Chen, R., Zhao, T., & Wu, F. (2015). From a historic review to horizons beyond: Lithium-sulphur batteries run on the wheels. In *Chemical Communications* (Vol. 51, Issue 1, pp. 18–33). Royal Society of Chemistry. https://doi.org/10.1039/c4cc05109b

Cheng, X., Pan, J., Zhao, Y., Liao, M., & Peng, H. (2018). Gel Polymer Electrolytes for Electrochemical Energy Storage. In *Advanced Energy Materials* (Vol. 8, Issue 7). Wiley-VCH Verlag. https://doi.org/10.1002/aenm.201702184

Colthorpe, A. (2020, July 7). *Solar farm fitted with batteries to meet grid output control requirements goes online in Japan | Energy Storage News*. https://www.energy-storage.news/news/solar-farm-fitted-with-batteries-to-meet-grid-output-control-requirements-g

Colthorpe, A. (2021, March 23). *Wisconsin utilities plan 250MW solar project with 75MW of battery storage | Energy Storage News*. https://www.energy-storage.news/news/wisconsin-utilities-plan-250mw-solar-project-with-75mw-of-battery-storage

COMSOL AB. (n.d.). *COMSOL Multiphysics® v. 5.5*. Retrieved July 27, 2020, from www.comsol.com

Croce, F., Appetecchi, G. B., Persi, L., & Scrosati, B. (1998). Nanocomposite polymer electrolytes for lithium batteries. *Nature 1998 394:6692*, *394*(6692), 456–458. https://doi.org/10.1038/28818

Ding, F., Xu, W., Graff, G. L., Zhang, J., Sushko, M. L., Chen, X., Shao, Y., Engelhard, M. H., Nie, Z., Xiao, J., Liu, X., Sushko, P. v., Liu, J., & Zhang, J. G. (2013). Dendrite-free lithium deposition via self-healing electrostatic shield mechanism. *Journal of the American Chemical Society*, *135*(11), 4450–4456. https://doi.org/10.1021/ja312241y

Ding, L., Xu, G., Ge, Q., Wu, T., Yang, F., & Xiang, M. (2017). Effect of Fumed SiO 2 on Pore Formation Mechanism and Various Performances of β - i PP Microporous Membrane Used for Lithium-ion Battery Separator. *Chinese Journal of Polymer Science 2017 36:4*, *36*(4), 536–545. https://doi.org/10.1007/S10118-018-2029-7

Ding, N., Zhou, L., Zhou, C., Geng, D., Yang, J., Chien, S. W., Liu, Z., Ng, M. F., Yu, A., Hor, T. S. A., Sullivan, M. B., & Zong, Y. (2016a). Building better lithium-

sulfur batteries: From LiNO2 to solid oxide catalyst. *Scientific Reports*, *6*(1), 1–10. https://doi.org/10.1038/srep33154

Ding, N., Zhou, L., Zhou, C., Geng, D., Yang, J., Chien, S. W., Liu, Z., Ng, M.-F., Yu, A., Hor, T. S. A., Sullivan, M. B., & Zong, Y. (2016b). Building better lithium-sulfur batteries: from LiNO 3 to solid oxide catalyst. *Scientific Reports 2016 6:1*, *6*(1), 1–10. https://doi.org/10.1038/srep33154

Ding, Y., Hou, H., Zhao, Y., Zhu, Z., & Fong, H. (2016). Electrospun polyimide nanofibers and their applications. *Progress in Polymer Science*, *61*, 67–103. https://doi.org/10.1016/J.PROGPOLYMSCI.2016.06.006

Dunn, B., Kamath, H., & Tarascon, J. M. (2011). Electrical energy storage for the grid: A battery of choices. In *Science* (Vol. 334, Issue 6058, pp. 928–935). American Association for the Advancement of Science. https://doi.org/10.1126/science.1212741

Feng, X., Ouyang, M., Liu, X., Lu, L., Xia, Y., & He, X. (2018). Thermal runaway mechanism of lithium ion battery for electric vehicles: A review. *Energy Storage Materials*, *10*, 246–267. https://doi.org/10.1016/J.ENSM.2017.05.013

Girishkumar, G., McCloskey, B., Luntz, A. C., Swanson, S., & Wilcke, W. (2010). Lithium-air battery: Promise and challenges. *Journal of Physical Chemistry Letters*, *1*(14), 2193–2203. https://doi.org/10.1021/jz1005384

Halim, W., Lee, J. H., Park, S. M., Zhang, R., Sarkar, S., O'Neil, T., Chiang, Y. C., & Joo, Y. L. (2019). Directly deposited binder-free sulfur electrode enabled by air-controlled electrospray process. *ACS Applied Energy Materials*, *2*(1), 678–686. https://doi.org/10.1021/acsaem.8b01694

Hasanuzzaman, M., Zubir, U. S., Ilham, N. I., & Seng Che, H. (2017). Global electricity demand, generation, grid system, and renewable energy polices: a review. *WIREs Energy and Environment*, *6*(3), e222. https://doi.org/https://doi.org/10.1002/wene.222

Herbert, D., & Ulam, J. (1958). *United States Patent Office l 3,043,896 ELECTRIC DRY CELLS AND STORAGE BATTERES*.

Höök, M., & Tang, X. (2013). Depletion of fossil fuels and anthropogenic climate change-A review. *Energy Policy*, *52*, 797–809. https://doi.org/10.1016/j.enpol.2012.10.046

Javed, K., Krumme, A., Viirsalu, M., Krasnou, I., Plamus, T., Vassiljeva, V., Tarasova, E., Savest, N., Mere, A., Mikli, V., Danilson, M., Kaljuvee, T., Lange, S., Yuan, Q., Topham, P. D., & Chen, C. M. (2018). A method for producing conductive graphene biopolymer nanofibrous fabrics by exploitation of an ionic liquid dispersant in electrospinning. *Carbon*, *140*, 148–156. https://doi.org/10.1016/J.CARBON.2018.08.034

Jeddi, K., Sarikhani, K., Qazvini, N. T., & Chen, P. (2014). Stabilizing lithium/sulfur batteries by a composite polymer electrolyte containing mesoporous silica particles. *Journal of Power Sources*, *245*, 656–662. https://doi.org/10.1016/j.jpowsour.2013.06.147

Jeon, H., Yeon, D., Lee, T., Park, J., Ryou, M. H., & Lee, Y. M. (2016). A water-based Al2O3 ceramic coating for polyethylene-based microporous separators for lithium-ion batteries. *Journal of Power Sources*, *315*, 161–168. https://doi.org/10.1016/J.JPOWSOUR.2016.03.037

Ji, X., Lee, K. T., & Nazar, L. F. (2009). A highly ordered nanostructured carbon-sulphur cathode for lithium-sulphur batteries. *Nature Materials*, *8*(6), 500–506. https://doi.org/10.1038/nmat2460

Ji, X., & Nazar, L. F. (2010). Advances in Li-S batteries. *Journal of Materials Chemistry*, *20*(44), 9821–9826. https://doi.org/10.1039/b925751a

Kamyshny Alexey, Gun, J., Rizkov, D., Voitsekovski, T., & Lev, O. (2007). Equilibrium Distribution of Polysulfide Ions in Aqueous Solutions at Different Temperatures by Rapid Single Phase Derivatization. *Environmental Science & Technology*, *41*(7), 2395–2400. https://doi.org/10.1021/es062637+

Killis, A., le Nest, J. F., Gandini, A., Cheradame, H., & Cohen-Addad, J. P. (1984). Correlation among transport properties in ionically conducting cross-linked networks. *Solid State Ionics*, *14*(3), 231–237. https://doi.org/10.1016/0167-2738(84)90104-8

Kozen, A. C., Lin, C. F., Pearse, A. J., Schroeder, M. A., Han, X., Hu, L., Lee, S. B., Rubloff, G. W., & Noked, M. (2015). Next-Generation Lithium Metal Anode Engineering via Atomic Layer Deposition. *ACS Nano*, *9*(6), 5884–5892. https://doi.org/10.1021/acsnano.5b02166

Lee, D. J., Lee, H., Kim, Y. J., Park, J. K., & Kim, H. T. (2016). Sustainable Redox Mediation for Lithium-Oxygen Batteries by a Composite Protective Layer on the Lithium-Metal Anode. *Advanced Materials*, *28*(5), 857–863. https://doi.org/10.1002/adma.201503169

Lei, T., Chen, W., Lv, W., Huang, J., Zhu, J., Chu, J., Yan, C., Wu, C., Yan, Y., He, W., Xiong, J., Li, Y., Yan, C., Goodenough, J. B., & Duan, X. (2018). Inhibiting Polysulfide Shuttling with a Graphene Composite Separator for Highly Robust Lithium-Sulfur Batteries. *Joule*, *2*(10), 2091–2104. https://doi.org/10.1016/j.joule.2018.07.022

Li, N. W., Yin, Y. X., Yang, C. P., & Guo, Y. G. (2016). An Artificial Solid Electrolyte Interphase Layer for Stable Lithium Metal Anodes. *Advanced Materials*, *28*(9), 1853–1858. https://doi.org/10.1002/adma.201504526

Li, T., Bai, X., Gulzar, U., Bai, Y. J., Capiglia, C., Deng, W., Zhou, X., Liu, Z., Feng, Z., & Proietti Zaccaria, R. (2019). A Comprehensive Understanding of Lithium–Sulfur Battery Technology. In *Advanced Functional Materials* (Vol. 29, Issue 32). Wiley-VCH Verlag. https://doi.org/10.1002/adfm.201901730

Liu, K., Zhuo, D., Lee, H. W., Liu, W., Lin, D., Lu, Y., & Cui, Y. (2017). Extending the Life of Lithium-Based Rechargeable Batteries by Reaction of Lithium Dendrites with a Novel Silica Nanoparticle Sandwiched Separator. *Advanced Materials*, *29*(4). https://doi.org/10.1002/adma.201603987

Liu, Y., Lin, D., Liang, Z., Zhao, J., Yan, K., & Cui, Y. (2016). Lithium-coated polymeric matrix as a minimum volume-change and dendrite-free lithium metal anode. *Nature Communications*, *7*(1), 1–9. https://doi.org/10.1038/ncomms10992

Love, C. T. (2011). Thermomechanical analysis and durability of commercial micro-porous polymer Li-ion battery separators. *Journal of Power Sources*, *196*(5), 2905–2912. https://doi.org/10.1016/J.JPOWSOUR.2010.10.083

Lu, Y., Das, S. K., Moganty, S. S., & Archer, L. A. (2012). Ionic liquid-nanoparticle hybrid electrolytes and their application in secondary lithium-metal batteries. *Advanced Materials*, *24*(32), 4430–4435. https://doi.org/10.1002/adma.201201953

Lu, Y., Tikekar, M., Mohanty, R., Hendrickson, K., Ma, L., & Archer, L. A. (2015). Stable cycling of lithium metal batteries using high transference number electrolytes. *Advanced Energy Materials*, *5*(9). https://doi.org/10.1002/aenm.201402073

Lu, Y., Tu, Z., & Archer, L. A. (2014). Stable lithium electrodeposition in liquid and nanoporous solid electrolytes. *Nature Materials*, *13*(10), 961–969. https://doi.org/10.1038/nmat4041

Lu, Z., Sui, F., Miao, Y. E., Liu, G., Li, C., Dong, W., Cui, J., Liu, T., Wu, J., & Yang, C. (2021). Polyimide separators for rechargeable batteries. *Journal of Energy Chemistry*, *58*, 170–197. https://doi.org/10.1016/J.JECHEM.2020.09.043

Luo, W., Zhou, L., Fu, K., Yang, Z., Wan, J., Manno, M., Yao, Y., Zhu, H., Yang, B., & Hu, L. (2015). A Thermally Conductive Separator for Stable Li Metal Anodes. *Nano Letters*, *15*(9), 6149–6154. https://doi.org/10.1021/acs.nanolett.5b02432

Marceaux, S., Bressy, C., Perrin, F. X., Martin, C., & Margaillan, A. (2014). Development of polyorganosilazane–silicone marine coatings. *Progress in Organic Coatings*, *77*(11), 1919–1928. https://doi.org/10.1016/J.PORGCOAT.2014.06.020

McBrayer, J. D., Beechem, T. E., Perdue, B. R., Apblett, C. A., & Garzon, F. H. (2018). Polysulfide Speciation in the Bulk Electrolyte of a Lithium Sulfur Battery. *Journal of The Electrochemical Society*, *165*(5), A876–A881. https://doi.org/10.1149/2.0441805jes

Mikhaylik, Y. v., & Akridge, J. R. (2004). Polysulfide Shuttle Study in the Li/S Battery System. *Journal of The Electrochemical Society*, *151*(11), A1969. https://doi.org/10.1149/1.1806394

Munsell, M. (2018, March 6). *US Energy Storage Market Tops the 1 GWh Milestone in 2017 | Greentech Media*. GTM Research Article: A Wood Mackenzie Business. https://www.greentechmedia.com/articles/read/us-energy-storage-market-tops-the-gwh-milestone-in-2017

Murata, K., Izuchi, S., & Yoshihisa, Y. (2000a). An overview of the research and development of solid polymer electrolyte batteries. *Electrochimica Acta*, *45*(8–9), 1501–1508. https://doi.org/10.1016/S0013-4686(99)00365-5

Murata, K., Izuchi, S., & Yoshihisa, Y. (2000b). Overview of the research and development of solid polymer electrolyte batteries. *Electrochimica Acta*, *45*(8), 1501–1508. https://doi.org/10.1016/S0013-4686(99)00365-5

Nunes-Pereira, J., Costa, C. M., & Lanceros-Méndez, S. (2015). Polymer composites and blends for battery separators: State of the art, challenges and future trends. *Journal of Power Sources*, *281*, 378–398. https://doi.org/10.1016/J.JPOWSOUR.2015.02.010

Park, J., Jeong, J., Lee, Y., Oh, M., Ryou, M. H., & Lee, Y. M. (2016). Micro-Patterned Lithium Metal Anodes with Suppressed Dendrite Formation for Post Lithium-Ion Batteries. *Advanced Materials Interfaces*, *3*(11). https://doi.org/10.1002/admi.201600140

Peled, E., Shekhtman, I., Mukra, T., Goor, M., Belenkaya, I., & Golodnitsky, D. (2018). Improving the Durability and Minimizing the Polysulfide Shuttle in the Li/S

Battery. *Journal of The Electrochemical Society*, *165*(1), A6051–A6057. https://doi.org/10.1149/2.0101801jes

Pfleging, W. (2018). A review of laser electrode processing for development and manufacturing of lithium-ion batteries. *Nanophotonics*, *7*(3), 549–573. https://doi.org/10.1515/NANOPH-2017-0044

Qie, L., & Manthiram, A. (2016). High-Energy-Density Lithium-Sulfur Batteries Based on Blade-Cast Pure Sulfur Electrodes. *ACS Energy Letters*, *1*(1), 46–51. https://doi.org/10.1021/acsenergylett.6b00033

Rana, M., Ahad, S. A., Li, M., Luo, B., Wang, L., Gentle, I., & Knibbe, R. (2019). Review on areal capacities and long-term cycling performances of lithium sulfur battery at high sulfur loading. In *Energy Storage Materials* (Vol. 18, pp. 289–310). Elsevier B.V. https://doi.org/10.1016/j.ensm.2018.12.024

Rand, D. A. J. (2011). A journey on the electrochemical road to sustainability. *Journal of Solid State Electrochemistry*, *15*(7), 1579–1622. https://doi.org/10.1007/s10008-011-1410-z

Reddy, M. v., Mauger, A., Julien, C. M., Paolella, A., & Zaghib, K. (2020). Brief history of early lithium-battery development. *Materials*, *13*(8). https://doi.org/10.3390/MA13081884

Ryou, M. H., Lee, D. J., Lee, J. N., Lee, Y. M., Park, J. K., & Choi, J. W. (2012). Excellent cycle life of lithium-metal anodes in lithium-ion batteries with mussel-inspired polydopamine-coated separators. *Advanced Energy Materials*, *2*(6), 645–650. https://doi.org/10.1002/aenm.201100687

Ryou, M. H., Lee, Y. M., Lee, Y., Winter, M., & Bieker, P. (2015). Mechanical surface modification of lithium metal: Towards improved Li metal anode performance by directed Li plating. *Advanced Functional Materials*, *25*(6), 834–841. https://doi.org/10.1002/adfm.201402953

Salem, N., & Abu-Lebdeh, Y. (2012). *Effect of Nanoparticles on Electrolytes and Electrode/Electrolyte Interface*. 221–244. https://doi.org/10.1007/978-1-4614-4605-7_9

Seh, Z. W., Li, W., Cha, J. J., Zheng, G., Yang, Y., McDowell, M. T., Hsu, P. C., & Cui, Y. (2013). Sulphur-TiO 2 yolk-shell nanoarchitecture with internal void space for long-cycle lithium-sulphur batteries. *Nature Communications*, *4*. https://doi.org/10.1038/ncomms2327

Shebert, G. L., Zamani, S., Yi, C., & Joo, Y. L. (2020). Polysulfide entrapment and retardation in gel electrolyte Li–S batteries: experiments and modeling. *Journal of Materials Chemistry A*, *8*(8), 4341–4353. https://doi.org/10.1039/C9TA14234G

Thackeray, M. M., Wolverton, C., & Isaacs, E. D. (2012). Electrical energy storage for transportation - Approaching the limits of, and going beyond, lithium-ion batteries. In *Energy and Environmental Science* (Vol. 5, Issue 7, pp. 7854–7863). Royal Society of Chemistry. https://doi.org/10.1039/c2ee21892e

Vallée, A., Besner, S., & Prud'Homme, J. (1992). Comparative study of poly(ethylene oxide) electrolytes made with LiN(CF3SO2)2, LiCF3SO3 and LiClO4: Thermal properties and conductivity behaviour. *Electrochimica Acta*, *37*(9), 1579–1583. https://doi.org/10.1016/0013-4686(92)80115-3

Wang, D., Yu, J., Duan, G., Liu, K., & Hou, H. (2020). Electrospun polyimide nonwovens with enhanced mechanical and thermal properties by addition of trace plasticizer. *Journal of Materials Science 2020 55:13*, *55*(13), 5667–5679. https://doi.org/10.1007/S10853-020-04402-2

Wang, H. C., Cao, X., Liu, W., & Sun, X. (2019). Research Progress of the Solid State Lithium-Sulfur Batteries. In *Frontiers in Energy Research* (Vol. 7, p. 112). Frontiers Media S.A. https://doi.org/10.3389/fenrg.2019.00112

Wang, Q., Ping, P., Zhao, X., Chu, G., Sun, J., & Chen, C. (2012). Thermal runaway caused fire and explosion of lithium ion battery. *JPS*, *208*, 210–224. https://doi.org/10.1016/J.JPOWSOUR.2012.02.038

Wang, Q., Ping, P., Zhao, X., Chu, G., Sun, J., Chen, C., Wang, Q., Ping, P., Zhao, X., Chu, G., Sun, J., & Chen, C. (2012). Thermal runaway caused fire and explosion of lithium ion battery. *JPS*, *208*, 210–224. https://doi.org/10.1016/J.JPOWSOUR.2012.02.038

Whittingham, M. S. (2012). History, Evolution, and Future Status of Energy Storage. *Proceedings of the IEEE*, *100*(Special Centennial Issue), 1518–1534. https://doi.org/10.1109/JPROC.2012.2190170

Yamin, H., & Peled, E. (1983). Electrochemistry of a nonaqueous lithium/sulfur cell. *Journal of Power Sources*, *9*(3), 281–287. https://doi.org/10.1016/0378-7753(83)87029-3

Yan, K., Lu, Z., Lee, H. W., Xiong, F., Hsu, P. C., Li, Y., Zhao, J., Chu, S., & Cui, Y. (2016). Selective deposition and stable encapsulation of lithium through heterogeneous seeded growth. *Nature Energy*, *1*(3), 1–8. https://doi.org/10.1038/NENERGY.2016.10

Yang, C. P., Yin, Y. X., Zhang, S. F., Li, N. W., & Guo, Y. G. (2015). Accommodating lithium into 3D current collectors with a submicron skeleton towards long-life lithium metal anodes. *Nature Communications*, *6*(1), 1–9. https://doi.org/10.1038/ncomms9058

Yu, X., Wu, H., Koo, J. H., & Manthiram, A. (2020). Tailoring the Pore Size of a Polypropylene Separator with a Polymer Having Intrinsic Nanoporosity for Suppressing the Polysulfide Shuttle in Lithium–Sulfur Batteries. *Advanced Energy Materials*, *10*(1), 1902872. https://doi.org/10.1002/AENM.201902872

Zhang, J., Yue, L., Kong, Q., Liu, Z., Zhou, X., Zhang, C., Xu, Q., Zhang, B., Ding, G., Qin, B., Duan, Y., Wang, Q., Yao, J., Cui, G., & Chen, L. (2014). Sustainable, heat-resistant and flame-retardant cellulose-based composite separator for high-performance lithium ion battery. *Scientific Reports 2014 4:1*, *4*(1), 1–8. https://doi.org/10.1038/srep03935

Zhang, R., Cheng, X. B., Zhao, C. Z., Peng, H. J., Shi, J. le, Huang, J. Q., Wang, J., Wei, F., & Zhang, Q. (2016). Conductive Nanostructured Scaffolds Render Low Local Current Density to Inhibit Lithium Dendrite Growth. *Advanced Materials*, *28*(11), 2155–2162. https://doi.org/10.1002/adma.201504117

Zhang, Sheng S. (2013). Liquid electrolyte lithium/sulfur battery: Fundamental chemistry, problems, and solutions. In *Journal of Power Sources* (Vol. 231, pp. 153–162). Elsevier. https://doi.org/10.1016/j.jpowsour.2012.12.102

Zhang, Sheng S., & Read, J. A. (2012). A new direction for the performance improvement of rechargeable lithium/sulfur batteries. *Journal of Power Sources*, *200*, 77–82. https://doi.org/10.1016/j.jpowsour.2011.10.076

Zhang, Sheng S., & Tran, D. T. (2013). How a gel polymer electrolyte affects performance of lithium/sulfur batteries. *Electrochimica Acta*, *114*, 296–302. https://doi.org/10.1016/j.electacta.2013.10.069

Zhang, Sheng Shui. (2007). A review on the separators of liquid electrolyte Li-ion batteries. *Journal of Power Sources*, *164*(1), 351–364. https://doi.org/10.1016/J.JPOWSOUR.2006.10.065

Zhao, M., Li, B.-Q., Zhang, X.-Q., Huang, J.-Q., & Zhang, Q. (2020). A Perspective toward Practical Lithium−Sulfur Batteries. *Cite This: ACS Cent. Sci*, *2020*, 1095–1104. https://doi.org/10.1021/acscentsci.0c00449

Zheng, C., Wang, K., Li, L., Huang, H., Liang, C., Gan, Y., He, X., Zhang, W., & Zhang, J. (2021). High-Performance All-Solid-State Lithium–Sulfur Batteries Enabled by Slurry-Coated Li6PS5Cl/S/C Composite Electrodes. *Frontiers in Energy Research*, *8*, 416. https://doi.org/10.3389/FENRG.2020.606494

Zheng, G., Lee, S. W., Liang, Z., Lee, H. W., Yan, K., Yao, H., Wang, H., Li, W., Chu, S., & Cui, Y. (2014). Interconnected hollow carbon nanospheres for stable lithium metal anodes. *Nature Nanotechnology*, *9*(8), 618–623. https://doi.org/10.1038/nnano.2014.152

Zhong, W. (2016). Nanofibres for medical textiles. *Advances in Smart Medical Textiles: Treatments and Health Monitoring*, 57–70. https://doi.org/10.1016/B978-1-78242-379-9.00003-7

Zhou, D., Liu, R., He, Y. B., Li, F., Liu, M., Li, B., Yang, Q. H., Cai, Q., & Kang, F. (2016). SiO2 Hollow Nanosphere-Based Composite Solid Electrolyte for Lithium Metal Batteries to Suppress Lithium Dendrite Growth and Enhance Cycle Life. *Advanced Energy Materials*, *6*(7). https://doi.org/10.1002/aenm.201502214

Zou, P., Wang, Y., Chiang, S. W., Wang, X., Kang, F., & Yang, C. (2018). Directing lateral growth of lithium dendrites in micro-compartmented anode arrays for safe lithium metal batteries. *Nature Communications*, *9*(1), 1–9. https://doi.org/10.1038/s41467-018-02888-8

CHAPTER 3

PROBING THE SYNERGY BETWEEN GEL ELECTROLYTE AND POLYMER-CERAMIC HYBRID SEPARATOR SYSTEMS IN LITHIUM SULFUR BATTERIES

3.1 Abstract

In this chapter, the synergy between gel electrolyte (POSS) and polymer-ceramic hybrid separator (PI/OPSZ) in the lithium sulfur cell was evaluated. It was shown that the PI/OPSZ separators are more ideally suited than Celgard 2400 to be used in the Li-S cell. They show better compatibility with the Li-S gel electrolyte, better wettability, and electrolyte uptake. They have superior heat and flame tolerance and show a much higher ionic conductivity than Celgard 2400. Finally, tailored gelled PI/OPSZ cells have been shown to exhibit better cell performance. There reliability issues of these technology at high C cycling rates has also been addressed and possible solutions to mitigating these problems have been highlighted.

Graphical Abstract

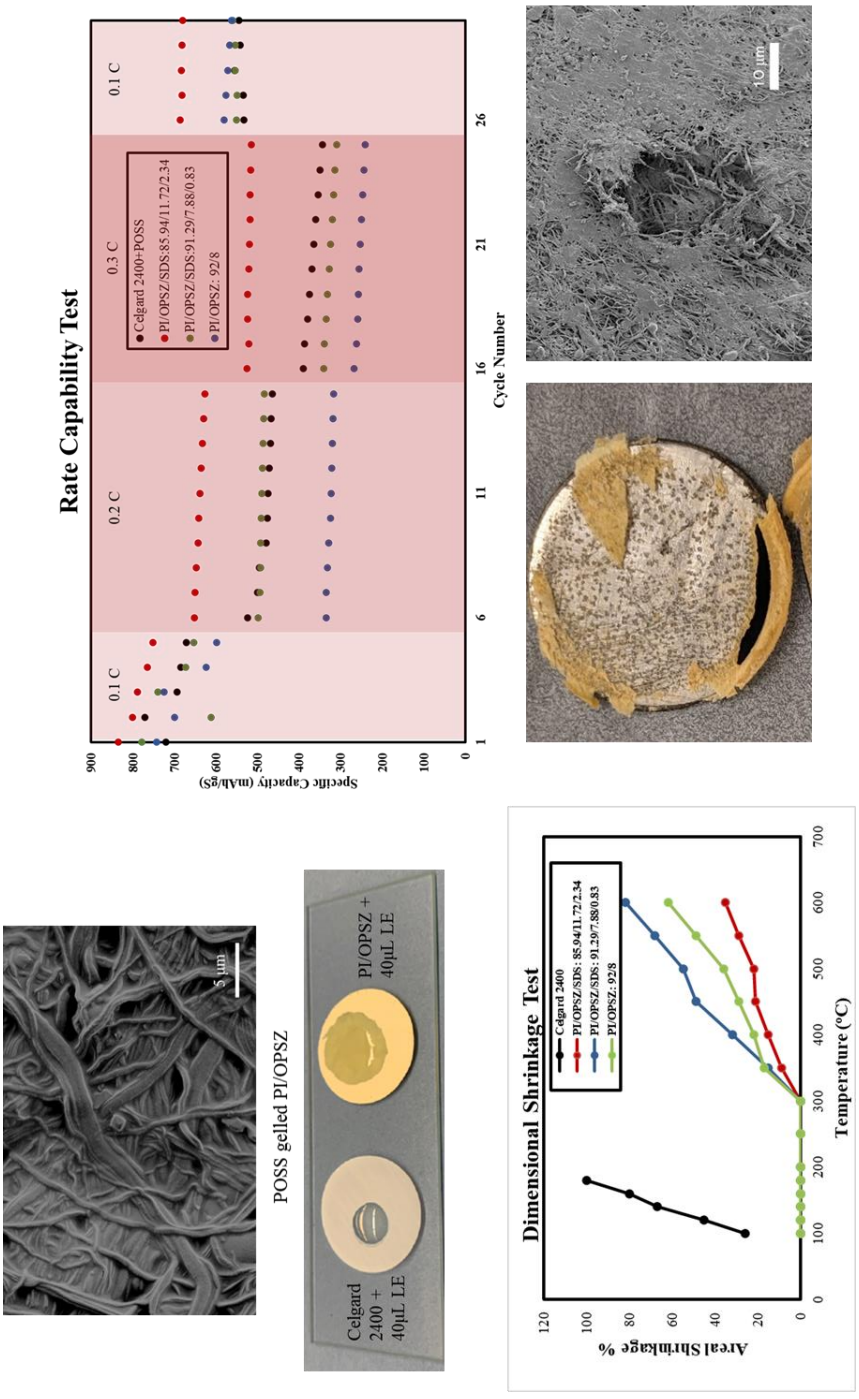

Figure 3.1: Graphical Abstract: Chapter 3

3.2 Introduction

3.2.1 Separators systems in batteries

A separator is a critical component in an electrochemical cell. It provides an effective insulating barrier separating the two active electrodes. Despite not actively taking part in the electrochemical reaction, it essentially controls the rate of active species diffusion across the electrochemical cell, that is, from one electrode to the other. It also acts as the electrolyte reservoir and so it is imperative to have good compatibility between the electrolyte component and the separator system. Theoretically, a cell may have the highest gravimetric capacity if the separator thickness is minimized which would lead to the least ion diffusion resistance. However, in the lithium-sulfur battery systems, practical problems like polysulfide shuttling and Li dendritic formation set a limitation on the thickness as if the separator is too thin, it would degrade its mechanical robustness leading to an increase in the cell-failure due to short-circuiting or Li degradation due to high flux polysulfide shuttling (Arora & Zhang, 2004). In a nutshell, the structure and properties of the separator drastically influence the overall capacity of the battery.

3.2.2 Requirements of an effective separator

The most essential requirement of an effective separator is that it should be electrochemically stable and inert to the cell chemistry. If the separator is not chemically inert, it might degrade during cycling, leading to poor cell performance, and in severe cases to complete battery failure. If the separator system has inherent impurities or any chemically active sites, it could lead to catastrophic side reactions which severely damage the performance of the cell. In the lithium sulfur battery chemistry, the harsh

materials, buttressed by strong oxidizing/reducing environment in the cell limit the types of materials that can be employed for use as a separator (Love, 2011).

In addition, the separator should also have high mechanical strength and should have enough robustness to withstand the pressure of the high-volume change of the S/KB cathode electrode during repeated charge/discharge cycles. The separator should also have a high puncture strength to withstand penetration from the needle-like Li dendritic formation on the anode side, or the rough passivation layer formed on the cathode side. A puncture in the separator will lead to the cell shorting and may be a severe safety hazard.

It is also important for the separator to be thermally stable. At high temperatures, the separator should be able to maintain its structural integrity. If the separator gives away at elevated temperatures, this could lead to a series of exothermic side-reactions which would further elevate the temperature causing grave fire safety risk (Q. Wang, Ping, Zhao, Chu, Sun, Chen, et al., 2012). This is especially important in EV applications, wherein the batteries are more likely to be exposed to elevated temperatures.

Furthermore, an essential requirement of the separator is to have adequate electrolyte uptake and wetting characteristics. An effective separator should be able to demonstrate good compatibility with the electrolyte and be able to sufficiently absorb the electrolyte to allow for efficient ion transport. A high electrolyte uptake leads to a reduction in the effective resistance of the cell, as it allows for facilitated Li^+ transport throughout cell during charge/discharge cycling. In addition to the hydrophilicity, the porosity and pore

size distribution also strongly affect the electrolyte uptake characteristics of the separator system.

For the Li-S battery system, the separator pore size needs to be small enough to effectively trap the polysulfide species from migrating towards the anode surface and at the same time, prevent dendritic structures from penetrating into cathodic half of the cell. It has been reported in literature that pore sizes under 1 μm would be ideal for the Li-S technology (Yu et al., 2020).

3.2.3 The need for specialized separator systems for Li-S batteries

Currently, due the lack of substantial research in separator systems specialized for the Li-S battery technology, most of the commonly used polyolefin microporous separators in Li-S cells have simply been borrowed from the Li-ion battery technology. Given, the vast difference in battery chemistry between the Li-S technology and the Li-ion technology, it is not surprising that the commonly used polyolefin microporous films – polypropylene (PP) and polyethylene (PE), despite their high strength, chemical stability, and low cost (Arora & Zhang, 2004) , are essentially incompatible with the Li-S battery electrolyte. The incompatibility of these separators stems from their intrinsic characteristics. The PP and PE polymers have poor electrolyte wettability and electrolyte uptake due to their non-polar, hydrophobic nature. Furthermore, these polymer films have very low porosity (approximately 35-50%) which results in a low Li^+ ion mobility and hence restricting the capacity of the batteries (Sheng Shui Zhang, 2007) .

In addition, these separator systems are extremely fragile when it comes to thermal tolerance and cannot maintain reasonable battery safety in the event of cell abuse or exposure to elevated temperatures.

At temperatures as low as 100^{o}C, these separators show potentially catastrophic shrinkage and they exhibit little to no tolerance for flames leading to severe thermal runways, and in some cases battery explosions (Feng et al., 2018) (Q. Wang, Ping, Zhao, Chu, Sun, & Chen, 2012). Several attempts have been made to retrofit the separators with ceramic coatings to decrease thermal shrinkage and improve electrolyte wettability to some extent (L. Ding et al., 2017)(Jeon et al., 2016). However, ceramic coated polyolefin separators still show low thermal tolerance above 150 ^{o}C and the coating peeling issues are common.

For the Li-S battery technology to maximize their capacity potential, every single component of the battery needs to be specialized for the system. In the recent years, the electrospinning technology has gathered considerable attention to produce non-woven separators for Li-S batteries with characteristics specifically tailored for Li-S battery chemistry. The Joo Research Group has been, for several years, working on optimizing the electrospinning technology for the specific reason of engineering high performance separator systems for various battery technologies. The next section gives a brief overview on the electrospinning technology.

3.2.4 Electrospinning

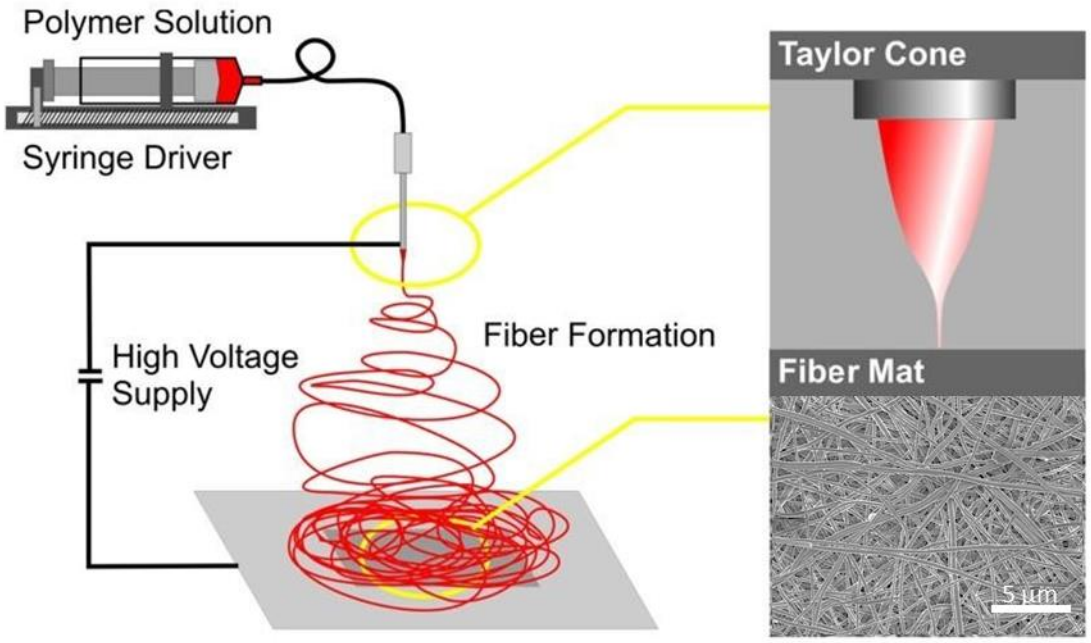

Figure 3.2: Schematic Diagram for Electrospinning process

Electrospinning is a method to produce nanofibers by charging and ejecting a polymer melt or solution through a spinneret under a high-voltage electric field and to solidify or coagulate it to form a filament (Zhong, 2016). In electrospinning, the electrostatic forces overcome the surface tension of the liquid/solution that is being sprayed, and this forms a jet that is ejected from the tip of the spinneret. As the solution is pumped through the spinneret, the charge builds up due to high applied voltage. At the tip of the spinneret, as the electrostatic forces build up, a Taylor cone develops. When the forces overcome the surface tension, fibers are ejected from the tip and travel to the grounded collector. Fig. 3.2 shows the typical setup for electrospinning.

To obtain good fiber morphology, parameters such as solution viscosity (concentration), applied voltage, spinneret tip-to-collector distance, and the solution feed rate need to be

optimized. Electrospinning is a facile, scalable and versatile method to form robust, high-performance nanofiber separators for battery applications. All the polymer ceramic hybrid separators used in this work had been fabricated using electrospinning.

3.2.5 Polyimide (PI) / ceramic hybrid separators

Given the inherent thermal safety problems with traditional polyolefins, a lot of recent research has been driven towards electrospinning thermally stable polymers for separators (D. Wang et al., 2020)(J. Zhang et al., 2014).

Polyimide (PI) is a thermally stable polymer that can withstand prolonged temperatures over 400^{o}C with minimal areal shrinkage issues (Y. Ding et al., 2016). Research on PI separators has shown that PI nanofiber separators have better electrolyte wettability and show better battery performance, much higher capacity and improved ionic conductivity compared to commercial Celgard separators (PP) (Z. Lu et al., 2021).

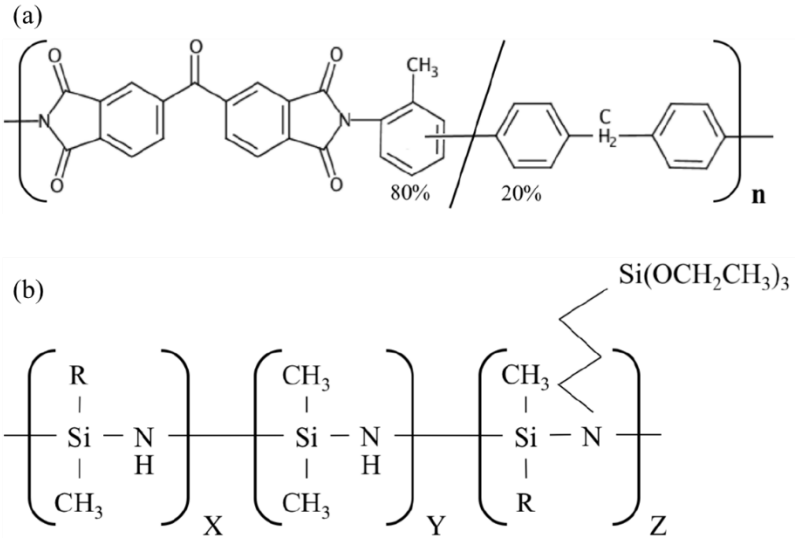

Figure 3.3: (a) Chemical structure of P84 co-polyimide. (b) Chemical structure of OPSZ (Durazane 1500 Slow Cure). In the OPSZ structure, R = -H or -CH_3

Further, it has long been established that ceramic additives to separator systems help improve the electrochemical performance (Croce et al., 1998; Nunes-Pereira et al., 2015; Salem & Abu-Lebdeh, 2012). Ceramic additives improve ionic conductivity leading to higher Li^+ ion transport through the cell. The ceramic additive further improves wettability and electrolyte interaction, and further improves the thermal stability. However, incorporating the ceramic filler into the polymeric strands is not a straightforward process and often improper impregnation leads to increased bulk resistance offsetting the benefits of better ionic conductivity.

The Joo Research Group has come up with a novel method to produce polymer ceramic hybrid separators by incorporating ceramic precursors to the separator solution before electrospinning.

Organopolysilazanes (OPSZ) are polymers in which silicon and nitrogen atoms alternate to form a ceramic precursor backbone. When coupled with trialkoxysilyl functional groups, OPSZs can cure at low temperatures resulting in highly cross-linked polymers, with Si-O-Si bonds in place of Si-N-Si and to form a polymer derived ceramic (PDC) (Marceaux et al., 2014). On further heat treatment, the conversion of the ceramic precursor is improved and remaining volatile group are removed that otherwise may cause side reactions. Previous work by Dr. Joe Carlin from the Joo Research Group had shown PI/OPSZ separators show better performance and battery safety for Li-ion batteries (Carlin et al., 2018).

In this work, synergy between PI/OPSZ separators and gel electrolyte has been probed. We have shown that PI/OPSZ performance have improved by increasing the OPSZ

content and improving heat treatment. Additionally, adding an ionic dispersant Sodium dodecyl sulfate (SDS) to the electrospinning solution was shown to result in better fiber morphology and improvement in battery performance. In this work, 3 prefabricated, commercial grade separators from SNT Corporation, Korea with different OPSZ and SDS content and with different heat treatment were used to probe the synergistic effects with gel electrolyte in the Li-S battery. We aim to show that the POSS gelled PI-OPSZ separator cells perform better than POSS gelled Celgard 2400 Li-S cells.

3.3 Experimental methods

3.3.1 Synthesis of Sulfur-Ketjen Black Cathode Systems

Sulfur powder (S, 1.5 g) was ground with Ketjen Black EC600JD (KB, 0.5 g, AkzoNobel) to obtain a 75:25 S:KB mixture. Then, the mixture was heat treated at 155 ^{0}C for at least 12 hours to ensure sulfur impregnation into the porous KB particles (Halim et al., 2019). The active material S/KB was then thoroughly mixed for 3 hours with Super C65 (MTI Corp.) and the binder polyvinylidene fluoride (PVDF, Aldrich) in N-methyl-2-pyrrolidone (NMP, BDH), in a weight ratio of 70 : 20 : 10 in a ball mill till honey-like consistency is achieved.

It was ensured that each milling session does not last over 10 mins for vibrations of over 20Hz to prevent overheating of the slurry. The slurry was then cast onto aluminum foil using a doctor blade and the sheets were dried in a fume hood at room temperature overnight followed by heat treatment in a 55^{0}C oven as seen in figure 2.2. The total thickness of aluminum + cathode was 54 microns, and sulfur areal loading was around 1 mg/cm^2 for all cells.

3.3.2 Electrolyte Fabrication

For the liquid electrolyte cells prepared, the electrolyte used was 1 M LiTFSI (99.95% trace metal basis, Sigma-Aldrich) and 0.1 M $LiNO_3$ (99.99% trace metals basis, Sigma – Aldrich) in a 1:1 volumetric ratio of 1,3 dioxolane (DOL) (≥ 99.5% purity, MilliporeSigma) and 1,2 dimethoxyethane (DME) (anhydrous, 99.5%, inhibitor-free, Sigma-Aldrich). For the gelled electrolyte cells prepared, the base liquid electrolyte solvent used was 1 M LiTFSI (99.95% trace metal basis, Sigma-Aldrich) and 0.1 M $LiNO_3$ (99.99% trace metals basis, Sigma – Aldrich) in a 1:1 volumetric ratio of 1,3 dioxolane (DOL) (≥ 99.5% purity, MilliporeSigma) and 1,2 dimethoxyethane (DME) (anhydrous, 99.5%, inhibitor-free, Sigma-Aldrich).

To make POSS gelled electrolyte cells, the base solution was mixed with 5 wt% polyhedral oligomeric silsesquioxane methacrylate (POSS-MA, ceramic-based) (99.99% pure, Sigma-Aldrich), a cage-like crosslinker, and 0.5 wt% AIBN were used. FTIR analysis was done to optimize the crosslinking density and it is observed that at 5% concentration of POSS-MA, the peak due to the C=C bond vanishes suggesting complete crosslinking.

The electrolyte added to the cells was weighted on sulfur basis, and the general electrolyte-to-sulfur ratio was maintained at 20 μL per mg of sulfur (unless mentioned otherwise). The fabrication process for all the electrolyte was essentially the same, however, for the gel electrolyte cells, a 30 min heat treatment at 70^{o}C to the prepared cells was carried out after resting the cells for 3 hours to gel the electrolyte *in situ.* The

entire electrolyte preparation process was conducted in an Argon environment glovebox with oxygen levels of lower than 0.1 ppm.

3.3.3 Coin Cell Assembly

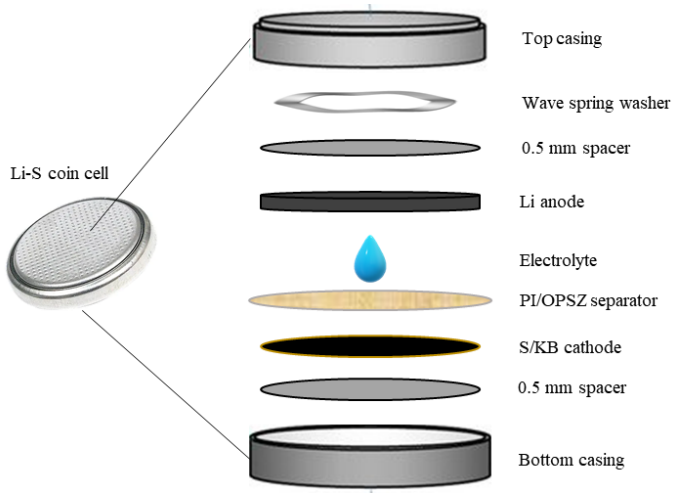

Figure 3.4: Schematic for cell setup using PI/OPSZ separators

The 2032 CR coin cells were constructed in an oxygen-free, argon environment glovebox. The construction for these cells was done using the following components in order: (1) 2032 CR coin cell bottom; (2) 0.5 mm thick stainless steel spacer (16 mm diameter); (3) Punched S/KB Cathode discs with Al current collector (16 mm); (4) Celgard 2400 separator (19 mm diameter) or PI/OPSZ separator (19 mm diameter); (5) Electrolyte added at ratio of 20 µL per mg of sulfur (unless mentioned otherwise); (6) Punched Li anode discs (0.75 mm thick, 16 mm diameter); (7) 0.5 mm thick stainless steel spacer (16 mm diameter); (8) Wave spring washer. Once the assembly was finished, the coin cells were, first, hand crimped using a manual hand crimper in the Ar environment glovebox. Then, later, the cells were re-crimped using MTI digital pressure controlled electric crimper at 0.8 T pressure which seals the coin cell.

3.3.4 Electrochemical Measurements

The galvanostatic charge-discharge measurements were performed using MTI Corporation Battery Analyzer at room temperature using BTSDA (Battery Testing System Data Analyzer) software for cycling and rate capability tests. Each test began with resting the cells for 6 hours and cycling for first 5 cycles at a formation rate of 0.1 C (1C = 1675 mAh/g_S) in the range of 1.8-2.8 V versus Li^+/Li.

For cycling tests, the cells were run for 5 cycles at 0.1 C rate and then the next 200 cycles at 0.2 C rate (or till end of cell life). Each charge and discharge step had an intermediate 5-minute resting step.

For rate capability tests, the cells were run for 5 cycles at 0.1 C rate (formation step) and then followed by 10 charge/discharge cycles at 0.2C and 0.3C and finally back to 5 cycles at 0.1C. All discharge capacities and current densities were standardized based on active sulfur mass in the cathode. Current densities were set according to a sulfur theoretical specific capacity of 1675 mAh/g.

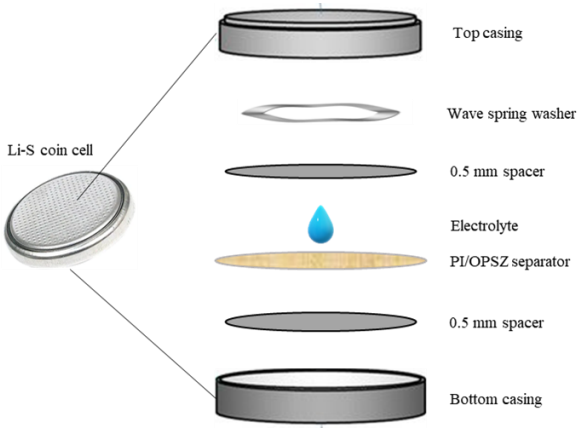

Figure 3.5: Schematic diagram for symmetric cells using PI/OPSZ separators

Ionic conductivity was measured using electrochemical impedance spectroscopy (EIS, Parstat 4000, Princeton Applied Materials). For these tests, the separators were soaked with 40 μL of electrolyte to mimic battery cell conditions and sandwiched between two stainless steel discs in a CR2032 coin cell. A frequency range from 10 kHz to 1 Hz was applied with an AC amplitude of 10 mV. Ionic conductivity was calculated according to the equation (C. Zheng et al., 2021):

$$Conductivity\ (\sigma) = \frac{d}{R_b \times A}$$

Where d is the thickness of the separator, R_b is the bulk resistance, and A is the surface area of the stainless-steel electrode (1.96 cm^2). R_b is defined as the high frequency intercept of the real axis.

3.3.5 Other characterization techniques

Dimensional thermal stability of the gelled separator system was determined with a shrinkage test by placing them in air convection oven for 1 hour at various temperatures been 100ºC – 600ºC. Thermal shrinkage of the separators (6 x 6 cm) was observed by measuring the dimensional change after heat treatment at varied temperatures. The shrinkage was measured using:

$$Shrinkage\ (\%) = \frac{A_i - A_f}{A_i} \times 100\%$$

Where, A_i and A_f are the initial and final areas of the separators, respectively.

Flammability of the separator materials was tested by soaking each membrane in electrolyte and lighting it with a butane torch.

Electrolyte uptake was determined by soaking the separators in electrolyte for two hours, and calculating the mass change with the equation:

$$Electrolyte\ Uptake\ (\%) = \frac{W_f - W_i}{W_i} \times 100$$

Where, W_i and W_f are the masses of the separator before and after soaking in liquid electrolyte for 2 hours, respectively.

The porosity of the separators was calculated by the *n*-butanol uptake method using the equation:

$$Porosity\ (\%) = 1 - \frac{M}{\rho_{PI} \times V}$$

Where, M is the separator weight, ρ_{PI} is the density of PI (P84) separators, and V is the apparent volume of the separator.

Scanning Electron Microscopy (Zeiss Gemini 500) was carried at an accelerating voltage of 3keV. The pore size distribution was done using image analysis of the SEM images.

3.3.6 PI/OPSZ separators used in the study.

For the purpose of the study, a series of separators with varying concentrations of PI & OPSZ components were analyzed. However, for the purpose of showing a performance trend based on the characteristics of the separators, in this thesis, the analysis results for 3 different separators with distinctly different compositions has been reported. The separators used in this study were commercially fabricated using air-controlled

electrospray technique by SNT Corp., South Korea. These separators had varying concentrations of PI, OPSZ and ionic dispersant sodium dodecyl sulfate (SDS).

The three separators used in the study were:

1) Separator 1:

PI/OPSZ: 92/8 %wt. Thickness: 19.3 μm

Heat Treatment: 300^{o}C for 4 hours; Roll Calendared: 180^{o}C at 0.5 m/min

2) Separator 2:

PI/OPSZ/SDS: 91.29/7.88/0.83 %wt. Thickness: 22.1 μm

Heat Treatment: 300^{o}C for 4 hours; Roll Calendared: 170^{o}C at 0.4 m/min

3) Separator 3:

PI/OPSZ/SDS: 85.94/11.72/2.34 %wt. Thickness: 23.2 μm

Heat Treatment: 300^{o}C for 4 hours; Roll Calendared: 170^{o}C at 0.3 m/min

3.4 Results and Discussions

3.4.1 Preliminary Performance Verification

In order to ensure that the PI-OPSZ separators are compatible with the Lithium Sulfur technology, a few initial verification tests were performed. First, the rate capability of the cells with liquid electrolyte was tested. Then, to test the compatibility with the gel electrolyte, the PI-OPSZ separators were gelled with POSS crosslinker. Finally, the first cycle discharge curve was analyzed. Figures 3.6, 3.7 and 3.8 show the result obtained from the verification step.

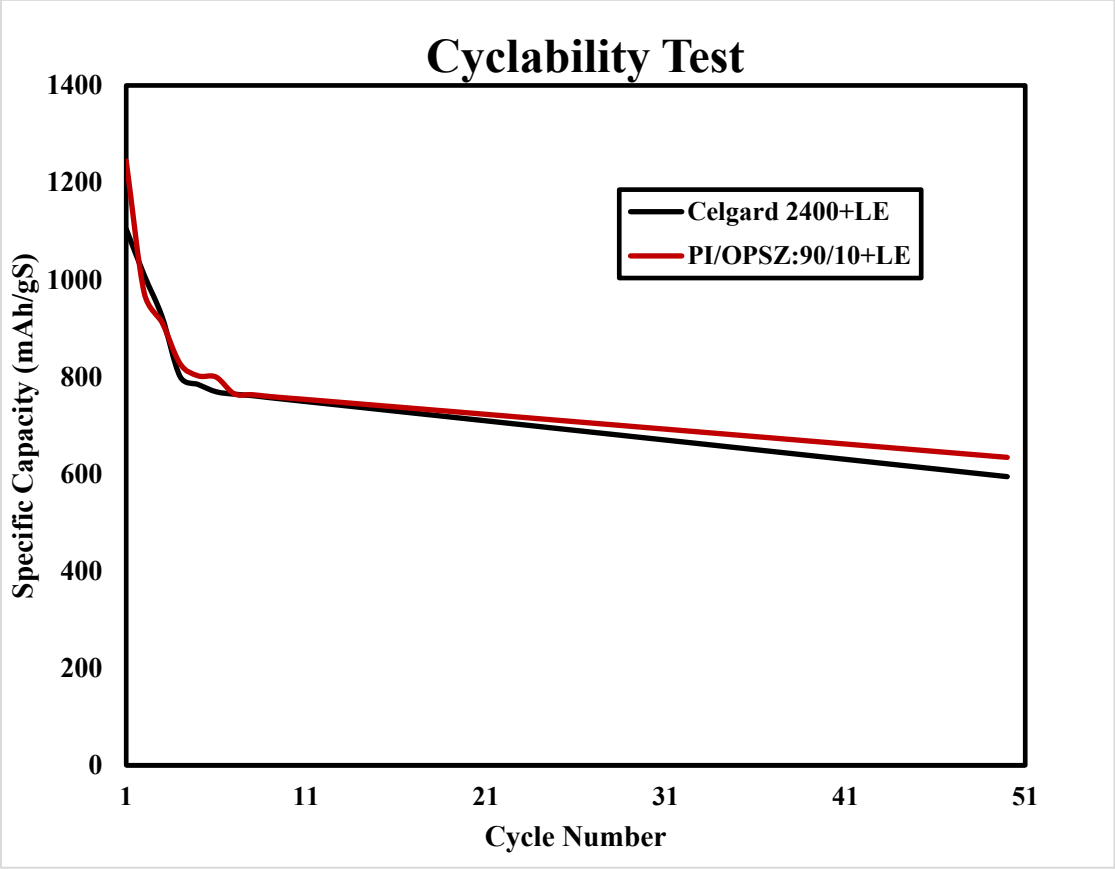

Figure 3.6: Cyclability test analysis between Celgard 2400 and PI/OPSZ separators with liquid electrolyte

Figure 3.6 shows the cyclability test comparison between Celgard 2400 and PI/OPSZ separators with liquid electrolyte. From the analysis, it is evident that PI/OPSZ separators showed a marginal improvement in capacity and that the cells fabricated with PI/OPSZ separators displayed higher capacity retention after 50 cycles – 86.0% for PI/OPSZ separator and 79.2% for Celgard separator.

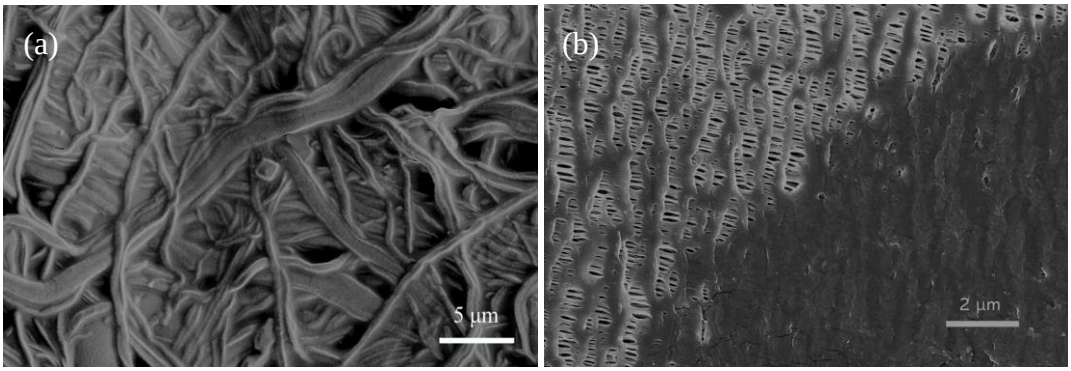

Figure 3.7: SEM images for POSS gelled: (a) PI/OPSZ separator, (b) Celgard 2400 separator

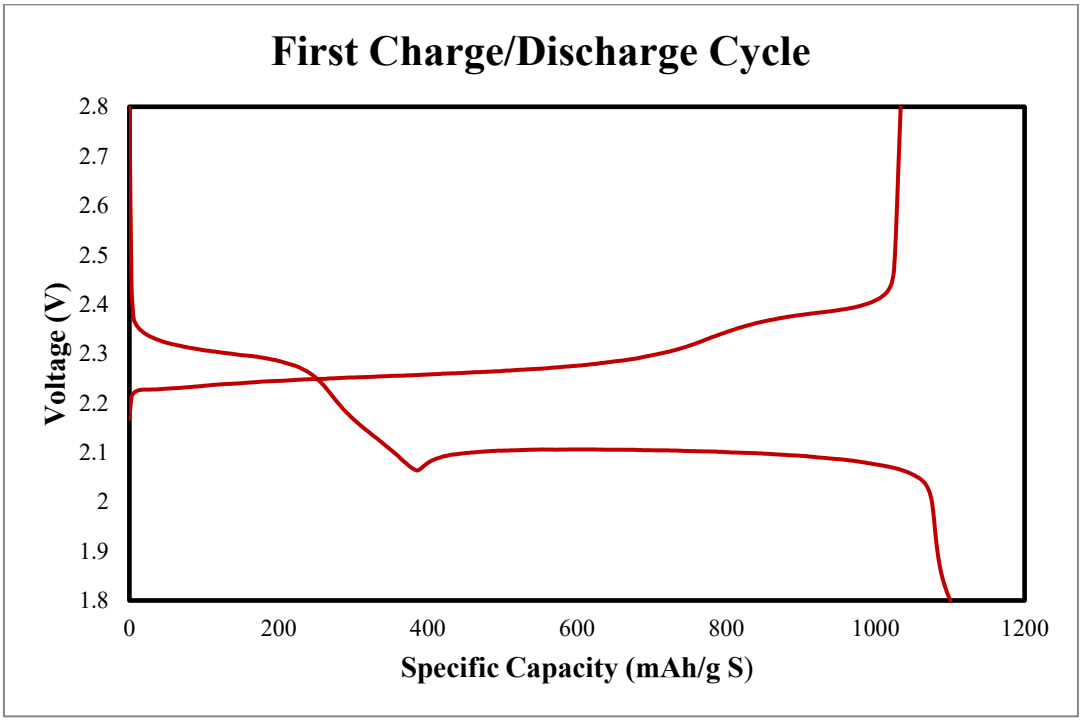

Figure 3.8: First Cycle Charge-Discharge characteristic curves (Voltage v/s Specific Capacity (mAh/gS)

Figure 3.7 shows the SEM images post gelation of the 2 separators – PI/OPSZ and Celgard 2400. From the images, it was clear that PI/OPSZ separators show much better wettability and compatibility with the gel electrolyte as compared to Celgard 2400 wherein, the gelation was seen to be incomplete due to the poor wettability of the polyolefin strands.

Further, it was also observed that the cell made using PI/OPSZ separator with liquid electrolyte showed a higher initial coulombic efficiency (88.4%) as compared to Celgard separator (~77.3%) as seen in figure 3.8.

Thus, it was verified that the PI/OPSZ separators showed better performance with liquid electrolyte – had a high capacity retention, high coulombic efficiency and showed much better gelation characteristics. This confirmed the potential of PI/OPSZ separators to be used in the lithium sulfur cell.

3.4.2 Morphology Analysis

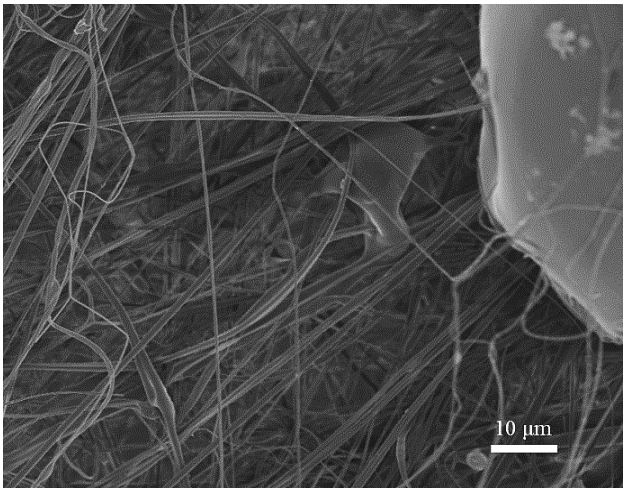

Figure 3.9: SEM image of Separator 1 (with visible beading)

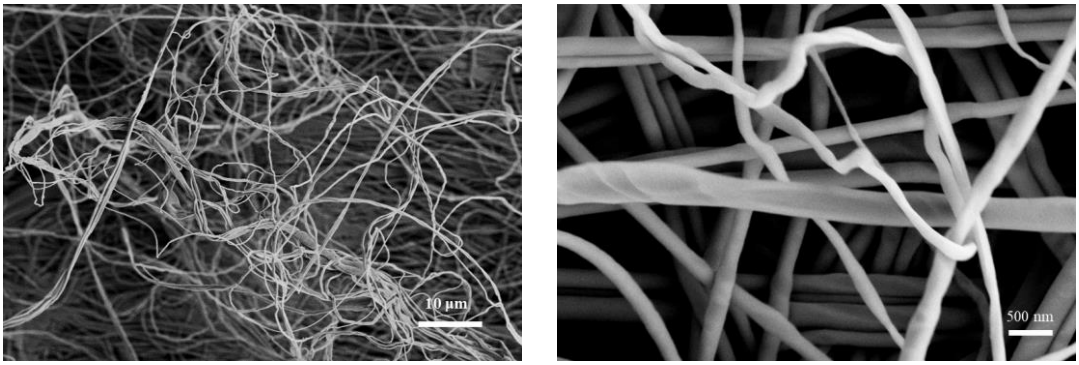

Figure 3.10: SEM images of Separator 2 (visible improvement in morphology due to SDS)

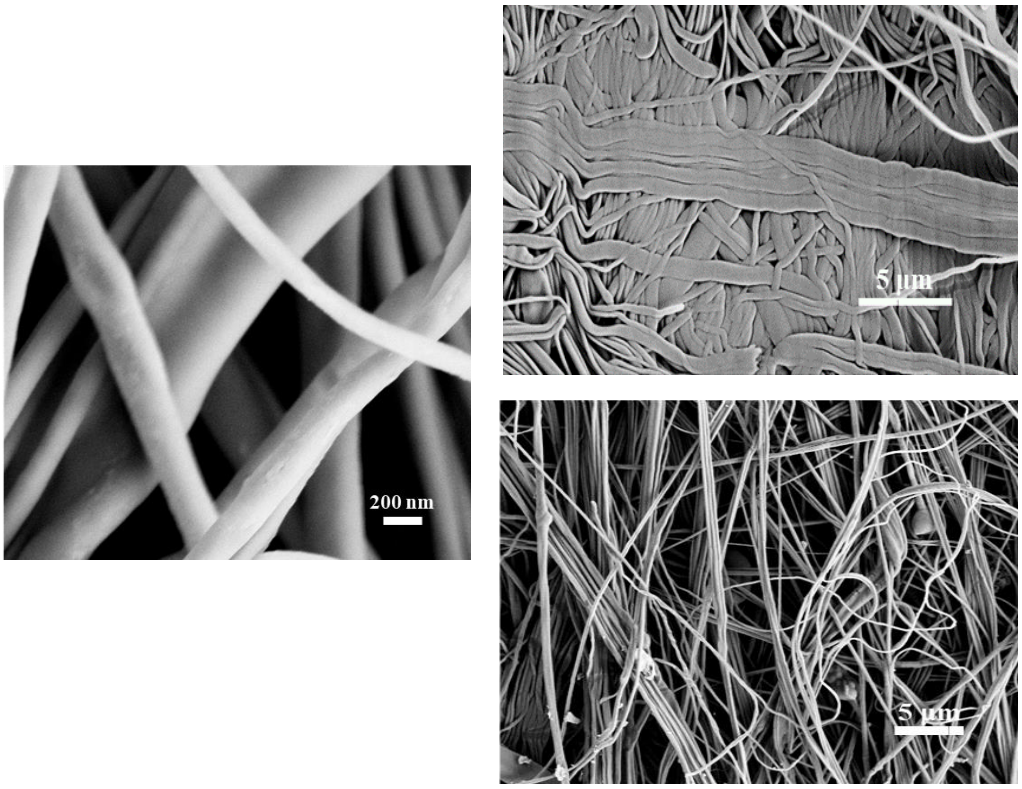

Figure 3.11: SEM images for Separator 3 (with best morphology and uniformity in strand diameter; impact of roll calendaring visible)

The SEM images (Figure 3.9, 3.10, 3.11) clearly show the impact of varying concentrations of the ionic dispersant (SDS) on the overall morphology and uniformity of the electrospun fibers. In figure 3.9, i.e., separator 1, a significant amount of bead formation is visible, and the fiber diameter is also not uniform – this leads to a loosely packed fiber mat system which is prone to peeling issues and severe degradation on handling.

As the concentration of SDS is increased, we saw a marked improvement in the fiber morphology and the dispersant even helps mitigate the formation of bead structures while electrospinning – significantly improving the separator robustness. Figure 3.10 (Separator 2) shows much lesser beads than Figure 3.9 (Separator 2), and Figure 3.11 (Separator 3) shows almost complete bead elimination in the strands.

Further, it can also be observed that the strands become thinner on addition of the dispersant – an expected outcome of the ionic dispersant in the electrospinning process (Javed et al., 2018). The impact of roll calendaring is visible in Figure 3.11.

3.4.3 Porosity Analysis

Table 3.1: Separator Porosity Analysis Results (n-butanol uptake test, SEM image analysis)

Separator	**Porosity**	**Surface Pore-size Distribution**
Celgard 2400	41	145-230 nm
PI/OPSZ: 92/8	54.4	505 – 765 nm
PI/OPSZ/SDS: 91.29/7.88/0.83	62.3	523 – 734 nm
PI/OPSZ/SDS: 85.94/11.72/2.34	61.8	587 – 754 nm

To understand the structural properties of PI/OPSZ separators and to detect possible trends, a porosity analysis using n-butanol uptake test and SEM image analysis was carried out. Table 3.1 reports the results for the porosity analysis comparison between the 3 PI/OPSZ separators and the Celgard 2400 separator.

The analysis conclusively proves that the PI/OPSZ separators exhibit a much higher porosity than compared to Celgard 2400. Additionally, the pore size distribution of the PI/OPSZ systems is wider – an expected outcome due to the inherent irregular nature of the electrospun fibers. Further, though PI/OPSZ separators exhibit a wider pore size distribution, the distribution becomes narrower on addition of SDS, indicating a much better morphology control on addition of SDS. It was also observed that the Separator 3 had the largest minimum pore size, this can be explained due to the impact of repulsive forces between the fibers during electrospinning caused due to the ionic dispersant.

3.4.4 Flammability & Thermal Tolerance Test

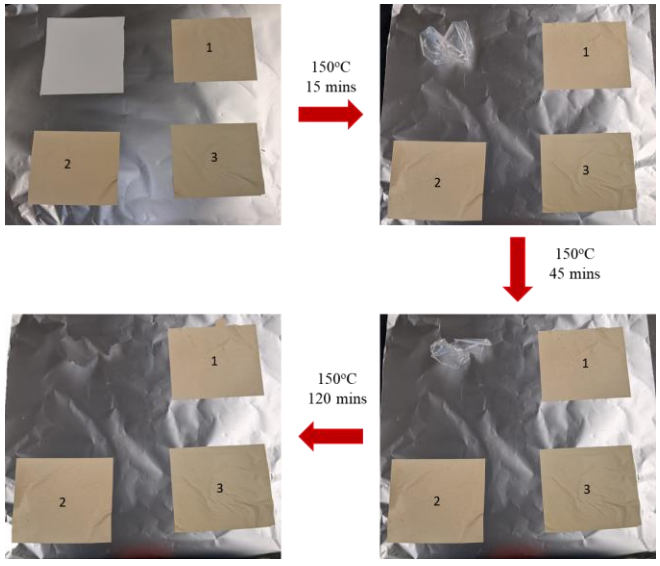

Figure 3.12: Qualitative analysis of elevated temperature stability test (Clockwise from top left: Celgard 2400, PI/OPSZ separator 1, separator 2 and separator 3)

Figure 3.12 shows the impact of high temperature on the separators. PI/OPSZ separators show much superior tolerance to high temperatures of about 150^{o}C, whereas in merely 15 minutes, the Celgard 2400 separator is destroyed. Further, as seen in Figure 3.13 PI/OPSZ separators show superior flame resistance unlike Celgard 2400 separators which burnt away almost immediately (See Chapter 2).

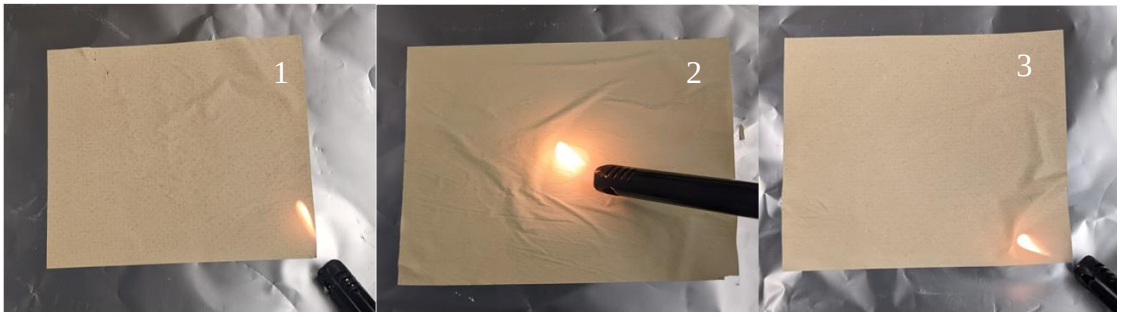

Figure 3.13: Flame tolerance test for PI/OPSZ separators.

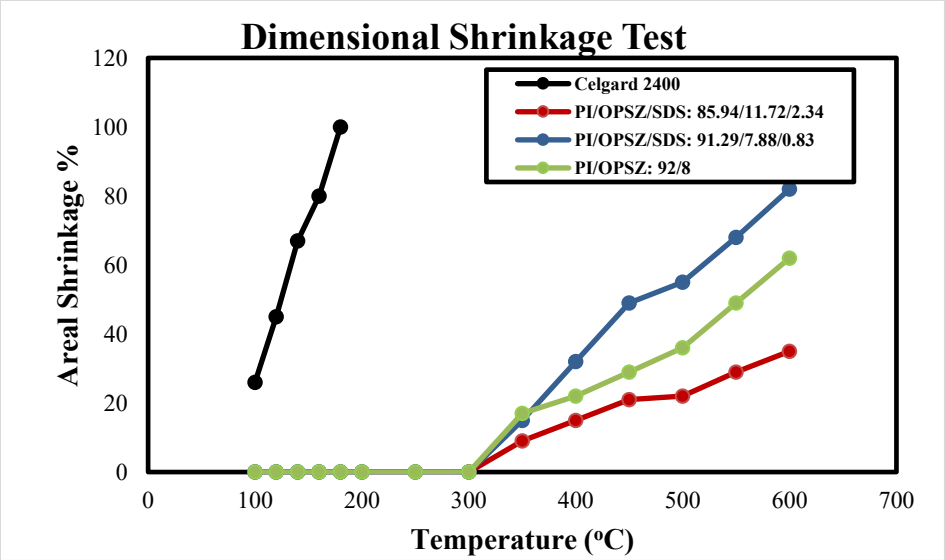

Figure 3.14: Results for dimensional stability test of the separator systems

From the dimensional stability test results (shown in fig. 3.14), it was observed that the areal shrinkage at elevated temperature reduced with increase in the OPSZ i.e. the ceramic content.

3.4.5 Wetting Analysis and Electrolyte Uptake

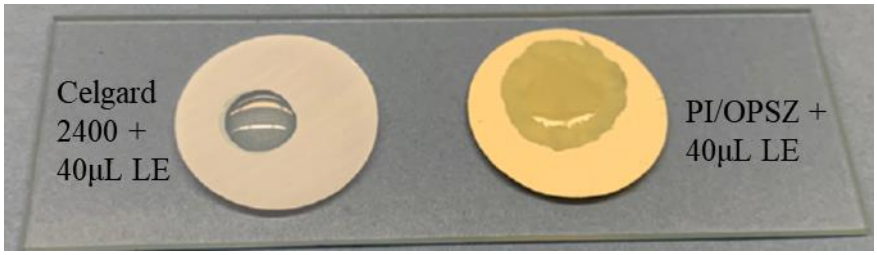

Figure 3.15: Result of electrolyte drop wetting test on the separators.

Table 3.2: Electrolyte uptake performance of the separators.

Separator	**Electrolyte Uptake (%)**
Celgard 2400	196
PI/OPSZ: 92/8	1064
PI/OPSZ/SDS: 91.29/7.88/0.83	960
PI/OPSZ/SDS: 85.94/11.72/2.34	1147

**Values averaged for 5 sets of each cell type*.

Figure 3.15 clearly shows the vast difference in wettability of the separator systems. PI/OPSZ separators are organophilic and absorb the electrolyte readily, whereas the Celgard 2400 separators are organophobic and the electrolyte remains as a drop with minimal wetting displayed.

From the electrolyte uptake test results shown in table 3.2, it can be seen that PI/OPSZ separators show 5 times the uptake potential as compared to Celgard 2400 and hence, are much more compatible with the lithium sulfur electrolyte.

3.4.6 Ionic Conductivity

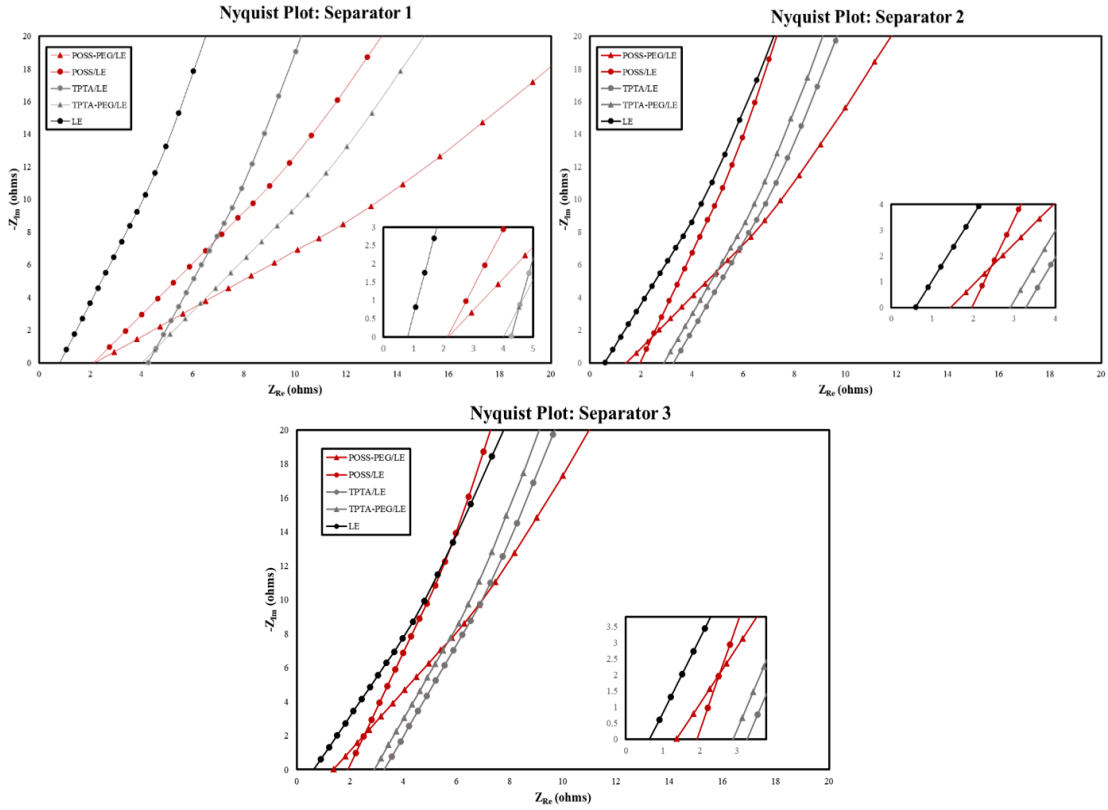

Figure 3.16: Nyquist plots from EIS analysis of stainless steel symmetric cells.

Table 3.3: Ionic Conductivity data for all the separator/electrolyte combinations

Separator	**Ionic Conductivity (mS/cm)**				
	POSS - PEG/LE	**POSS/LE**	**TPTA/LE**	**TPTA - PEG/LE**	**LE**
Celgard 2400	0.425	0.364	0.138	0.075	0.709
PI/OPSZ: 92/8	0.615	0.590	0.295	0.325	1.678
PI/OPSZ/SDS: 91.29/7.88/0.83	0.890	0.679	0.393	0.472	2.225
PI/OPSZ/SDS: 85.94/11.72/2.34	0.910	0.682	0.393	0.469	2.34

Figure 3.16 shows the Nyquist plots obtained from EIS analysis of the symmetric cells with PI/OPSZ separators. This data was used to evaluate the ionic conductivity of the different electrolyte/separator combinations reported in Table 3.2.

From the conductivity results, it is evident that PI/OPSZ separators show much superior ionic conductivity with all electrolyte configurations than Celgard. It was also observed that the ionic conductivity improves with increasing ceramic content with Separator 3 having the highest ionic conductivity.

Most of the characterization techniques relevant to battery systems show positive trends for the PI/OPSZ separators coupled with the gel electrolyte as compared to the Celgard system and hence, the cell performance of these separators was tested.

3.4.7 Cell Performance Analysis

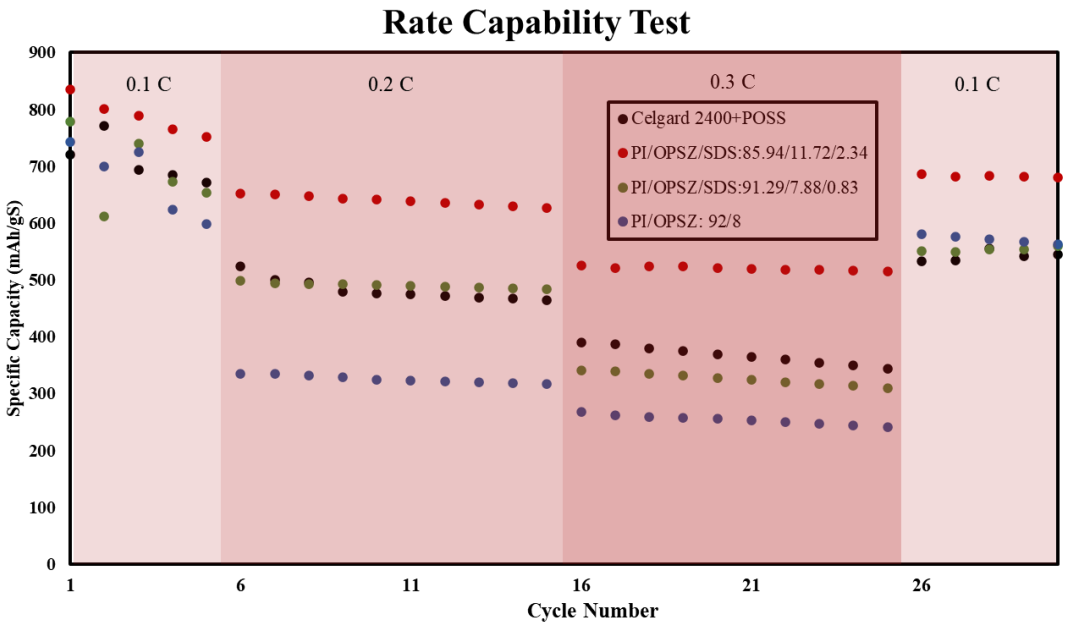

Figure 3.17: Rate capability testing cells made of POSS gelled Celgard 2400 and PI/OPSZ separators.

For the rate capability test, the cells were run for 5 initial cycles at 0.1 C, then 10 cycles for 0.2 C and 0.3 C and finally 5 additional cycles at 0.1C.

It was observed that Separator 3 displayed the maximum discharge capacity with POSS; the discharge being significantly greater than the Celgard 2400/POSS/LE reference cells.

It was observed that the specific discharge capacity improved with rising ceramic content owing to the improvement in the ionic conductivity. This clearly shows that PI/OPSZ separators coupled with gel electrolyte can be tailored to perform much better than POSS gelled Celgard separators.

However, an important observation was the fact that the capacity for separator 1 and 2 was lower than that for Celgard 2400 despite having much higher ionic conductivity. In order to further investigate this observation, the first cycle discharge curves were analyzed.

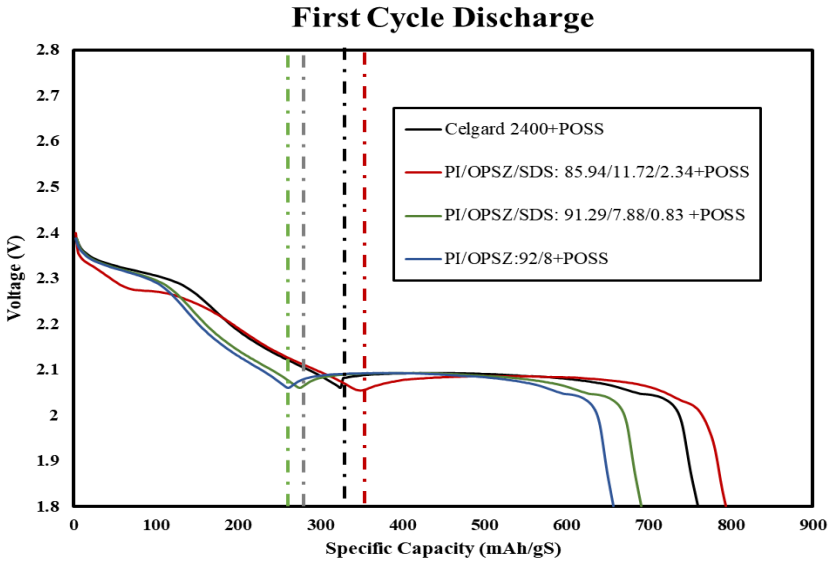

Figure 3.18: First cycle discharge profiles for gelled separator cells.

Figure 3.18 displays the first cycle discharge profiles of the cells with POSS-gelled separators. From the profiles, it could be confirmed that the separator 3 showed maximum first plateau discharge capacity and hence, the maximum overall capacity. Whereas, separator 1 showed the least first plateau discharge capacity and hence, performed the poorest. This reiterates the direct impact of trapping polysulfides during discharge of the cell on its performance.

The polysulfide losses in separator 1 was higher than Celgard 2400 – this could be partly explained due to the uneven, beady fiber morphology. Since we see improvement in the first plateau capacity and overall capacity for separator 2 and even more so for separator 3. It can be concluded that the morphology of the electrospun fibers lays a critical role in its cell performance. As the morphology of the fibers in the separator improves, so does the cell performance.

3.4.8 Scopes for improvement of separators: Postmortem Analysis.

Though, through the characterization and cell performance tests, we have shown that gelled PI/OPSZ separators show superior performance than their Celgard counterpart, the PI/OPSZ system it currently far from perfect.

The PI/OPSZ system still shows certain reliability issues and is plagued with a short cell life at high C rate cycling over 0.5 C. Out of the batch of 25 gelled-separator 3 cells that were fabricated, only 6 cells were able to cycle at 0.5 C and 1 C, and none were able to cycle at 2C.

Additionally, the cells would run into infinite charging cycles. This could be explained by the fact that the dissolved polysulfides potentially are able to diffuse faster through the highly porous non-woven separators than the narrow slit-like pores of Celgard 2400. This high-rate shuttling of the polysulfides led to an "infinite charge" where the cell voltage cannot reach the upper cutoff due to continuous oxidation of polysulfide species.

To investigate the issue of lack of reliability of these cells, extensive post-mortem analysis was carried. Some of the observations have been highlighted in this section.

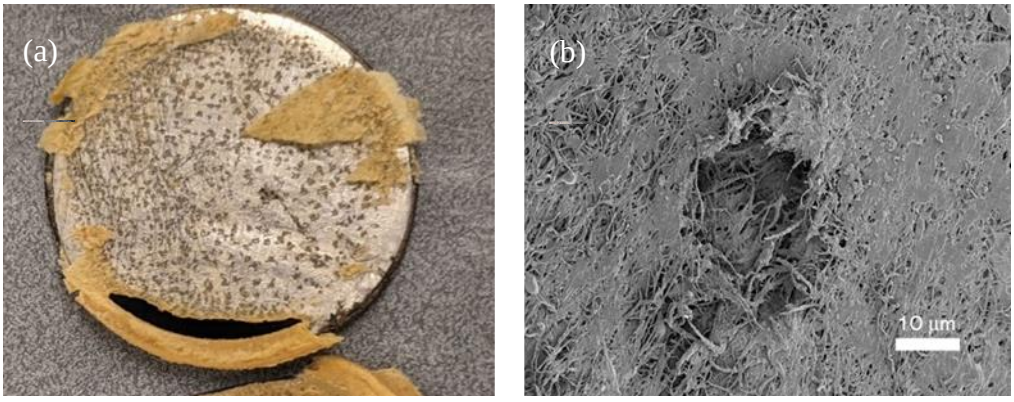

Figure 3.19: (a) Anode surface showing dendritic growth after cell post-mortem. (b) Dendritic lump impression on anode side of the separator.

First, for many cells that died prematurely, the anode surface showed extensive dendritic formations. Figure 3.19 shows the observed dendritic growth on the anode surface and the corresponding dendritic lumps on the separator. This lithium dendritic formation led to cell shorting and hence, the caused the cells to die prematurely. Due to the lack of sufficient mechanical strength displayed by the non-woven fibrous electrospun separators, the dendritic formations are able to easily penetrate them and cause the cell to short. In order to mitigate this issue, the mechanical strength of the PI/OPSZ separators needs to be enhanced.

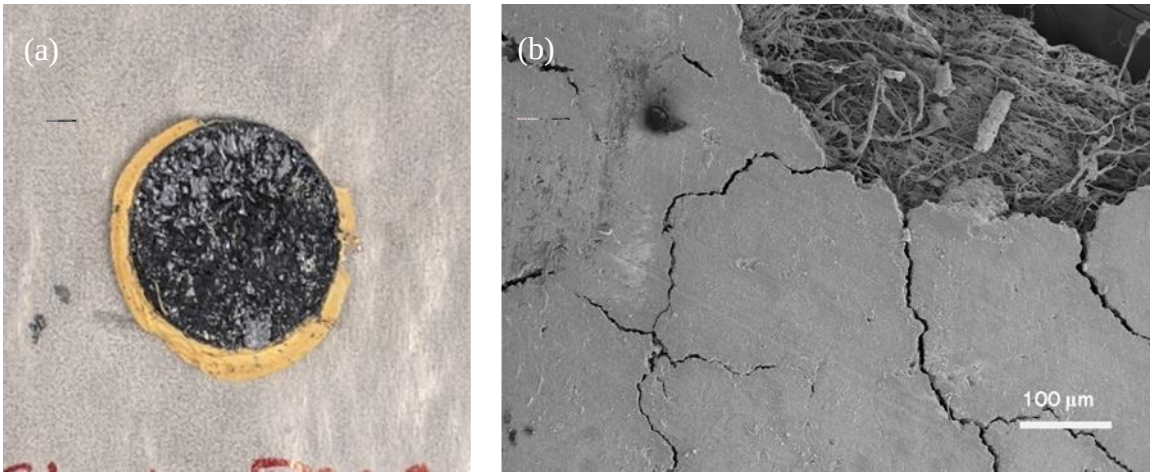

Figure 3.20: (a) Separator showing cathodic lamination post cell failure. (b) SEM image of the cathodic lamination onto the separator surface.

Second, a significant amount of cathodic lamination on the separator was observed. The hypothesis is that due to the high electrolyte uptake of the separators, significant capillary pressure develops on the cathodic surface which causes the delamination if the cathode. This phenomenon is caused due to the inherent fibrous, porous structural properties of the non-woven separator mat. Possible research in polymer interlayers may help alleviate this issue.

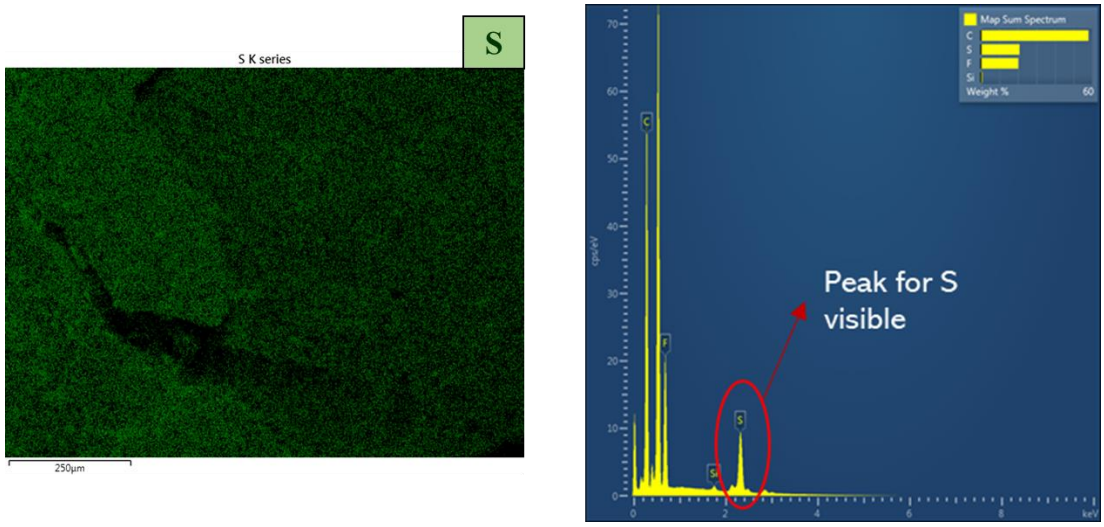

Figure 3.21: EDS analysis of anode surface post cell failure.

Finally, on carrying out the EDS analysis of the anode from a cell run at 1C cycling rate, we see a S peak which is higher than that observed for the background LiTFSI molecule. This shows the presence of sulfur compounds on the anode – indicating high polysulfide shuttling losses at high C rate cycling. At high C rate cycling, the polysulfide entrapping ability of the separators is not sufficient to arrest shuttling and hence, there needs to a study on optimizing the balance between the porosity and thickness of the membrane and the ionic conductivity to ensure maximum trapping of the soluble polysulfide intermediates.

Thus, these observations prove that despite the fact the PI/OPSZ separators show much superior performance than Celgard 2400, the PI/OPSZ technology, as it stands today, is far from perfect and there are several avenues of possible improvements.

3.5 Conclusion

From the synergy studies, we can conclude that PI/OPSZ separators show better compatibility and wettability to Li-S electrolyte than Celgard 2400 owing to the fibrous and porous morphology of the non-woven separators. They show much better ionic conductivity for all liquid electrolyte and gelled electrolyte combinations and the ionic conductivity was observed to improve with increase in the ceramic content (OPSZ). Thus, it can be concluded that the PI/OPSZ fibers can be tailored to optimize the ionic conductivity.

Further, it can be concluded that morphology of the fibers has a significant effect on the cell performance and tailoring the morphology can help achieve high discharge capacities with better capacity retention over long cycling.

PI/OPSZ separators also show much higher tolerance to heat and flame as compared to Celgard 2400 and hence significantly enhance the heat tolerance of the cell. From the postmortem analysis of the cells, it was concluded that the fibrous nature of the separators lacks sufficient mechanical strength to combat Li dendritic formation and the porous geometry leads to cathodic delamination and polysulfide shuttling at high C rate cycling.

Thus, it can be concluded that the PI/OPSZ separators exhibit good synergy with the gel electrolyte and are promising candidates to be used as separators in the lithium sulfur cell. That said, despite the superior performance, the path to commercialization for PI/OPSZ separators in the lithium sulfur battery is distant and needs significant amount of research.

3.6 Future Work

Reiterating from the conclusion in the previous section, despite the high performance displayed by the PI/OPSZ separator systems, there are still several opportunities of improving the technology to cover the current limitations of the PI/OPSZ system and improve their performance in the Li-S cell.

First, on analysis of discharge profiles for cells that failed to operate, many cells showed complete absence of the first plateau and/or showed irregular spikes in voltage levels profiles while charging suggesting towards the presence of some side-reactions. These could have been cause due to some unreacted functional groups left on the separator fibers. We plan to increase the duration and amount of heat treatment on the fibers to ensure complete removal of the unreacted functional groups and then evaluate the difference in cell performance.

Since, it has been established that the separator morphology and characteristics is critical to cell performance, a possible extension to this technology may be to test the impact of layered electrospinning of different polymer ceramic precursors to specifically tailor the characteristics of the fibers.

Further, other separator systems developed by our group – PI/Al and PI/PSSQ have shown good mechanical properties and superior cell performance respectively in Li-based battery systems. As future work, we plan to test the impact of double stacking the separators with PI/Al separators and PI/PSSQ separators produced in the group.

Finally, the strength of the gelled electrolyte could be exploited to improve the mechanical strength of the separators. To do so we plan to increase the crosslinking density of the gel electrolyte and analyze the subsequent change in performance.

3.7 References

Amine, K., Kanno, R., & Tzeng, Y. (2014). Rechargeable lithium batteries and beyond: Progress, challenges, and future directions. *MRS Bulletin*, *39*(5), 395–401. https://doi.org/10.1557/mrs.2014.62

Angulakshmi, N., & Stephan, A. M. (2015). Efficient electrolytes for lithium-sulfur batteries. In *Frontiers in Energy Research* (Vol. 3, Issue MAY, p. 17). Frontiers Media S.A. https://doi.org/10.3389/fenrg.2015.00017

Arora, P., & Zhang, Z. (2004). *Battery Separators*. https://doi.org/10.1021/cr020738u

Barchasz, C., Leprêtre, J. C., Alloin, F., & Patoux, S. (2012). New insights into the limiting parameters of the Li/S rechargeable cell. *Journal of Power Sources*, *199*, 322–330. https://doi.org/10.1016/j.jpowsour.2011.07.021

Birk, J. R., & Steunenberg, R. K. (1974). CHEMICAL INVESTIGATIONS OF LITHIUM-SULFUR CELLS. *Adv Chem Ser*, *140*, 186–202. https://doi.org/10.1021/ba-1975-0140.ch012

Bruce, P. G., Freunberger, S. A., Hardwick, L. J., & Tarascon, J. M. (2012). LigO2 and LigS batteries with high energy storage. In *Nature Materials* (Vol. 11, Issue 1, pp. 19–29). Nature Publishing Group. https://doi.org/10.1038/nmat3191

Cao, R., Xu, W., Lv, D., Xiao, J., & Zhang, J. G. (2015). Anodes for Rechargeable Lithium-Sulfur Batteries. In *Advanced Energy Materials* (Vol. 5, Issue 16, p. 1402273). Wiley-VCH Verlag. https://doi.org/10.1002/aenm.201402273

Carlin, J. M., Joo, Y. L., & Smith, S. (2018). *Hybrid separators and the manufacture thereof*.

Chen, R., Zhao, T., & Wu, F. (2015). From a historic review to horizons beyond: Lithium-sulphur batteries run on the wheels. In *Chemical Communications* (Vol. 51, Issue 1, pp. 18–33). Royal Society of Chemistry. https://doi.org/10.1039/c4cc05109b

Cheng, X., Pan, J., Zhao, Y., Liao, M., & Peng, H. (2018). Gel Polymer Electrolytes for Electrochemical Energy Storage. In *Advanced Energy Materials* (Vol. 8, Issue 7). Wiley-VCH Verlag. https://doi.org/10.1002/aenm.201702184

Colthorpe, A. (2020, July 7). *Solar farm fitted with batteries to meet grid output control requirements goes online in Japan | Energy Storage News*. https://www.energy-storage.news/news/solar-farm-fitted-with-batteries-to-meet-grid-output-control-requirements-g

Colthorpe, A. (2021, March 23). *Wisconsin utilities plan 250MW solar project with 75MW of battery storage | Energy Storage News*. https://www.energy-storage.news/news/wisconsin-utilities-plan-250mw-solar-project-with-75mw-of-battery-storage

COMSOL AB. (n.d.). *COMSOL Multiphysics® v. 5.5.* Retrieved July 27, 2020, from www.comsol.com

Croce, F., Appetecchi, G. B., Persi, L., & Scrosati, B. (1998). Nanocomposite polymer electrolytes for lithium batteries. *Nature 1998 394:6692*, *394*(6692), 456–458. https://doi.org/10.1038/28818

Ding, F., Xu, W., Graff, G. L., Zhang, J., Sushko, M. L., Chen, X., Shao, Y., Engelhard, M. H., Nie, Z., Xiao, J., Liu, X., Sushko, P. v., Liu, J., & Zhang, J. G. (2013). Dendrite-free lithium deposition via self-healing electrostatic shield mechanism. *Journal of the American Chemical Society*, *135*(11), 4450–4456. https://doi.org/10.1021/ja312241y

Ding, L., Xu, G., Ge, Q., Wu, T., Yang, F., & Xiang, M. (2017). Effect of Fumed SiO 2 on Pore Formation Mechanism and Various Performances of β - i PP Microporous Membrane Used for Lithium-ion Battery Separator. *Chinese Journal of Polymer Science 2017 36:4*, *36*(4), 536–545. https://doi.org/10.1007/S10118-018-2029-7

Ding, N., Zhou, L., Zhou, C., Geng, D., Yang, J., Chien, S. W., Liu, Z., Ng, M. F., Yu, A., Hor, T. S. A., Sullivan, M. B., & Zong, Y. (2016a). Building better lithium-

sulfur batteries: From LiNO2 to solid oxide catalyst. *Scientific Reports*, *6*(1), 1–10. https://doi.org/10.1038/srep33154

Ding, N., Zhou, L., Zhou, C., Geng, D., Yang, J., Chien, S. W., Liu, Z., Ng, M.-F., Yu, A., Hor, T. S. A., Sullivan, M. B., & Zong, Y. (2016b). Building better lithium-sulfur batteries: from LiNO 3 to solid oxide catalyst. *Scientific Reports 2016 6:1*, *6*(1), 1–10. https://doi.org/10.1038/srep33154

Ding, Y., Hou, H., Zhao, Y., Zhu, Z., & Fong, H. (2016). Electrospun polyimide nanofibers and their applications. *Progress in Polymer Science*, *61*, 67–103. https://doi.org/10.1016/J.PROGPOLYMSCI.2016.06.006

Dunn, B., Kamath, H., & Tarascon, J. M. (2011). Electrical energy storage for the grid: A battery of choices. In *Science* (Vol. 334, Issue 6058, pp. 928–935). American Association for the Advancement of Science. https://doi.org/10.1126/science.1212741

Feng, X., Ouyang, M., Liu, X., Lu, L., Xia, Y., & He, X. (2018). Thermal runaway mechanism of lithium ion battery for electric vehicles: A review. *Energy Storage Materials*, *10*, 246–267. https://doi.org/10.1016/J.ENSM.2017.05.013

Girishkumar, G., McCloskey, B., Luntz, A. C., Swanson, S., & Wilcke, W. (2010). Lithium-air battery: Promise and challenges. *Journal of Physical Chemistry Letters*, *1*(14), 2193–2203. https://doi.org/10.1021/jz1005384

Halim, W., Lee, J. H., Park, S. M., Zhang, R., Sarkar, S., O'Neil, T., Chiang, Y. C., & Joo, Y. L. (2019). Directly deposited binder-free sulfur electrode enabled by air-controlled electrospray process. *ACS Applied Energy Materials*, *2*(1), 678–686. https://doi.org/10.1021/acsaem.8b01694

Hasanuzzaman, M., Zubir, U. S., Ilham, N. I., & Seng Che, H. (2017). Global electricity demand, generation, grid system, and renewable energy polices: a review. *WIREs Energy and Environment*, *6*(3), e222. https://doi.org/https://doi.org/10.1002/wene.222

Herbert, D., & Ulam, J. (1958). *United States Patent Office l 3,043,896 ELECTRIC DRY CELLS AND STORAGE BATTERES*.

Höök, M., & Tang, X. (2013). Depletion of fossil fuels and anthropogenic climate change-A review. *Energy Policy*, *52*, 797–809. https://doi.org/10.1016/j.enpol.2012.10.046

Javed, K., Krumme, A., Viirsalu, M., Krasnou, I., Plamus, T., Vassiljeva, V., Tarasova, E., Savest, N., Mere, A., Mikli, V., Danilson, M., Kaljuvee, T., Lange, S., Yuan, Q., Topham, P. D., & Chen, C. M. (2018). A method for producing conductive graphene biopolymer nanofibrous fabrics by exploitation of an ionic liquid dispersant in electrospinning. *Carbon*, *140*, 148–156. https://doi.org/10.1016/J.CARBON.2018.08.034

Jeddi, K., Sarikhani, K., Qazvini, N. T., & Chen, P. (2014). Stabilizing lithium/sulfur batteries by a composite polymer electrolyte containing mesoporous silica particles. *Journal of Power Sources*, *245*, 656–662. https://doi.org/10.1016/j.jpowsour.2013.06.147

Jeon, H., Yeon, D., Lee, T., Park, J., Ryou, M. H., & Lee, Y. M. (2016). A water-based Al2O3 ceramic coating for polyethylene-based microporous separators for lithium-ion batteries. *Journal of Power Sources*, *315*, 161–168. https://doi.org/10.1016/J.JPOWSOUR.2016.03.037

Ji, X., Lee, K. T., & Nazar, L. F. (2009). A highly ordered nanostructured carbon-sulphur cathode for lithium-sulphur batteries. *Nature Materials*, *8*(6), 500–506. https://doi.org/10.1038/nmat2460

Ji, X., & Nazar, L. F. (2010). Advances in Li-S batteries. *Journal of Materials Chemistry*, *20*(44), 9821–9826. https://doi.org/10.1039/b925751a

Kamyshny Alexey, Gun, J., Rizkov, D., Voitsekovski, T., & Lev, O. (2007). Equilibrium Distribution of Polysulfide Ions in Aqueous Solutions at Different Temperatures by Rapid Single Phase Derivatization. *Environmental Science & Technology*, *41*(7), 2395–2400. https://doi.org/10.1021/es062637+

Killis, A., le Nest, J. F., Gandini, A., Cheradame, H., & Cohen-Addad, J. P. (1984). Correlation among transport properties in ionically conducting cross-linked networks. *Solid State Ionics*, *14*(3), 231–237. https://doi.org/10.1016/0167-2738(84)90104-8

Kozen, A. C., Lin, C. F., Pearse, A. J., Schroeder, M. A., Han, X., Hu, L., Lee, S. B., Rubloff, G. W., & Noked, M. (2015). Next-Generation Lithium Metal Anode Engineering via Atomic Layer Deposition. *ACS Nano*, *9*(6), 5884–5892. https://doi.org/10.1021/acsnano.5b02166

Lee, D. J., Lee, H., Kim, Y. J., Park, J. K., & Kim, H. T. (2016). Sustainable Redox Mediation for Lithium-Oxygen Batteries by a Composite Protective Layer on the Lithium-Metal Anode. *Advanced Materials*, *28*(5), 857–863. https://doi.org/10.1002/adma.201503169

Lei, T., Chen, W., Lv, W., Huang, J., Zhu, J., Chu, J., Yan, C., Wu, C., Yan, Y., He, W., Xiong, J., Li, Y., Yan, C., Goodenough, J. B., & Duan, X. (2018). Inhibiting Polysulfide Shuttling with a Graphene Composite Separator for Highly Robust Lithium-Sulfur Batteries. *Joule*, *2*(10), 2091–2104. https://doi.org/10.1016/j.joule.2018.07.022

Li, N. W., Yin, Y. X., Yang, C. P., & Guo, Y. G. (2016). An Artificial Solid Electrolyte Interphase Layer for Stable Lithium Metal Anodes. *Advanced Materials*, *28*(9), 1853–1858. https://doi.org/10.1002/adma.201504526

Li, T., Bai, X., Gulzar, U., Bai, Y. J., Capiglia, C., Deng, W., Zhou, X., Liu, Z., Feng, Z., & Proietti Zaccaria, R. (2019). A Comprehensive Understanding of Lithium–Sulfur Battery Technology. In *Advanced Functional Materials* (Vol. 29, Issue 32). Wiley-VCH Verlag. https://doi.org/10.1002/adfm.201901730

Liu, K., Zhuo, D., Lee, H. W., Liu, W., Lin, D., Lu, Y., & Cui, Y. (2017). Extending the Life of Lithium-Based Rechargeable Batteries by Reaction of Lithium Dendrites with a Novel Silica Nanoparticle Sandwiched Separator. *Advanced Materials*, *29*(4). https://doi.org/10.1002/adma.201603987

Liu, Y., Lin, D., Liang, Z., Zhao, J., Yan, K., & Cui, Y. (2016). Lithium-coated polymeric matrix as a minimum volume-change and dendrite-free lithium metal anode. *Nature Communications*, *7*(1), 1–9. https://doi.org/10.1038/ncomms10992

Love, C. T. (2011). Thermomechanical analysis and durability of commercial micro-porous polymer Li-ion battery separators. *Journal of Power Sources*, *196*(5), 2905–2912. https://doi.org/10.1016/J.JPOWSOUR.2010.10.083

Lu, Y., Das, S. K., Moganty, S. S., & Archer, L. A. (2012). Ionic liquid-nanoparticle hybrid electrolytes and their application in secondary lithium-metal batteries. *Advanced Materials*, *24*(32), 4430–4435. https://doi.org/10.1002/adma.201201953

Lu, Y., Tikekar, M., Mohanty, R., Hendrickson, K., Ma, L., & Archer, L. A. (2015). Stable cycling of lithium metal batteries using high transference number electrolytes. *Advanced Energy Materials*, *5*(9). https://doi.org/10.1002/aenm.201402073

Lu, Y., Tu, Z., & Archer, L. A. (2014). Stable lithium electrodeposition in liquid and nanoporous solid electrolytes. *Nature Materials*, *13*(10), 961–969. https://doi.org/10.1038/nmat4041

Lu, Z., Sui, F., Miao, Y. E., Liu, G., Li, C., Dong, W., Cui, J., Liu, T., Wu, J., & Yang, C. (2021). Polyimide separators for rechargeable batteries. *Journal of Energy Chemistry*, *58*, 170–197. https://doi.org/10.1016/J.JECHEM.2020.09.043

Luo, W., Zhou, L., Fu, K., Yang, Z., Wan, J., Manno, M., Yao, Y., Zhu, H., Yang, B., & Hu, L. (2015). A Thermally Conductive Separator for Stable Li Metal Anodes. *Nano Letters*, *15*(9), 6149–6154. https://doi.org/10.1021/acs.nanolett.5b02432

Marceaux, S., Bressy, C., Perrin, F. X., Martin, C., & Margaillan, A. (2014). Development of polyorganosilazane–silicone marine coatings. *Progress in Organic Coatings*, *77*(11), 1919–1928. https://doi.org/10.1016/J.PORGCOAT.2014.06.020

McBrayer, J. D., Beechem, T. E., Perdue, B. R., Apblett, C. A., & Garzon, F. H. (2018). Polysulfide Speciation in the Bulk Electrolyte of a Lithium Sulfur Battery. *Journal of The Electrochemical Society*, *165*(5), A876–A881. https://doi.org/10.1149/2.0441805jes

Mikhaylik, Y. v., & Akridge, J. R. (2004). Polysulfide Shuttle Study in the Li/S Battery System. *Journal of The Electrochemical Society*, *151*(11), A1969. https://doi.org/10.1149/1.1806394

Munsell, M. (2018, March 6). *US Energy Storage Market Tops the 1 GWh Milestone in 2017 | Greentech Media*. GTM Research Article: A Wood Mackenzie Business. https://www.greentechmedia.com/articles/read/us-energy-storage-market-tops-the-gwh-milestone-in-2017

Murata, K., Izuchi, S., & Yoshihisa, Y. (2000a). An overview of the research and development of solid polymer electrolyte batteries. *Electrochimica Acta*, *45*(8–9), 1501–1508. https://doi.org/10.1016/S0013-4686(99)00365-5

Murata, K., Izuchi, S., & Yoshihisa, Y. (2000b). Overview of the research and development of solid polymer electrolyte batteries. *Electrochimica Acta*, *45*(8), 1501–1508. https://doi.org/10.1016/S0013-4686(99)00365-5

Nunes-Pereira, J., Costa, C. M., & Lanceros-Méndez, S. (2015). Polymer composites and blends for battery separators: State of the art, challenges and future trends. *Journal of Power Sources*, *281*, 378–398. https://doi.org/10.1016/J.JPOWSOUR.2015.02.010

Park, J., Jeong, J., Lee, Y., Oh, M., Ryou, M. H., & Lee, Y. M. (2016). Micro-Patterned Lithium Metal Anodes with Suppressed Dendrite Formation for Post Lithium-Ion Batteries. *Advanced Materials Interfaces*, *3*(11). https://doi.org/10.1002/admi.201600140

Peled, E., Shekhtman, I., Mukra, T., Goor, M., Belenkaya, I., & Golodnitsky, D. (2018). Improving the Durability and Minimizing the Polysulfide Shuttle in the Li/S

Battery. *Journal of The Electrochemical Society*, *165*(1), A6051–A6057. https://doi.org/10.1149/2.0101801jes

Pfleging, W. (2018). A review of laser electrode processing for development and manufacturing of lithium-ion batteries. *Nanophotonics*, *7*(3), 549–573. https://doi.org/10.1515/NANOPH-2017-0044

Qie, L., & Manthiram, A. (2016). High-Energy-Density Lithium-Sulfur Batteries Based on Blade-Cast Pure Sulfur Electrodes. *ACS Energy Letters*, *1*(1), 46–51. https://doi.org/10.1021/acsenergylett.6b00033

Rana, M., Ahad, S. A., Li, M., Luo, B., Wang, L., Gentle, I., & Knibbe, R. (2019). Review on areal capacities and long-term cycling performances of lithium sulfur battery at high sulfur loading. In *Energy Storage Materials* (Vol. 18, pp. 289–310). Elsevier B.V. https://doi.org/10.1016/j.ensm.2018.12.024

Rand, D. A. J. (2011). A journey on the electrochemical road to sustainability. *Journal of Solid State Electrochemistry*, *15*(7), 1579–1622. https://doi.org/10.1007/s10008-011-1410-z

Reddy, M. v., Mauger, A., Julien, C. M., Paolella, A., & Zaghib, K. (2020). Brief history of early lithium-battery development. *Materials*, *13*(8). https://doi.org/10.3390/MA13081884

Ryou, M. H., Lee, D. J., Lee, J. N., Lee, Y. M., Park, J. K., & Choi, J. W. (2012). Excellent cycle life of lithium-metal anodes in lithium-ion batteries with mussel-inspired polydopamine-coated separators. *Advanced Energy Materials*, *2*(6), 645–650. https://doi.org/10.1002/aenm.201100687

Ryou, M. H., Lee, Y. M., Lee, Y., Winter, M., & Bieker, P. (2015). Mechanical surface modification of lithium metal: Towards improved Li metal anode performance by directed Li plating. *Advanced Functional Materials*, *25*(6), 834–841. https://doi.org/10.1002/adfm.201402953

Salem, N., & Abu-Lebdeh, Y. (2012). *Effect of Nanoparticles on Electrolytes and Electrode/Electrolyte Interface*. 221–244. https://doi.org/10.1007/978-1-4614-4605-7_9

Seh, Z. W., Li, W., Cha, J. J., Zheng, G., Yang, Y., McDowell, M. T., Hsu, P. C., & Cui, Y. (2013). Sulphur-TiO 2 yolk-shell nanoarchitecture with internal void space for long-cycle lithium-sulphur batteries. *Nature Communications*, *4*. https://doi.org/10.1038/ncomms2327

Shebert, G. L., Zamani, S., Yi, C., & Joo, Y. L. (2020). Polysulfide entrapment and retardation in gel electrolyte Li–S batteries: experiments and modeling. *Journal of Materials Chemistry A*, *8*(8), 4341–4353. https://doi.org/10.1039/C9TA14234G

Thackeray, M. M., Wolverton, C., & Isaacs, E. D. (2012). Electrical energy storage for transportation - Approaching the limits of, and going beyond, lithium-ion batteries. In *Energy and Environmental Science* (Vol. 5, Issue 7, pp. 7854–7863). Royal Society of Chemistry. https://doi.org/10.1039/c2ee21892e

Vallée, A., Besner, S., & Prud'Homme, J. (1992). Comparative study of poly(ethylene oxide) electrolytes made with LiN(CF3SO2)2, LiCF3SO3 and LiClO4: Thermal properties and conductivity behaviour. *Electrochimica Acta*, *37*(9), 1579–1583. https://doi.org/10.1016/0013-4686(92)80115-3

Wang, D., Yu, J., Duan, G., Liu, K., & Hou, H. (2020). Electrospun polyimide nonwovens with enhanced mechanical and thermal properties by addition of trace plasticizer. *Journal of Materials Science 2020 55:13*, *55*(13), 5667–5679. https://doi.org/10.1007/S10853-020-04402-2

Wang, H. C., Cao, X., Liu, W., & Sun, X. (2019). Research Progress of the Solid State Lithium-Sulfur Batteries. In *Frontiers in Energy Research* (Vol. 7, p. 112). Frontiers Media S.A. https://doi.org/10.3389/fenrg.2019.00112

Wang, Q., Ping, P., Zhao, X., Chu, G., Sun, J., & Chen, C. (2012). Thermal runaway caused fire and explosion of lithium ion battery. *JPS*, *208*, 210–224. https://doi.org/10.1016/J.JPOWSOUR.2012.02.038

Wang, Q., Ping, P., Zhao, X., Chu, G., Sun, J., Chen, C., Wang, Q., Ping, P., Zhao, X., Chu, G., Sun, J., & Chen, C. (2012). Thermal runaway caused fire and explosion of lithium ion battery. *JPS*, *208*, 210–224. https://doi.org/10.1016/J.JPOWSOUR.2012.02.038

Whittingham, M. S. (2012). History, Evolution, and Future Status of Energy Storage. *Proceedings of the IEEE*, *100*(Special Centennial Issue), 1518–1534. https://doi.org/10.1109/JPROC.2012.2190170

Yamin, H., & Peled, E. (1983). Electrochemistry of a nonaqueous lithium/sulfur cell. *Journal of Power Sources*, *9*(3), 281–287. https://doi.org/10.1016/0378-7753(83)87029-3

Yan, K., Lu, Z., Lee, H. W., Xiong, F., Hsu, P. C., Li, Y., Zhao, J., Chu, S., & Cui, Y. (2016). Selective deposition and stable encapsulation of lithium through heterogeneous seeded growth. *Nature Energy*, *1*(3), 1–8. https://doi.org/10.1038/NENERGY.2016.10

Yang, C. P., Yin, Y. X., Zhang, S. F., Li, N. W., & Guo, Y. G. (2015). Accommodating lithium into 3D current collectors with a submicron skeleton towards long-life lithium metal anodes. *Nature Communications*, *6*(1), 1–9. https://doi.org/10.1038/ncomms9058

Yu, X., Wu, H., Koo, J. H., & Manthiram, A. (2020). Tailoring the Pore Size of a Polypropylene Separator with a Polymer Having Intrinsic Nanoporosity for Suppressing the Polysulfide Shuttle in Lithium–Sulfur Batteries. *Advanced Energy Materials*, *10*(1), 1902872. https://doi.org/10.1002/AENM.201902872

Zhang, J., Yue, L., Kong, Q., Liu, Z., Zhou, X., Zhang, C., Xu, Q., Zhang, B., Ding, G., Qin, B., Duan, Y., Wang, Q., Yao, J., Cui, G., & Chen, L. (2014). Sustainable, heat-resistant and flame-retardant cellulose-based composite separator for high-performance lithium ion battery. *Scientific Reports 2014 4:1*, *4*(1), 1–8. https://doi.org/10.1038/srep03935

Zhang, R., Cheng, X. B., Zhao, C. Z., Peng, H. J., Shi, J. le, Huang, J. Q., Wang, J., Wei, F., & Zhang, Q. (2016). Conductive Nanostructured Scaffolds Render Low Local Current Density to Inhibit Lithium Dendrite Growth. *Advanced Materials*, *28*(11), 2155–2162. https://doi.org/10.1002/adma.201504117

Zhang, Sheng S. (2013). Liquid electrolyte lithium/sulfur battery: Fundamental chemistry, problems, and solutions. In *Journal of Power Sources* (Vol. 231, pp. 153–162). Elsevier. https://doi.org/10.1016/j.jpowsour.2012.12.102

Zhang, Sheng S., & Read, J. A. (2012). A new direction for the performance improvement of rechargeable lithium/sulfur batteries. *Journal of Power Sources*, *200*, 77–82. https://doi.org/10.1016/j.jpowsour.2011.10.076

Zhang, Sheng S., & Tran, D. T. (2013). How a gel polymer electrolyte affects performance of lithium/sulfur batteries. *Electrochimica Acta*, *114*, 296–302. https://doi.org/10.1016/j.electacta.2013.10.069

Zhang, Sheng Shui. (2007). A review on the separators of liquid electrolyte Li-ion batteries. *Journal of Power Sources*, *164*(1), 351–364. https://doi.org/10.1016/J.JPOWSOUR.2006.10.065

Zhao, M., Li, B.-Q., Zhang, X.-Q., Huang, J.-Q., & Zhang, Q. (2020). A Perspective toward Practical Lithium−Sulfur Batteries. *Cite This: ACS Cent. Sci*, *2020*, 1095–1104. https://doi.org/10.1021/acscentsci.0c00449

Zheng, C., Wang, K., Li, L., Huang, H., Liang, C., Gan, Y., He, X., Zhang, W., & Zhang, J. (2021). High-Performance All-Solid-State Lithium–Sulfur Batteries Enabled by Slurry-Coated Li6PS5Cl/S/C Composite Electrodes. *Frontiers in Energy Research*, *8*, 416. https://doi.org/10.3389/FENRG.2020.606494

Zheng, G., Lee, S. W., Liang, Z., Lee, H. W., Yan, K., Yao, H., Wang, H., Li, W., Chu, S., & Cui, Y. (2014). Interconnected hollow carbon nanospheres for stable lithium metal anodes. *Nature Nanotechnology*, *9*(8), 618–623. https://doi.org/10.1038/nnano.2014.152

Zhong, W. (2016). Nanofibres for medical textiles. *Advances in Smart Medical Textiles: Treatments and Health Monitoring*, 57–70. https://doi.org/10.1016/B978-1-78242-379-9.00003-7

Zhou, D., Liu, R., He, Y. B., Li, F., Liu, M., Li, B., Yang, Q. H., Cai, Q., & Kang, F. (2016). SiO2 Hollow Nanosphere-Based Composite Solid Electrolyte for Lithium Metal Batteries to Suppress Lithium Dendrite Growth and Enhance Cycle Life. *Advanced Energy Materials*, *6*(7). https://doi.org/10.1002/aenm.201502214

Zou, P., Wang, Y., Chiang, S. W., Wang, X., Kang, F., & Yang, C. (2018). Directing lateral growth of lithium dendrites in micro-compartmented anode arrays for safe lithium metal batteries. *Nature Communications*, *9*(1), 1–9. https://doi.org/10.1038/s41467-018-02888-8

CHAPTER 4

ANALYSIS OF Li_2S_6 DIFFUSIVITY THROUGH GELLED AND NON-GELLED SEPARATOR SYSTEMS

4.1 Abstract

In this chapter, Li_2S_6 diffusivity analysis was done to study and understand the dynamics of the soluble polysulfide intermediates through gelled separator systems. First, an experimental approach was used to probe the diffusivity of the Li_2S_6 though gelled and non-gelled PI/OPSZ and Celgard 2400 separators to ascertain the polysulfide trapping characteristics of the PI/OPSZ separators when used in tandem with the gel electrolyte. The experimental results show a 6-fold reduction in the amount of polysulfide diffusing through the POSS-gelled PI/OPSZ separator compared to a Celgard 2400 separator with liquid electrolyte.

Second, to computationally study the diffusion profile in a separator, a numerical model solved using Finite Element Method on a 2-D mapped mesh grid using COMSOL Multiphysics 5.5 was built. The boundary conditions were defined to closely mimic the diffusion experiment. The model was checked for robustness via tortuosity calculations. The model can be easily expanded to incorporate more complex 3D topologies to closely mimic the separator geometry and be extended to include cell chemistry for computational analysis of electrochemical performance.

Graphical Abstract

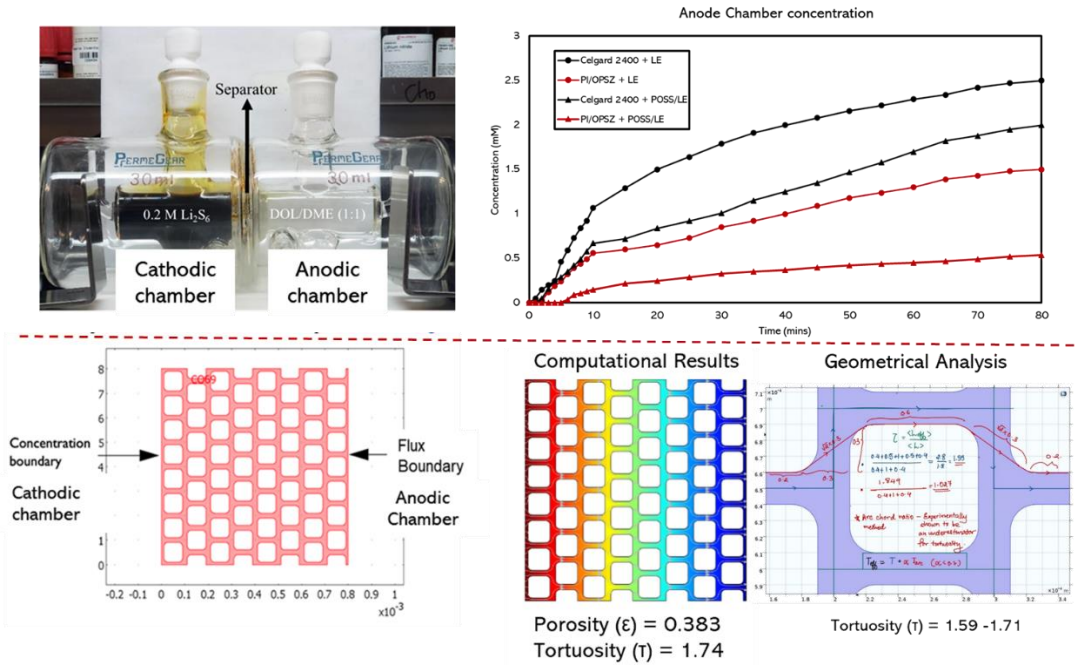

Figure 4.1: Graphical Abstract for Chapter 4

4.2 Experimental Methods

4.2.1 Synthesis of Li_2S_6 polysulfide solution

Under an Argon-filled and oxygen-free glovebox, elemental sulfur (pure) and lithium sulfide (Li_2S) (Alfa Aesar) were mixed in a 5:1 molar ratio in a 250 mL glass (VWR). The mixture was then added to a 1:1 volume ratio of 1,2-dimethoxyethane (DME) and 1,3-Dioxolane (DOL) to form a 0.2M lithium sulfide (Li_2S_6) solution, which should produce a deep orange/brown polysulfide solution. The solution is then placed on a hot stir plate (Thermo Fisher Scientific) for approximately 24 hours at 80^oC. The mixture was then fully mixed for another 24 hours without heat. Solution was utilized within a few days due to polysulfides degrading under air and water in Argon atmosphere.

4.2.2 Synthesis of Gelled separators.

The Liquid Electrolyte (LE) consisted of 1M bis(trifluoromethane)sulfonimide lithium salt (LiTFSI), 0.15M of lithium nitrate ($LiNO_3$) in a 1:1 volume ratio of 1,2-dimethoxyethane (DME) and 1,3-Dioxolane (DOL). Electrolyte materials were purchased from Sigma and prepared inside an Argon-filled and oxygen free glovebox.

To make the POSS gelled electrolyte, 5 wt% polyhedral oligomeric silsesquioxane methacrylate (POSS-MA, Sigma-Aldrich) a ceramic-based cross-linker along with 0.5 wt% azobisisobutyronitrile (AIBN, Sigma-Aldrich) initiator was added to the base liquid electrolyte solution.

After the gel precursor was prepared, 4” x 4” of square separator sheets (Celgard 2400 and PI-OPSZ) were submerged in the POSS precursor solution and heat treated at 70oC for 30 minutes on a hot plate inside an Argon-filled and oxygen-free glovebox.

4.2.3 Synthesis of DOL:DME mixture

30 mL of 1:1 volume ratio of 1,2-dimethoxyethane (DME) and 1,3-Dioxolane (DOL) was mixed and placed in a separate glass container.

4.2.4 Diffusion Test Setup

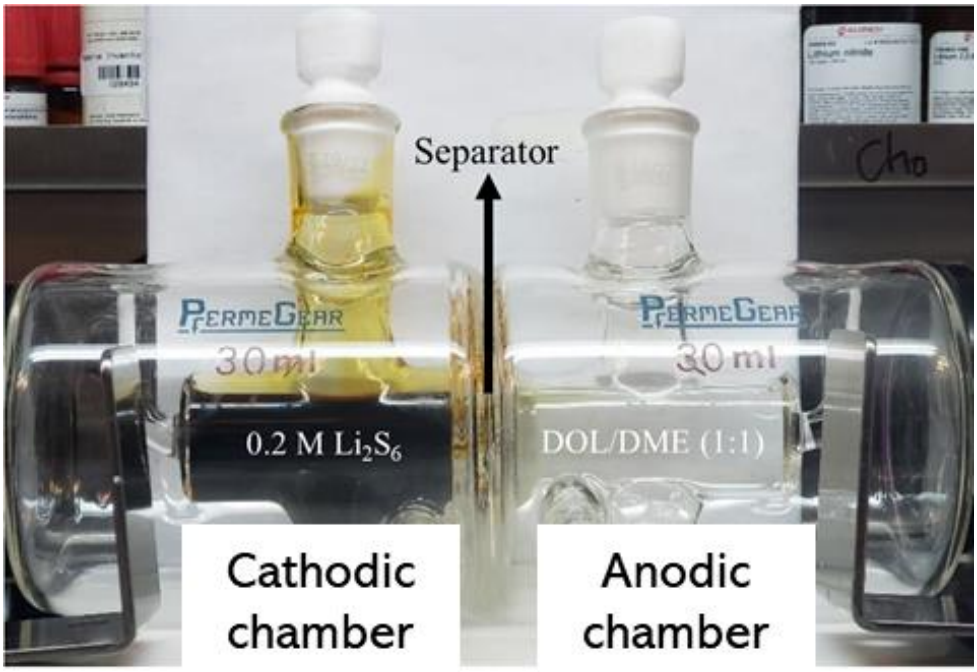

Figure 4.2: Polysulfide Diffusion Experiment Setup

The polysulfide diffusion experiment was set up using “side-bi-side” cells purchased from PermeGear. A white background was provided to accentuate the color of the chambers filled with solution and DOL:DME solvent. The two compartments acted as the cathode (polysulfide mixture) and anode (DOL:DME solvent). Celgard 2400 and the gelled polymer electrolyte separator were placed in between the two glass chambers

in which clear lubricant grease was used to provide adhesion and prevent leakage of solution. The DOL:DME solution was then added from the opening of the right chamber immediately followed by pouring the polysulfide mixture on the left chamber. Time and pictures were immediately recorded and taken at increments of 1 min for the first 20 minutes and subsequently for 5 minutes afterwards. Next, 2 mL samples from each chamber were taken in the first 5 minutes for further analysis using UV-Vis spectroscopy. After all samples were taken, a side-by-side picture was taken for polysulfide comparisons.

4.2.5 Constructing a Calibration Curve

Concentration of polysulfides were analyzed using Ultraviolet-visible (UV-Vis) spectrophotometer (Varian Cary 5000 UV-Vis-NIR) from the Hanrath group. Samples were drawn and placed in a quartz cuvette inside Argon-filled and oxygen-free glovebox. The samples were then carefully transported to the UV-Vis for further analysis using the Varian Cary WinUV software program. All samples were analyzed in the range of 350 to 600 nm.

To produce a calibration curve of the concentrations, the absorbances of standard (known) concentrations between 3mM and 0.75mM were obtained against a baseline of DOL:DME at 430 nm peak (Figure 4.3). The 5 absorbance values were used to plot a calibration line in congruence to the Beer-Lambert Law of absorption. The calibration plot was then used to extrapolate the concentration of any solution based on its absorbance value at 430 nm.

4.3 Results and Discussion

4.3.1 Calibration Curve for Polysulfide Concentration

The absorption curves for the standard concentrations of Li_2S_6 showed a peak at 430 nm (because the yellowish hue of the Li_2S_6 compound. The absorption values were tabulated and plotted against concentration to construct a calibration line (Figure 4.4)

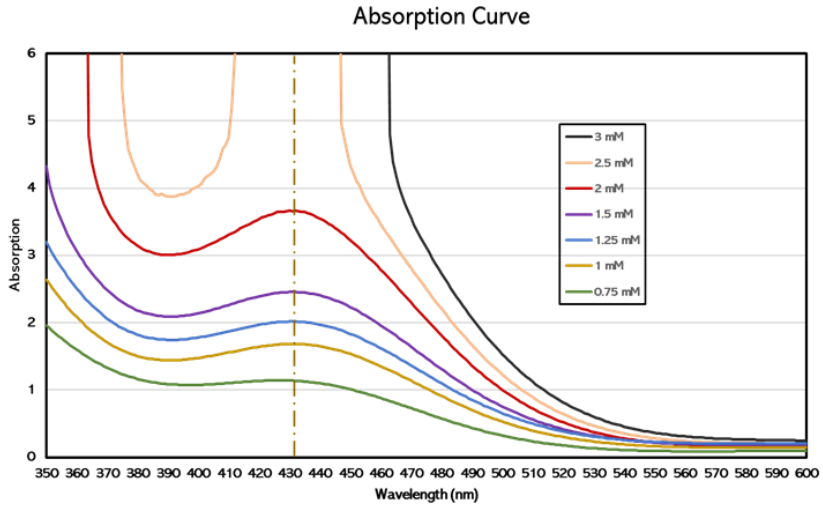

Figure 4.3: Absorption Curve

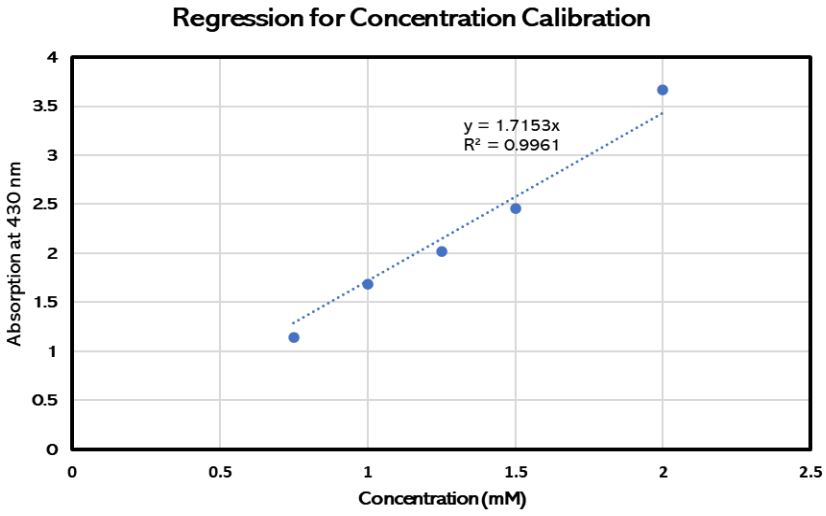

Figure 4.4: Regression line for concentration calibration

The regression line equation was Abs = 1.7153*(Concentration (mM)) and the R^2 value was 0.9961

4.3.2 Diffusion Results

From the time-lapse snapshots (figure 4.6) and the concentration profile (figure 4.5), it can be clearly seen that the diffusivity of Li_2S_6 is the least in the gelled PI/OPSZ separators and in fact diffusion rate through the ungelled PI/OPSZ separator was also lesser than the gelled Celgard separator. This observation is interesting as despite having a much larger porosity than Celgard, the PI/OPSZ separators can better trap the polysulfide species, and this confirms the effectiveness of these separators at mitigating polysulfide shuttling. This performance may be linked to more tortuosity in the randomly oriented electrospun PI/OPSZ fibers and also due to the presence of ceramic content in the PI/OPSZ fibers which due to their polar nature help in trapping the polysulfide species.

Though it should be noted that this diffusion study doesn't exactly mimic the cell conditions and the rates of diffusion, diffusion pathway and intermediate – separator interaction may vary at high electric fields.

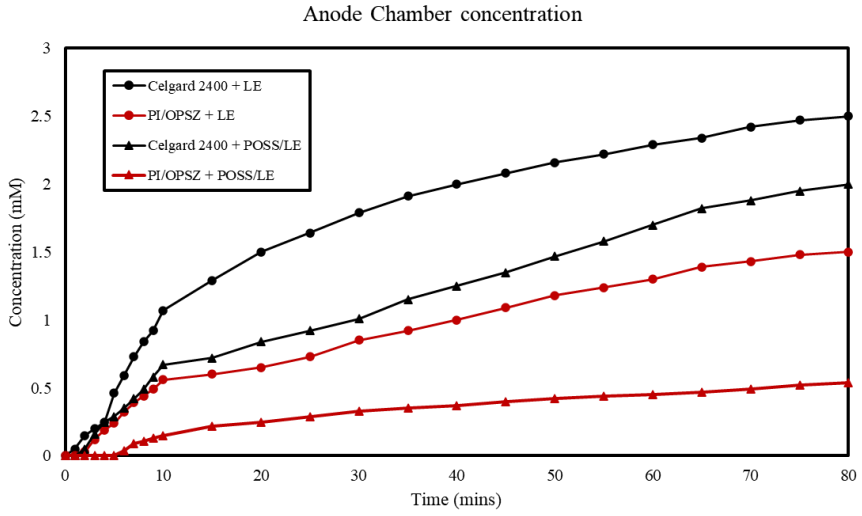

Figure 4.5: Anode chamber concentration profile.

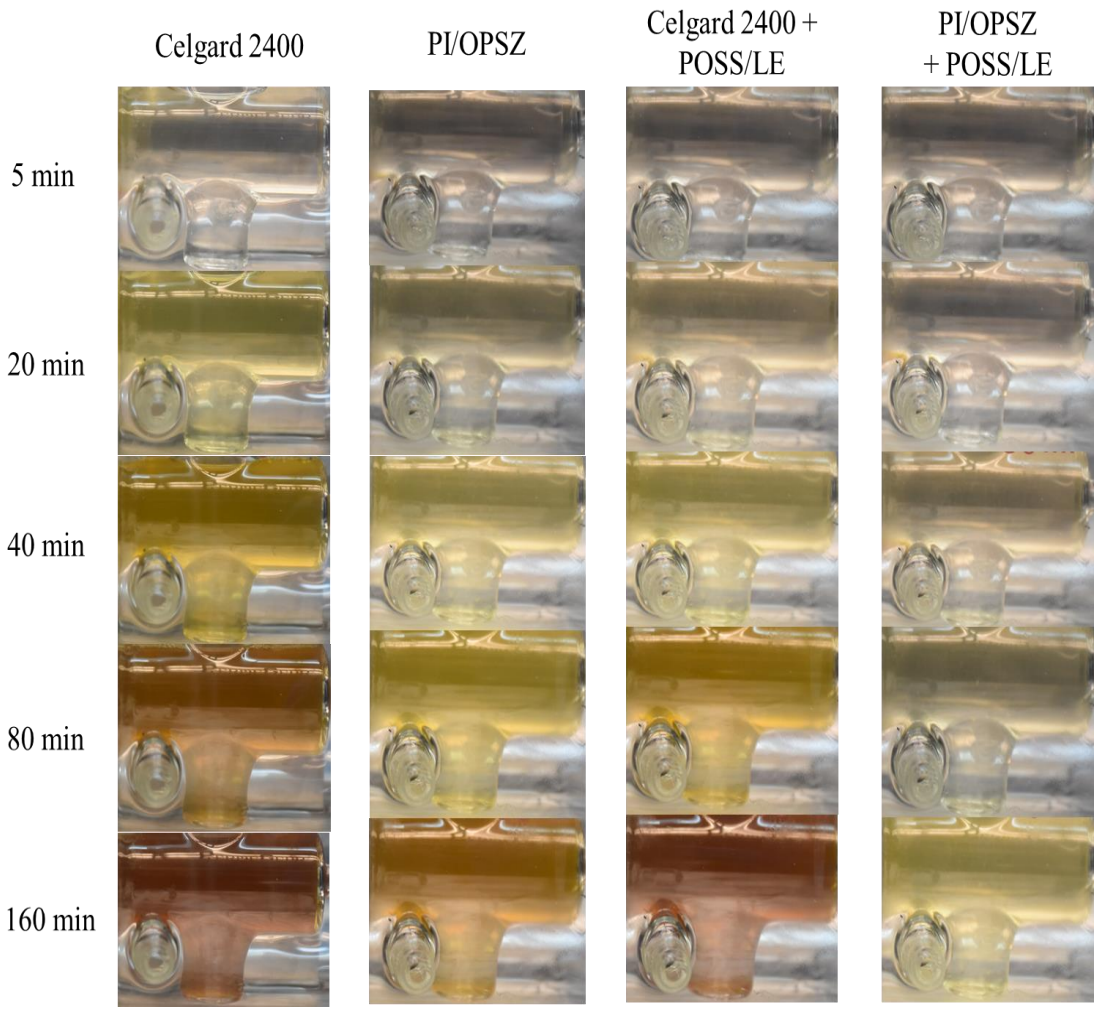

Figure 4.6: Time lapse photograph of the Li_2S_6 diffusion from the cathode chamber through gelled and non-gelled Celgard 2400 and PI/OPSZ separators

4.4 Numerical Model: Finite Element Analysis

4.4.1 Introduction

The motivation of this work was to build a microscale module to study the diffusion of species through any defined porous geometry; with the eventual goal of extending the work to include specific cell chemistry, material interactions and battery dynamics to mimic the operation of a working cell. This would help study the impact of species diffusion throughout the cell on the cell electrochemical performance.

Typically, transport through porous media is usually studied using a simplified homogeneous model with effective transport properties. This is a necessity in most of the cases, as typically, the sizes of pores and particles that make up the component are several orders of magnitude smaller than the domain size that needs to be studied[1]. PI/OPSZ separators have a thickness of 21-25μm, however modelling such a large domain would be quite computationally expensive and hence, in the study a micro-domain has been used to model the behavior of the separator.

In this model, to study the diffusion dynamics in the separator system, a numerical model solved using Finite Element Method on a mapped mesh grid using COMSOL Multiphysics® 5.5 was built. The model is still in its rudimentary phase and can be easily developed by adding material characteristics and chemistry to better mimic the

[1]Effective Diffusivity in Porous Materials, COMSOL Multiphysics® v. 5.5. COMSOL AB, Stockholm, Sweden. 2020

actual interactions between the electrolyte, separator, and the soluble polysulfide intermediates.

4.4.2 Model Definition

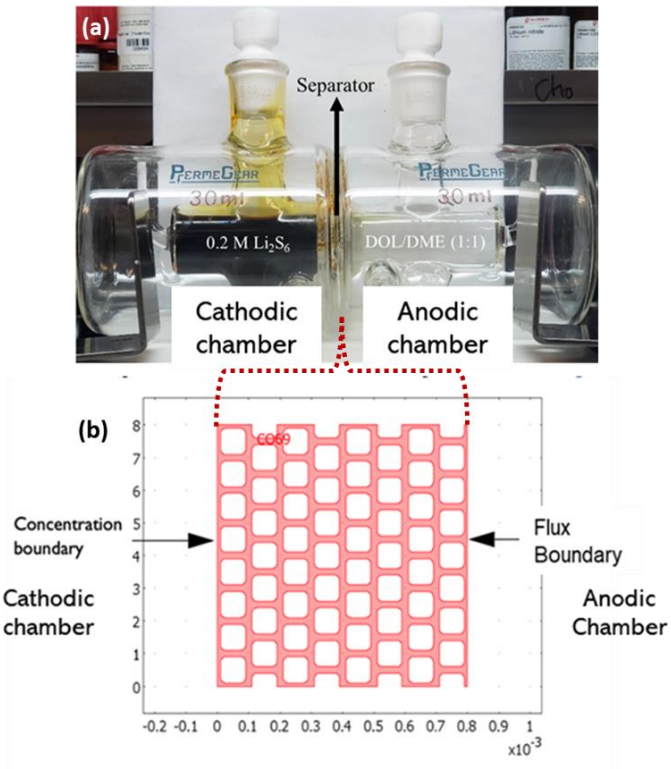

Figure 4.7: Model definition

The model was made to closely mimic the conditions of the experimental diffusion analysis. First, a symmetric 'test' geometry was constructed to check for the robustness of the model before shifting onto more *realistic* geometries. This was done because geometric analysis of the regular, symmetric geometry is easier and can be easily verified against model evaluated parameters to check for robustness of the system.

The model equation in the domain shown in figure 4.7 is the standard transient diffusion equation (Fickian Diffusion):

$$\frac{\partial c}{\partial t} + \nabla.(-D\nabla c) = 0$$

Where, c denotes concentration (mol/m^3 using S.I. units), and D is the diffusion coefficient (m^2/s) of the solute.

The boundary conditions are of three different kinds. The large concentration of Li_2S_6 on the cathodic side was assumed to remain constant throughout the analysis and so a constant concentration boundary was set up on the cathodic side.

$$c = c_0$$

Where, c_0 is a given concentration.

Next, the anodic boundary was set to a flux boundary with Danckwert boundary conditions.

$$(-D\nabla c).n = k_m(c - c_{out})$$

Where, k_m is the mass transfer coefficient (m/s), and c_{out} is the concentration in a bulk solution outside of the porous structure (Anodic chamber)

The other boundaries were insulated to prevent flux out of these surfaces.

$$(-D\nabla c).n = 0$$

The model evaluates a species' effective diffusivity in a medium:

Effective Diffusivity is evaluated according to:

$$D^{eff}\frac{(c_0 - c_{out})}{L_1} = N_{average}$$

$$N_{average} = \frac{1}{L_0}\int_0^{L_0}(-D\nabla c).n\, dS$$

Where, L_0 and L_1 are the length across x and y axis, and $N_{average}$ is the average flux at exit.

Next, the model is checked for robustness by evaluating the tortuosity of the known geometry by : (1) numerical evaluation by solving the model using Finite Element Method, (2) geometrical evaluation using Arc-Chord Method (Figure 4.8)

The porosity and tortuosity calculations were done by evaluating these equations:

$$\varepsilon = \frac{1}{L_0 L_1}\iint_0^{L_0 L_1} 1.\, dxdy$$

$$D^{eff} = D\,\frac{\varepsilon}{\tau}$$

Where, ε is the porosity and τ is the tortuosity.

4.5 Results and Discussion

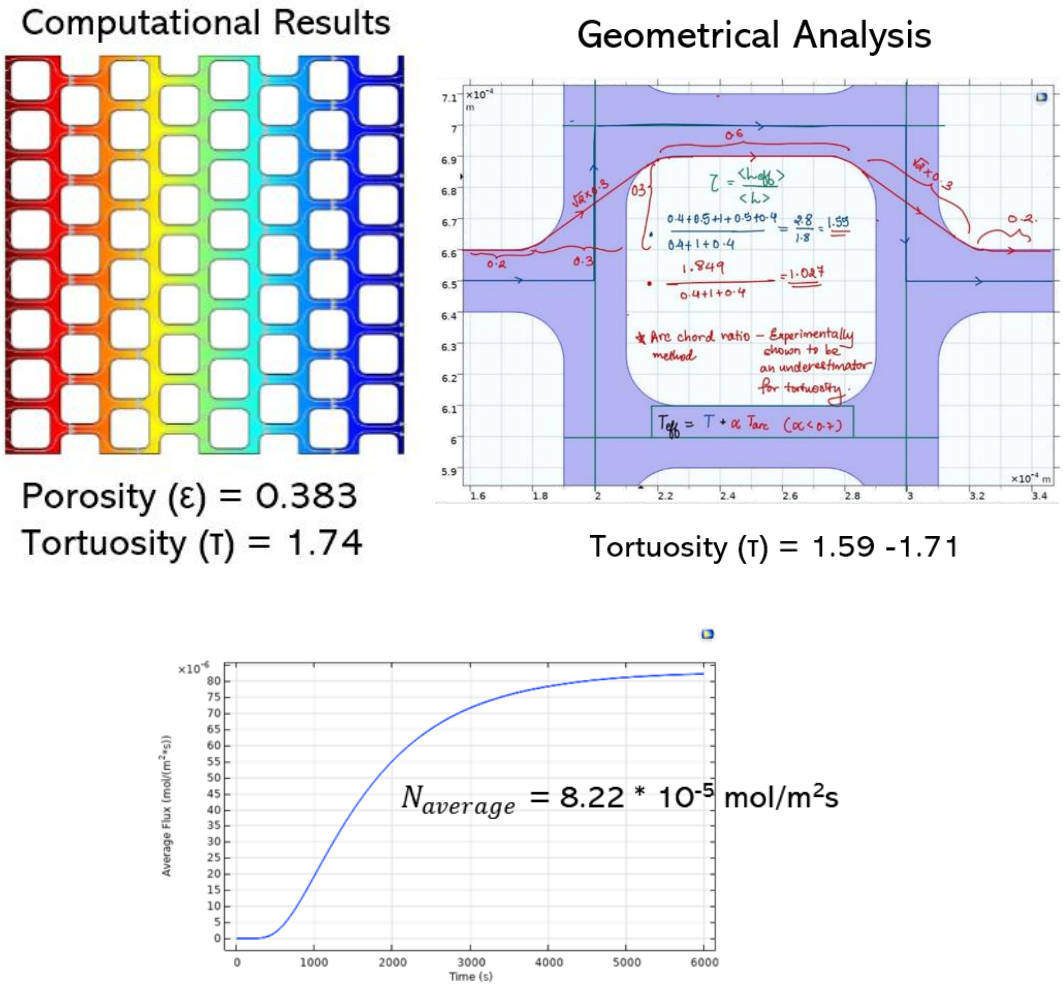

Figure 4.8: Model results and Robustness evaluation

Figure 4.8 shows the steady-state concentration profile across the test geometry. The tortuosity evaluated by the model matches closely with that obtained by the geometric evaluation and hence, the model can be concluded to be robust. Next, the model was extended to a more 'realistic' separator geometry.

Due to high computational expenditure of modeling a 3D separator topology on COMSOL and the resource limitation during the lab shut down during the pandemic, a

SEM image generated 2D separator geometry produced using MATLAB was used. (fig. 4.9)

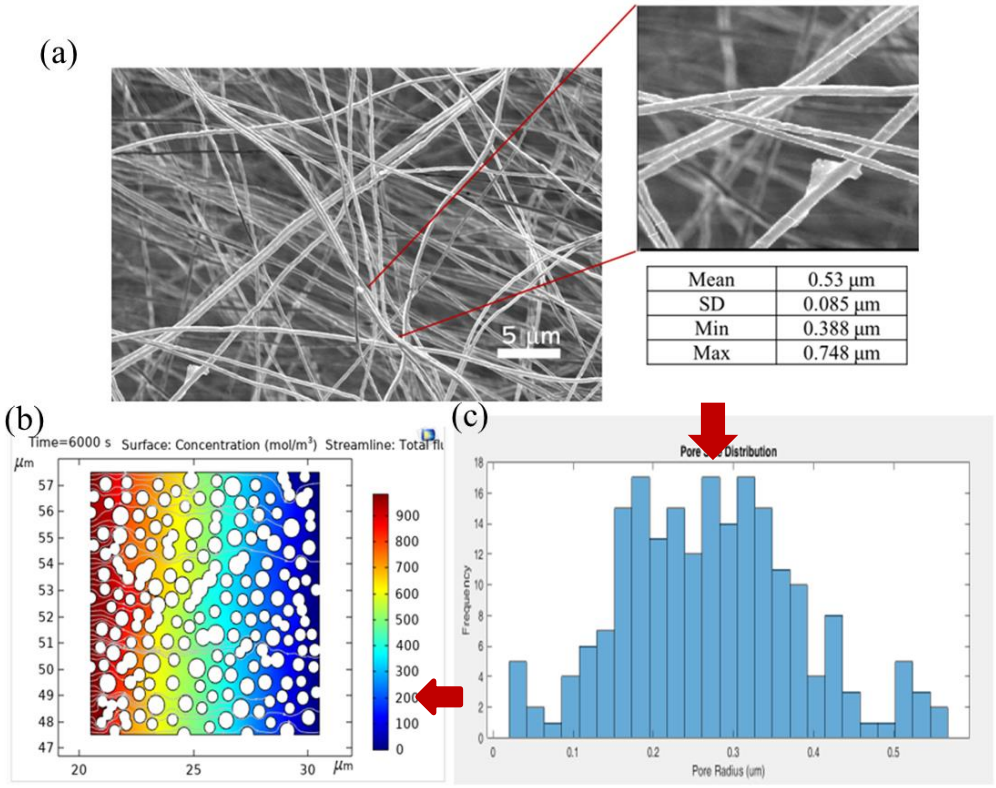

Figure 4.9: (a) SEM image analyzed using ImageJ. (b) Final concentration profile on random 2D topology generated using MATLAB. (c) Pore size distribution of the random 2D geometry.

The SEM image of the electrospun separator was analyzed using ImageJ – an open source image processing software. The data was then used to produce a 'random' 2D domain using MATLAB, with structural characteristics like the geometry in the SEM image and the model was run. Figure 4.9 and Table 4.1 shows the results of the model run on the new geometry. The tortuosity parameter is constant for each species showing good convergence in the model. The model can easily incorporate any 3D geometry from tomographic images, and we plan on extending the work to incorporate several other features relevant to the cell performance.

Table 4.1: Results from simulation using new geometry.

Species	Initial Concentration (mol/m^3)	Diffusivity (m^2/s) ($x10^{10}$)	Average Molecular Flux (mol/m^2s)	Porosity	Effective Diffusivity (m^2/s) ($x10^{10}$)	Tortuosity
S_8^{2-}	0.175	6	$4x10^{-6}$	0.566	2.285	1.49
S_6^{2-}	0.319	6	$7.29x10^{-6}$	0.566	2.288	1.49
S_4^{2-}	0.0197	1	$7.49x10^{-8}$	0.566	0.381	1.49

* Concentration and diffusivity data from Dr. J. Carlin's computational LiS cell model

4.6 Conclusion

The experimental analysis clearly shows that the diffusivity of Li_2S_6 is the least in the gelled PI/OPSZ separators and in fact the diffusion rate through the ungelled PI/OPSZ separator was also lesser than the gelled Celgard separator. This performance may be linked to more tortuosity in the randomly oriented electrospun PI/OPSZ fibers and also due to the presence of ceramic content in the PI/OPSZ fibers which due to their polar nature help in trapping the polysulfide species. This undoubtably verifies the effectiveness of PI/OPSZ separators in trapping the polysulfide intermediates and hence, aid in mitigating polysulfide shuttling in the cell.

Further, the numerical diffusion model was successfully checked for robustness and though it is still very rudimentary, it can be easily extended to incorporate more complex 3D topologies and specific cell chemistry to better model the separator in actual cell conditions.

4.7 Future Work

Given that the COMSOL model is still in an elementary phase, there are several possible extensions that can be added to improve the model. Also, given the versatility of the COMSOL program, the model can also be incorporated in various modules to simulate and study various performance conditions.

Currently, the model only simulates simple transient diffusion. Integrating electric field into the model will help better study the diffusion of the polar, charged intermediates through the separator and the electrolyte. Additionally, we plan to incorporate the electrolyte molecules and molecular interactions (potential fields) to closely model 'real' cell environment.

Also, given the limitations of 2D geometries, the obvious next step is to shift to a 3D geometry built using tomographic imaging to better incorporate the complex random nature of the electrospun fibers and gel polymer networks. Only on using a 3D geometry would we be able to evaluate the true tortuosity of the geometry and hence, be able to better compare between different separator systems.

Further, the COMSOL package comes with an extensive electrochemistry module which can be incorporated into the model to simulate electrochemical performance tests quickly, eliminating the need of time-consuming trial-and error experimental analysis of the various separator systems.

Finally, a possible extension to the work may be to incorporate functional groups on the separator and gel networks to closely mimic polysulfide interactions with the gelled separator systems.